Benha University
Faculty of medicine
Radio diagnosis department

Role of different image modalities in diagnosis of skin lesions

Essay

Submitted for fulfillment of master degree in
Radio diagnosis
By

Dr. Shaimaa Fathy Mohamed Lotfy
M.B.B.CH.

Under supervision of

Prof.Dr. Medhat Mohamed Refaat
Professor of Radiodiagnosis
Faculty of medicine
Benha University

Dr. Hesham Mohamed Farouk
Assistant Professor of Radiodiagnosis
Faculty of medicine
Benha University

2011

Acknowledgement

Thanks first and last to ***Allah,*** *the God who create us, as we owe him for his great care, support and guidance in every step in our life.*

I would like to express my profound gratitude and cordial appreciation to for

Dr. Medhat Mohamed Refaat ***Professor of Radiology, Faculty of Medicine, Benha University*** *for his moral support, valuable supervision and for enabling me to fulfill this work.*

I would like also to thank ***Dr. Hesham Mohammed Farouk,*** ***Ass.Professor of Radiology, Faculty of Medicine, Benha University,*** *for his continued advice, constructive and valuable suggestions, meticulous follow up and supervision of every step of this work till its final form.*

I deeply thank ***my husband,*** *the human whom I wish always the best of everything , for his valuable support and encouragement , and* ***my family*** *who putting me at the right way.*

Shaimaa fathy Mohammed.

List of content

Title	Page
List of abbreviation	1
List of diagram	2
List of figure	3
List of table	6
Introduction	7
Aim of the work	9
Chapter 1	**10-58**
Anatomy of the skin	10
Histology of the skin	20
Pathology of the skin lesions	31
Chapter 2	**59-93**
Technique	59
Radiological diagnosis of	
Malignant Melanoma	68
Squamous Cell Carcinoma	77
Basal cell carcinoma	80
Pigmented nevi	82
Sebrrheic keratosis	82
Subcutaneous abscess	83
Psoriasis	
Summary	94
Reference	97
Arabic summary	109

List of abbreviation

ALMs	Acral Lentiginous Melanomas.
BCC	Basal Cell Carcinoma.
CCD	Charge-Coupled Device
Cglc	Circulating glucose level.
CT	Computed Tomography
FTR- IR	Fourier Transform Raman &Infra Red vibrational
LMMs	Lentigo Malignant Melanomas
MLMs	Mucosal Lentiginous Melanomas
MM	Malignant Melanoma
MRI	Magnetic Resonance Image
MR spectroscopy	Magnetic Resonance spectroscopy
NMs	Nodular Melanomas
PET/CT	Positron Emission tomography/ Computed Tomography
PN	Pigmented Nevus
RF	Radio Frequancy
ROS	Reactive Oxygen Species
RST	Relaxed Skin Tension Lines
SCC	Squamous Cell Carcinoma
SK	Seborrheic keratoses
SSMs	Superficial Spreading Melanomas
U/S	Ultrasonography

List of Diagrams

Diagram		Page
Diagram 1	Layers of the skin.	10
Diagram 2	Anatomy of the hair follicle.	15
Diagram 3	Four main facial lines.	17
Diagram 4	Layers of the epidermis.	21
Diagram 5	Blood vessel network of the skin.	٢٦
Diagram 6	Free nerve ending of the skin.	٢٧
Diagram 7	The principle of Raman spectroscopy.	63
Diagram 8	The principle of ELastography.	66
Diagram 9	A schematic showing the process of computing the strain in a tissue segment.	67
Diagram 10	NIR-FT Raman spectra of normal skin, PN, BCC MM and SK.	69
Diagram 11	NIR-FT Raman spectra of normal skin, PN, BCC, MM and SK.	70
Diagram 12	Sensitivity map of neural network.	73
Diagram 13	Line diagram depicting location of band A, B, C in high frequency U/S image of plaque of psoriasis.	92

List of figures

Figure		Page
Figure 1	Histological slide of layers of the skin.	20
Figure 2	Histological slide of melanocyte attachment	٢٣
Figure 3	Histological slide of langerhans cells.	23
Figure 4	Histological slide of layers of the dermis.	24
Figure 5	Histological slide of papillary and reticular layers of the dermis.	25
Figure 6	Histological slide of hair follicle.	27
Figure 7	Histological slide of nail eponychium.	28
Figure 8	Histological slide of sebaceous gland.	29
Figure 9	Histological slide of apocrine sweat gland.	30
Figure 10	Pathological slide of of hyperkeratosis and parakeratosis of Psoriasis.	31
Figure 11	Macroscopic picture of psoriasis.	32
Figure 12	Pathological slide of downword elongation of ridge in Psoriasis.	32
Figure 13	Pathological slide of malignant melanoma.	3٣
Figure 14	Macroscopic picture of malignant melanoma.	٣٤
Figure 15	Macroscopic picture of malignant melanoma.	٣٥
Figure 16	Macroscopic picture of lentigo malignant melanoma.	٣٥
Figure 17	Pathological slide of dysplastic melanocytic cells.	٣٦
Figure 18	Pathological slide of nodular melanoma.	٣٧
Figure 19	Different macroscopic pictures of squamous cell carcinoma.	٤٠
Figure 20	Pathological slide of squamous cell carcinoma.	٤١
Figure 21	Pathological slide of basal cell carcinoma.	٤٢
Figure 22	Pathological slide of basal cell carcinoma.	٤٢

Figure 23	Macroscopic picture of nodular basal cell carcinoma.	٤٣
Figure 24	Macroscopic picture of superficial basal cell carcinoma.	٤٣
Figure 25	Macroscopic picture of large superficial basal cell carcinoma	٤٣
Figure 26	Macroscopic picture of nodular basal cell carcinoma.	٤٤
Figure 27	Macroscopic picture of seborrheic keratoses.	٤٧
Figure 28	Macroscopic picture of seborrheic keratoses in autosomally dominant mode of inheritance.	٤٧
Figure 29	Macroscopic picture of a Clark (dysplastic nevus).	٥٣
Figure 30	Macroscopic picture of a compound Clark (dysplastic nevus)	٥٣
Figure 31	Macroscopic picture of junctional spitz nevus.	٥٤
Figure 32	Pathological slide of congenital nevus.	٥٤
Figure 33	Pathological slide of conventional compound pigmented nevus.	٥٥
Figure 34	Pathological slide of spitz nevus.	٥٦
Figure 35	Pathological slide of spitz nevus.	٥٧
Figure 36	Pathological slide of blue nevus.	٥٨
Figure 37	Ultrasound image of superficial spreading melanoma.	٧٦
Figure 38	Ultrasound and elastography images of malignant melanoma.	٧٦
Figure 39	Trans-axial multi spin-echo MRI of normal skin and tumors On different stages of growth.	٧٨
Figure 40	The loss of dermis and epidermis interphase accompanied By the invasion of tumor in squamous cell carcinoma.	٧٩
Figure 41	Ultrasound and elastography images of squamous cell carcinoma.	٨٠
Figure 42	Ultrasound and elastography images of squamous cell carcinoma.	٨٠
Figure 43	Basal cell carcinoma, histological slide, B mode ultrasound and elastography.	٨١
Figure 44	Abscess cavity visualized with B mode imaging and Elastography.	٨٤
Figure 45	Elastographic imaging of isoechoic abscesses.	٨٥
Figure 46	Elastographic color spectrum of skin abscesses.	٨٦

Figure 47	Elastographic color pattern of skin abscesses.	٨٧
Figure 48	Elastographic image of soft tissue induration.	٨٨
Figure 49	Elastographic pattern of skin infection induration.	٨٩
Figure 50	Elastographic color spectrum of skin infection induration.	٩٠
Figure 51	Comparison between histologic section and high frequency ultrasound image of plaque of psoriasis.	٩٢
Figure 52	Ultrasound image of a psoriatic plaque before treatment.	٩٣

List of tables

Table		Page
Table I	The Fitzpatrick Scale.	١٨
Table II	Major protein and lipid band positions of NIR-FT Raman Spectra of Normal skin (NOR), PN, BCC and SK.	٧٠
Table III	Major band ratio in NIR-FT Raman Spectra of Normal skin (NOR), PN, BCC and SK.	٧١
Table IV	Confusion map of the neural network prediction of Normal skin (NOR), PN, BCC and SK	٧٢

Introduction

Introduction

Skin diseases classified either according to its origin to primary skin disease and secondary skin diseases or according to the causative agent to: non- infectious skin diseases as urticaria, dermatitis, angio-neurotic edema and infectious skin diseases (viral, bacterial, mystic and parasitic diseases) and other diseases (congenital, granulomatous, neoplasm lesions) **(Kenneth.Katz, 2001).**

Recently, high-frequency ultrasonography has been introduced to dermatology, currently; the most often used frequency for skin imaging is between 20 and 25 MHZ. Ultrasound images can be generated in different modes, i.e. one-dimensional A mode, tow-dimensional B mode and C mode. This type of skin imaging is known as a non invasive, reproducible and quantitative method, which can be used to evaluate skin characteristics in a variety of dermatologic diseases. It can found application in the assessment of skin tumors, morphea, psoriasis, lipodermatosclerosis, skin aging and photo damage, hypertrophic scars, wound healing processes and allergic reactions **(Zmudzinska etal., 2008).**

Magnetic resonance image (MRI) is finding an interesting clinical application in evaluating skin tumors because the thickness of skin is small, MRI of the skin demands high resolution and high sensitivity. Recent development in surface coil technology and high field scanners have made MRI useful to study superficial skin structures at high resolution. The application of MRI in dermatology can give a detailed picture of a tumor and its depth of invasion in relation to adjacent anatomic structures **(Moganty etal., 2003).**

MR spectroscopy has been used to differentiate the diseased skin from the normal skin, Recently, Raman spectroscopy has been used for skin lesion detection. FT-Raman spectroscopy is a modern analytical tool and its used for cancer diagnosis will lead to several advantages for the patient as, for example, real time and less invasive diagnosis. The primary objective of this work was to use FT-Raman spectroscopy to detect spectral changes between benign and malignant skin tissue. Those spectral changes can provide important formation about the biochemical ultrations between these two types of tissues **(Lilian etal.,2003).**

Elastic light scattering spectroscopy used to differentiate between malignant and benign skin lesions. The system consists of a UV spectrometer, a single optical fiber probe and a laptop. The single optical fiber probe was used for both delivery and detection of white light to tissue and from tissue. Single optical fiber probe received singly scattered

photons rather than diffused photons in tissue. Therefore, the spectra are correlated with morphological difference of the cells **(Canpolat etal., 2007).**

Elastography was found to distinguish between benign and malignant lesions not by their visible appearance but by measuring their elasticity or stiffness. Since malignancies are stiffer than benign growths, elastography, when added to high-frequency ultrasound imaging of the skin, has potential to improve the accuracy of traditional clinical diagnosis of skin cancers and, in some cases, eliminate unnecessary biopsies of benign skin lesions. The procedure is noninvasive, convenient and inexpensive **(Giovagnorio etal., 1999).**

Simple, safe, and inexpensive x-ray imaging using the mammography technique is the hallmark in diagnosis of arteriolar calcification of patients with calcific uremic arteriolopathy (CUA) **(Wissam etal., 2006).**

Computed tomography (CT) has been useful in staging mycosis fungoidesand which is uncommon primary malignant T cell lymphoma of the skin. And in defining the extent of adenopathy. Typical finding include focal skin thickening due to dermal and epidermal infiltration **(Malloy etal., 1998).**

Aim Of The Work

To determine the role of different image modalities in the diagnosis of some skin lesions including: X-rays, Ultrasonography (US), Elastography, Computed Tomography (CT), Magnetic Resonance Image (MRI) and MR Spectroscopy and other new modalities.

Chapter 1

Anatomy Of The Skin

Anatomy of the skin

The skin covers the entire external surface of the human body and is the principal site of interaction with the surrounding world. It serves as a protective barrier that prevents internal tissues from exposure to trauma, ultraviolet radiation, temperature extremes, toxins, and bacteria. Other important functions include sensory perception, immunologic surveillance, thermoregulation, and control of insensible fluid loss.

The integument consists of 2 mutually dependent layers, the epidermis and dermis, which rest on a fatty subcutaneous layer, the panniculus adiposus. The epidermis is derived primarily from surface ectoderm but is colonized by pigment-containing melanocytes of neural crest origin, antigen-processing Langerhans cells of bone marrow origin, and pressure-sensing Merkel cells of neural crest origin. The dermis is derived primarily from mesoderm and contains collagen, elastic fibers, blood vessels, sensory structures, and fibroblasts **(Carlson, 1998).**

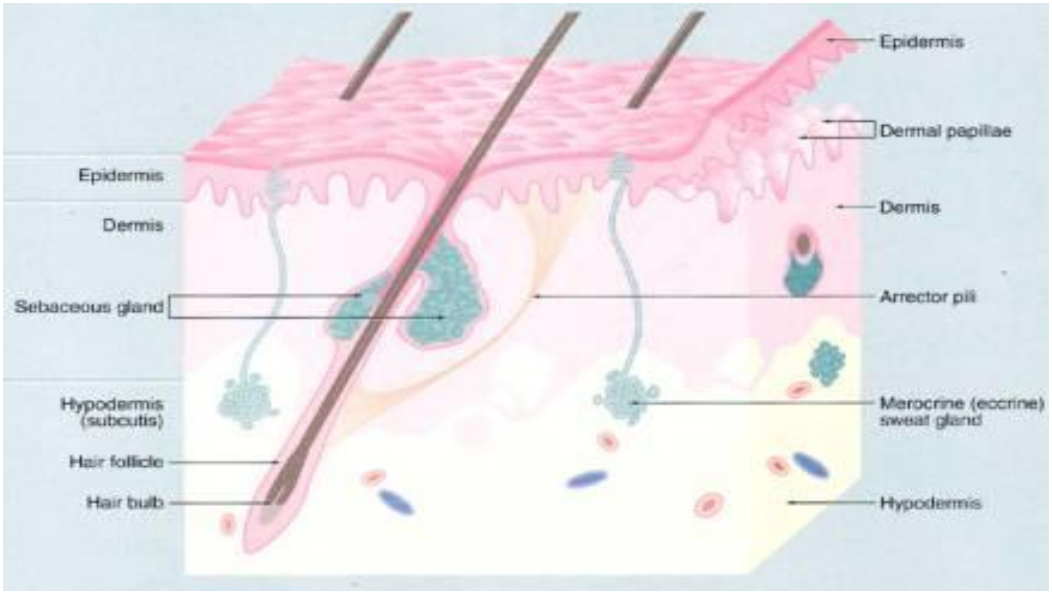

Diagram 1: Layers of the skin **(Wheater 2005).**

During the fourth week of embryologic development, the single cell thick ectodermand underlying mesoderm begin to proliferate and differentiate. The specialized structures formed by the skin, including hair follicles, fingernails, toenails, sebaceous glands, sweat glands, apocrine glands, and mammary glands also begin to appear during this period in development. Teeth, hair, and hair follicles are formed by the epidermis and dermis in concert, while fingernails and toenails are formed by the epidermis alone. Hair follicles, sebaceous glands, sweat glands, apocrine glands, and mammary glands are considered epidermal glands or epidermal appendages, because they develop as downgrowths or diverticula of the epidermis into the dermis .The definitive multi-layered skin is present at birth, but skin is a dynamic organ that undergoes

continuous changes throughout life as outer layers are shed and replaced by inner layers. Skin also varies in thickness among anatomic location, sex, and age of the individual.This varying thickness primarily represents a difference in dermal thickness, as epidermal thickness is rather constant throughout life and from one anatomic location to another **(Moore and Persuad, 1998).**

Skin is thickest on the palms and soles of the feet (1.5 mm thick), while the thinnest skin is found on the eyelids and in the postauricular region (0.05 mm thick). Male skin is characteristically thicker than female skin in all anatomic locations. Children have relatively thin skin, which progressively thickens until the fourth or fifth decade of life when it begins to thin. This thinning is also primarily a dermal change, with loss of elastic fibers, epithelial appendages, and ground substance **(Burns etal., 2004).**

Epidermis:

The epidermis contains no blood vessels and is entirely dependent on the underlying dermis for nutrient delivery and waste disposal via diffusion through the dermoepidermal junction. The epidermis is a stratified squamous epithelium that consists primarily of keratinocytes in progressive stages of differentiation from deeper to more superficial layers. The named layers of the epidermis include the stratum germinativum, stratum spinosum, stratum granulosum, and stratum corneum. The stratum germinativum or the basal layer is immediately superficial to the dermoepidermal junction. This single cell layer of keratinocytes is attached to the basement membrane via hemidesmosomes. As keratinocytes divide and differentiate, they move from this deeper layer to the more superficial layers. Once they reach the stratum corneum, they are fully differentiated keratinocytes devoid of nuclei and are subsequently shed in the process of epidermal turnover. Cells of the stratum corneum are the largest and most abundant of the epidermis. This layer ranges in thickness from 15-100 or more cells depending on anatomic location and is the primary protective barrier from the external environment. Melanocytes, derived from neural crest cells, primarily function to produce a pigment, melanin, which absorbs radiant energy from the sun and protects the skin from the harmful effects of ultraviolet radiation. Melanin accumulates in organelles termed melanosomes that are incorporated into dendrites anchoring the melanosome to the surrounding keratinocytes. Ultimately, the melanosomes are transferred via phagocytosis to the adjacent keratinocytes where they remain as granules. Melanocytes are found in the basal layer of the epidermis as well as in hair follicles, the retina, uveal tract, and leptomeninges. These cells are the sites of origin of melanoma **(Carlson, 1998).**

In areas exposed to the sun, the ratio of melanocytes to keratinocytes is approximately 1:4. In areas not exposed to solar radiation, the ratio may be as small as 1:30. Absolute numbers of melanosomes are the same among the sexes and various races. Differing pigmentation among individuals is related to melanosome size rather than cell number. Sun exposure, melanocyte-stimulating hormone (MSH), adrenocorticotropic hormone (ACTH), estrogens, and progesterones stimulate melanin production. With aging, a decline is observed in the number of melanocytes populating the skin of an individual. Since these cells are of neural crest origin, they have no ability to reproduce. Langerhans cells originate from the bone marrow and are found in the basal, spinous, and granular layers of the epidermis. They serve as antigen-presenting cells. They are capable of ingesting foreign antigens, processing them into small peptide fragments, binding them with major histocompatibility complexes, and subsequently presenting them to lymphocytes for activation of the immune system. An example of activation of this component of the immune system is contact hypersensitivity. Merkel cells, also derived from neural crest cells, are found on the volar aspect of digits, in nail beds, on the genitalia, and in other areas of the skin. These cells are specialized in the perception of light touch **(Carlson, 1998).**

Dermis:

The primary function of the dermis is to sustain and support the epidermis. The dermis is a more complex structure and is composed of 2 layers, the more superficial papillary dermis and the deeper reticular dermis. The papillary dermis is thinner, consisting of loose connective tissue containing capillaries, elastic fibers, reticular fibers, and some collagen. The reticular dermis consists of a thicker layer of dense connective tissue containing larger blood vessels, closely interlaced elastic fibers, and coarse bundles of collagen fibers arranged in layers parallel to the surface. The reticular layer also contains fibroblasts, mast cells, nerve endings, lymphatics, and epidermal appendages. Surrounding the components of the dermis is the gel-like ground substance, composed of mucopolysaccharides (primarily hyaluronic acid), chondroitin sulfates, and glycoproteins. The deep surface of the dermis is highly irregular and borders the subcutaneous layer, the panniculus adiposus, which additionally cushions the skin **(Moore and Persuad, 1998)**.

The fibroblast is the major cell type of the dermis. These cells produce and secrete procollagen and elastic fibers. Procollagen is terminally cleaved by proteolytic enzymes into collagen that aggregates and becomes cross-linked. These tightly cross-linked collagen fibers provide tensile strength and resistance to shear and other mechanical forces. Collagen makes up 70% of the weight of the dermis, primarily Type I (85% of the total collagen) and TypeIII (15% of the total collagen). Elastic fibers constitute less than

1% of the weight of the dermis, but they play an enormous functional role by resisting deformational forces and returning the skin to its resting shape **(Burns etal., 2004)**.

Dermoepidermal Junction:

The dermoepidermal junction is an undulating basement membrane that adheres the epidermis to the dermis. It is composed of 2 layers, the lamina lucida and lamina densa. The lamina lucida is thinner and lies directly beneath the basal layer of epidermal keratinocytes. The thicker lamina densa is in direct contact with the underlying dermis. These structures are the target of immunologic injury in bullous pemphigoid and epidermolysis bullosa. Dermal papillae from the papillary dermis contain a plexus of capillaries and lymphatics oriented perpendicular to the skin surface. These fingerlike projections are surrounded by similar projections of the epidermis. This highly irregular junction greatly increases the surface area over which oxygen, nutrients, and waste products are exchanged between the dermis and the avascular epidermis **(Carlson, 1998)**.

Epidermal Appendages:

Epidermal appendages are intradermal epithelial structures lined with epithelial cells with the potential for division and differentiation. These are important as a source of epithelial cells, which accomplish re-epithelialization should the overlying epidermis be removed or destroyed in situations such as partial thickness burns, abrasions, or split-thickness skin graft harvesting. Epidermal appendages include sebaceous glands, sweat glands, apocrine glands, mammary glands, and hair follicles. They often are found deep within the dermis, and in the face may even lie in the subcutaneous fat beneath the dermis. This accounts for the remarkable ability of the face to re-epithelialize even the deepest cutaneous wounds.

Sebaceous glands:

Sebaceous glands, or holocrine glands, are found over the entire surface of the body except the palms, soles, and dorsum of the feet. They are largest and most concentrated in the face and scalp where they are the sites of origin of acne. The normal function of sebaceous glands is to produce and secrete sebum, a group of complex oils including triglycerides and fatty acid breakdown products, wax esters, squalene, cholesterol esters, and cholesterol. Sebum lubricates the skin to protect against friction and makes it more impervious to moisture.

Sweat glands:

Sweat glands, or eccrine glands, are found over the entire surface of the body except the vermillion border of the lips, external ear canal, the nail beds, labia minora, the glans penis, and the inner aspect of the prepuce. They are most concentrated in the palms and

soles and the axillae. Each gland consists of a coiled secretory intradermal portion that connects to the epidermis via a relatively straight distal duct. The normal function of the sweat gland is to produce sweat, which cools the body by evaporation. The thermoregulatory center in the hypothalamus controls sweat gland activity through sympathetic nerve fibers that innervate the sweat glands. Sweat excretion is triggered when core body temperature reaches or exceeds a set point.

Apocrine glands:

Apocrine glands are similar in structure but not identical to eccrine glands. They are found in the axillae, in the anogenital region, and, as modified glands, in the external ear canal (ceruminous glands), in the eyelid (Moll's glands), and in the breast (mammary glands). They produce odor and do not function prior to puberty, which means they probably serve a vestigial function. The mammary gland is considered a modified and highly specialized type of apocrine gland **(Poblet etal., 2004).**

Hair follicles:

Hair follicles are complex structures formed by the epidermis and dermis. They are found over the entire surface of the body except the soles of the feet, palms, glans penis, clitoris, labia minora, mucocutaneous junction, and portions of the fingers and toes. Sebaceous glands often open into the hair follicle rather than directly onto the skin surface, and the entire complex is termed the pilosebaceous unit. Caucasian hair follicles are oriented obliquely to the skin surface, whereas the hair follicles of black persons are oriented almost parallel to the skin surface. Asian persons have vertically oriented follicles that produce straight hairs.These anatomic variations are an important consideration in avoiding alopecia when making incisions in the scalp. The base of the hair follicle, or hair bulb, lies deep within the dermis and, in the face, may actually lie in the subcutaneous fat. This accounts for the remarkable ability of the face to re-epithelialize even the deepest cutaneous wounds. A band of smooth muscle, the arrector pili, connects the deep portion of the follicle to the superficial dermis.Contraction of this muscle, under control of the sympathetic nervous system, causes the follicle to assume a more vertical orientation **(Prost-Squarcioni , 2006).**

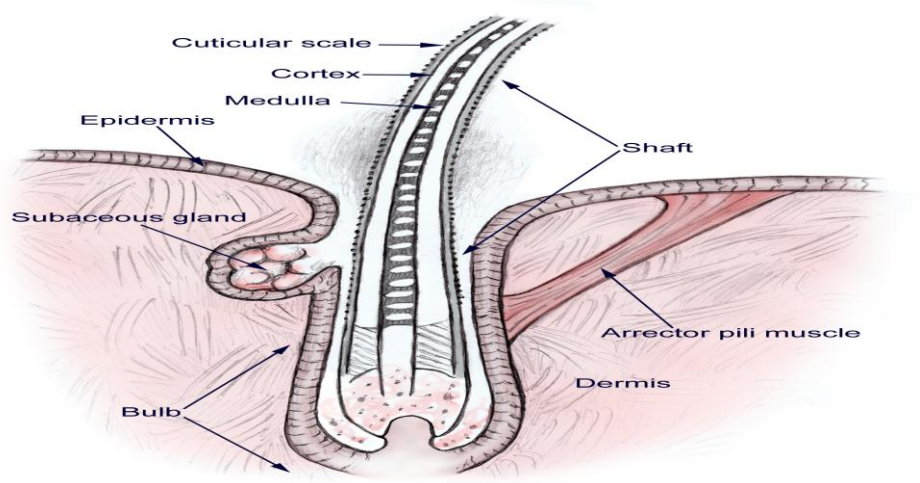

Diagram 2: Anatomy of hair follicle **(Carlson ,1998).**

Anatomy of hair follicle:

Hair growth exhibits a cyclical pattern. The anagen phase is the growth phase, whereas the telogen phase is the resting state. The transition between anagen and telogen is termed the catagen phase. Phases vary in length according to anatomic location, and the length of the anagen phase is proportional to the length of the hair produced. At any one time at an anatomic location, follicles are found in all 3 phases of hair growth. This is extremely important for laser hair removal, because follicles in the anagen phase are susceptible to destruction, whereas resting follicles are more resistant. This explains why multiple treatments of an area may be necessary to ensure adequate hair removal **(Prost-Squarcioni, 2006).**

Blood Supply of the Skin:

Cutaneous vessels ultimately arise from underlying named source vessels. Each source vessel supplies a 3-dimensional vascular territory from bone to skin termed an angiosome. Adjacent angiosomes have vascular connections via reduced caliber (choke) vessels or similar caliber (true) anastomotic vessels.The cutaneous vessels originate either directly from the source arteries (septocutaneous or fasciocutaneous perforators) or as terminal branches of muscular vessels (musculocutaneous perforators) **(Taylor and Pen, 1998).**

During their course to the skin, they travel within or adjacent to the connective tissue framework and supply branches to each tissue with which they come into close contact (bone, muscle, fascia, nerve and fat). They emerge from the deep fascia in the vicinity of the intermuscular or intramuscular septa or near tendons and travel toward the skin, where they form extensive subdermal and dermal plexuses. The dermis contains horizontally arranged superficial and deep plexuses, which are interconnected via communicating

vessels oriented perpendicular to the skin surface. Cutaneous vessels ultimately anastomose with other cutaneous vessels to form a continuous vascular network within the skin. Clinically, this extensive horizontal network of vessels allows for random skin flap survival **(Lamberty and Cormack, 1999).**

In addition to the skin's natural heat conductivity and loss of heat from the evaporation of sweat, convection from cutaneous vessels is a vital component of thermoregulation. Cutaneous blood flow is 10-20 times that required for essential oxygenation and metabolism, and large amounts of heat can be exchanged through the regulation of cutaneous blood flow. The thermoregulatory center in the hypothalamus controls vasoconstriction and vasodilatation of cutaneous vessels through the sympathetic nervous system **(McGregor and Morgan, 2000).**

Lymphatics:

Skin lymphatics parallel the blood supply and function to conserve plasma proteins and scavenge foreign material, antigenic substances, and bacteria. Blind-ended lymphatic capillaries arise within the interstitial spaces of the dermal papillae.These unvalved superficial dermal vessels drain into valved deep dermal and subdermal plexuses. These then coalesce to form larger lymphatic channels, which course through numerous filtering lymph nodes on their way to join the venous circulation near the subclavian vein-internal jugular vein junction bilaterally **(Crockett , 1998).**

Skin Innervation:

Sensory perception is critically important in the avoidance of pressure, mechanical or traumatic forces, and extremes of temperature. Numerous specialized structures are present in the skin to detect various stimuli. As previously mentioned, Merkel cells of the epidermis detect light touch. Meissner corpuscles also detect light touch. These are found in the dermal papillae and are most concentrated in the fingertips. Pacini corpuscles are found deep within the dermis or even in the subcutaneous tissue. These structures are specialized to detect pressure **(Morris and Gibbins, 1997).**

Pain is transmitted through naked nerve endings located in the basal layer of the epidermis. Krause bulbs detect cold, whereas Raffini corpuscles detect heat. Heat, cold, and proprioception also are located in the superficial dermis. Cutaneous nerves follow the route of blood vessels to the skin. The area supplied by a single spinal nerve, or single segment of the spinal cord, is termed a dermatome. Adjacent dermatomes may overlap

considerably, of importance to note when performing field blocks with local anesthesia **(Carlson, 1998).**

Surface Anatomy:

Lines and creases are evident over major and minor joints. Skin contraction produces wrinkles and creases that lie perpendicular to the underlying muscular vector force. Relaxed skin tension lines (RSTL), however, are formed during relaxation and often follow a different direction than age and contracting wrinkles. Relaxed skin tension lines are created by the natural tension on the skin from underlying structures. Papillary ridges on the tips of the digits of the hands and feet and the surface of palms and soles are often used for personal identification. These are also known as friction ridges, since they assist in the ability to grasp **(Fongo etal., 1999).**

Diagram 3: Four main facial lines show the direction of relaxed skin tension lines **(Fongo etal., 1999).**

They are formed during fetal development and are unique to each individual, including identical twins. This distinct pattern does not change with aging. Stratum mucosum composes the outer surface of the ridges with underlying dermal papillae. Sweat pores are usually located at the top of the ridges **(Ashbaugh , 1999).**

Skin Phototype:

The amount of melanin pigment in the skin determines an individual's skin color (skin phototype). Skin pigment can be inherited genetically or acquired by various diseases. Hormonal changes during pregnancy can also vary the amount of pigmentation.

The Fitzpatrick Scale is used to classify skin complexion and response to ultraviolet exposure. This classification is based on a personal history of sun burning and sun tanning.

This classification is used clinically for evaluation of facial skin pigmentation before resurfacing procedures and is important for predicting outcomes and adverse effects **(Goldman etal., 2007).**

Skin Type	Color	Features
I	White or freckled skin	Always burns, never tans
II	White skin	Burns easily, tans poorly
III	Olive skin	Mild burn, gradually tans
IV	Light brown skin	Burns minimally, tans easily
V	Dark brown skin	Rarely burns, tans easily
VI	Black skin	Never burns, always tans

Table 1: The Fitzpatrick Scale **(Goldman etal., 2007).**

Anatomy of Aging Skin:

Age-associated skin changes include thinning, skin laxity, fragility, and wrinkles. Sun-exposed areas demonstrate additional aging changes, including dyspigmentation, premature wrinkling, telangiectasia, and actinic elastosis **(Baumann, 2007).**

Cutaneous aging is characterized by intrinsic and extrinsic processes. Intrinsic or chronologic aging is a genetically determined and inevitable process in skin, which also includes photoprotected skin. Intrinsic aging naturally occurs and is exacerbated by extrinsic aging, which is environmentally induced. Aging at the cellular level is thought to be related to cellular senescence, specifically, the shortening of telomeres (the terminal portions of chromosomes) with each cell cycle **(Rabe etal., 2007).**

Telomere shortening ultimately results in cell-cycle arrest or apoptosis once a critical length is reached. Preventable environmental factors that amplify intrinsic aging include sun exposure and smoking. Long-term UVA radiation exposure accelerates intrinsic aging via the formation of reactive oxygen species (ROS). ROS lead to inflammatory cytokines

and the up-regulation of matrix metalloproteinases, which result in the breakdown of collagen. UVB radiation can also contribute to this aging process by causing direct DNA mutations. Histopathologically, photoaging is manifest as flattening of the dermal-epidermal junction resulting in decreased nutrient transfer between the layers, heliodermatitis or chronic inflammation, elongated and collapsed fibroblasts, disorganized collagen fibrils with overall decrease in collagen levels, and the accumulation of abnormal elastin-containing material termed solar elatosis **(Baumann , 2007).**

Histology Of The Skin

Histology of the skin

The skin is the heaviest single organ of the body, accounting for about 16% of total body weight; it is composed of the epidermis, an epithelial layer of ectodermal origin, and the dermis, layer of connective tissue of mesodermal origin. Based on the comparative thickness of the epidermis, thick and thin skin can be distinguished.

The junction of dermis and epidermis is irregular, and projections of the dermis called papillae interdigitate with evaginations of the epidermis known as epidermal ridges. In three dimensions these interdigitations may be of the peg -and –socket variety (Thin skin) or formed of ridges and grooves (thick skin). Epidermal derivatives include hair, nail, and sebaceous and sweat glands. Beneath the dermis lies the hypodermis or subcutaneous tissue, a loose connective tissue that may contain a pad of adipose cells, the panniculus adiposus. The hypodermis, which is not considered part of the skin, binds skin loosely to the subjacent tissues and corresponds to the superficial fascia of gross anatomy **(Wheater etal., 2005).**

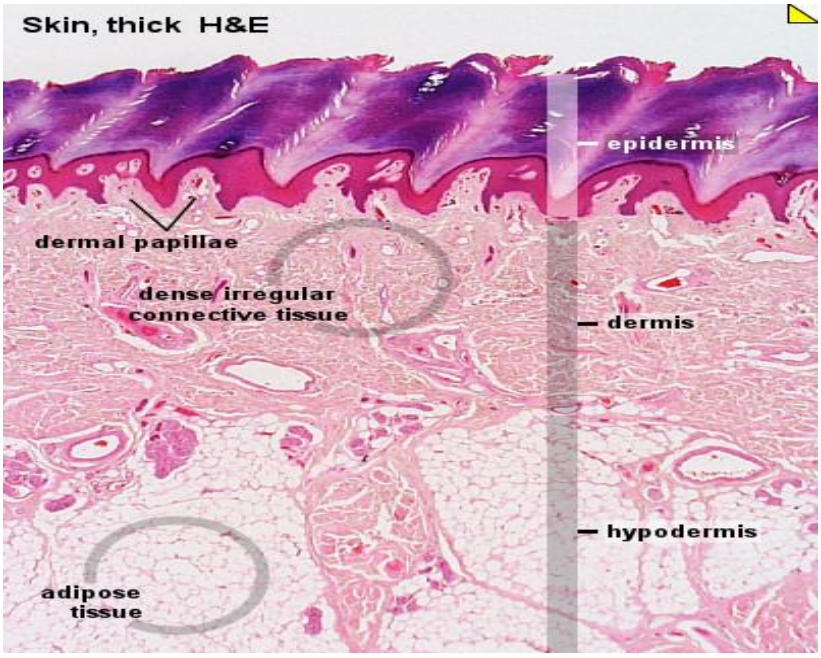

Figure 1: Layers of the skin **(Wheater, 2005).**

Epidermis:

The epidermis consists mainly of a stratified squamous keratinized epithelium, but it also contains three less abundant cell types; Melanocytes, Langerhans cells, and Merkel's cells. The keratinizing epidermal cells are called keratinocytes. The designations thick and thin refer to the thickness of the epidermal layer, which varies between 75 and 150nm for thin skin and 600nm for thick skin. Total skin thickness (epidermal plus dermis) also varies according to site. For example, skin on the back is

about 4mm thick, whereas that of the scalp is about 1.5mm thick.. From the dermis outward, the epidermis consists of five layers of keratin-producing cells (keratinocytes) **(Schwartz, 2002).**

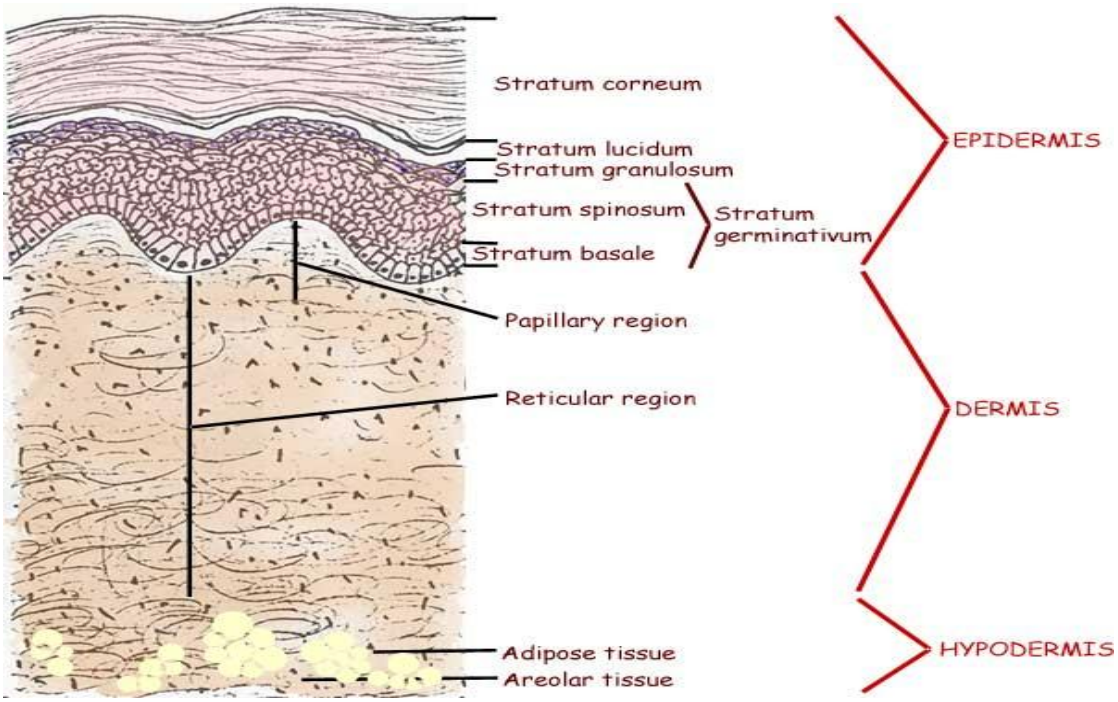

Diagram 4: Layers of epidermis **(Wheater , 2005).**

Stratum Basale (Stratum Germinativum):

It consists of a single layer of basophilic columnar or cuboidal cells resting on the basement membrane at the dermal-epidermal junction. Desmosom bind the cells of this layer together in their upper and lateral surface. All cells in the stratum basale contain intermediate keratin filaments about 10nm in diameter. As the number of filaments increases until they represent half the total protein in the stratum corneum.

Stratum Spinosum:

It consists of cuboidal, or slightly flattened, cells with central nucleus and cytoplasm whose processes are filled with bundle of keratin filaments. These keratin bundles, visible under the light microscope, are called tonofilaments, they end at and insert into the cytoplasmic densities of the desmosome. The filament plays an important role in maintaining cohesion among cells and resisting the effect of abrasion.

Stratum Granulosum

It consists of three to five layers of flattened polygonal cells whose cytoplasm is filled with coarse basophilic granules called keratohylin granules. Another characteristic

structure in the cells of the granular layer of the epidermis that can be seen with the electron microscope is the membrane coated lamellar granule, a small (0.1-0.3nm) ovoid or rod like structure containing lamellar disc that are formed by lipid bilayers. These granules fuse with the cell membrane and discharge their content into the intra cellular spaces of the stratum granulosum, where they are deposit in the form of sheets containing lipid. The function of this extruded material is similar to that of intracellular cement in that it acts as a barrier to penetration by foreign materials and provides a very important sealing effect in the skin.

Stratum Lucidum:

More apparent in thick skin, the stratum lucidumis a translucent, thin layer of extremely flattened eosinophilic epidermal cells. The organelles and nuclei are no longer evident, and the cytoplasm consists primarily of densely packed keratin filaments embedded in an electron-dense matrix. Desmosomes are still evident between adjacent cells

Stratum corneum:

It consist of 15-20 layers of flattened non nucleated keratinized cells whose cytoplasm is filled with a birefringent filamentous scleroprotein, keratin contains at least six different polypeptides with molecular mass ranging from 40to70 kDa. The composition of tonofilaments changes as epidermal cells differentiate **(Lodish etal.,2003).**

Melanocytes:

The color of the skin is the result of several factors, the most important of which are its content of melanin and carotene, the number of blood vessels in the dermis, and the color of blood flowing in them. Eumelanin is a dark brown pigment produce by the melanocyte, specialized cell of the epidermis found beneath or between the cells of the stratum basale and in the hair follicles.

The electron microscopic reveals a pale-staining cell containing numerous small mitochondria, a well-developed Golgi complex, and short cisternae of rough endoplasmic reticulum. Although melanocytes are not attached to the adjacent keratinocytes by desmosome, they are bound to the basal lamina by hemidesmosomes **(Wheater etal., 2005).**

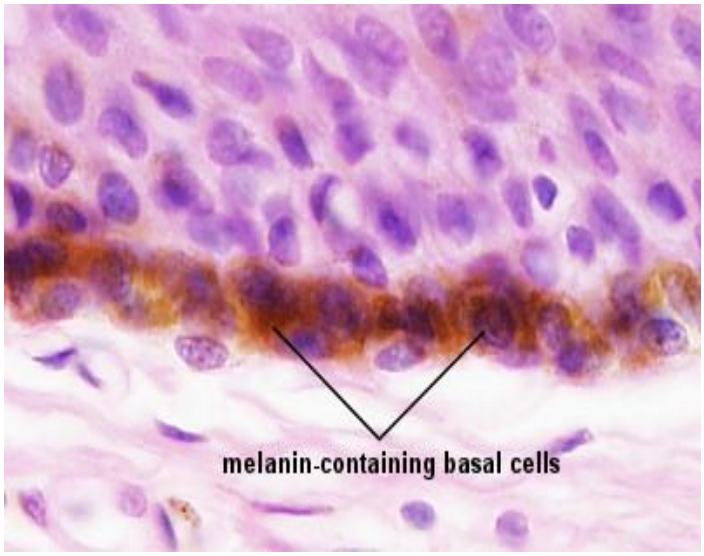

Figure 2: Melanocytes attachment **(Wheater, 2005).**

Langerhans cells:

Star shaped cells found mainly in the stratum spaniousum of the epidermis, represent 2-8 % of the epidermal cells. They are bone marrow derivative, carried to the skin by the blood, and capable in binding, processing, and present antigen the T lymphocytes, thus participating in the stimulation of these cells. Consequently, they have a significant role in immunological skin reactions. Langerhans cells are antigen-presenting cells **(Winklelmann , 1999).**

Figure 3: Langerhans cells **(Wheater, 2005).**

Merkel's cells:

Generally presenting in the thick skin of palms and soles, somewhat resemble the epidermal epithelial cells but have small dense granules in their cytoplasm. The composition of these granules is not known. Free nerves ending that form an expanded terminal disc are present at the base of Merkel's cells.

These cells can serve as mechanoreceptor, although other evidence suggests that they have function related to the diffuse neuroendocrine system **(Winklelmann , 1999).**

Immunological activity in the skin:

Because of the large size of the skin, the skin has impressive number of lymphocytes and antigen-presenting cells (Langerhans cells), and because of its location it is with close contact to many antigenic molecules. For this reason, the epidermis has important role in some types of immune responses. Most lymphocytes found in the skin are "homed" in the epidermis **(Edelson etal., 1999).**

Dermis:

The dermis is the connective tissue that supported the epidermis and binds it to the subcutaneous tissue (hypodermis). The thickness of the dermis varies according to the region of the body and reaches its maximum of 4mm on the back **(Wheater etal., 2005).**

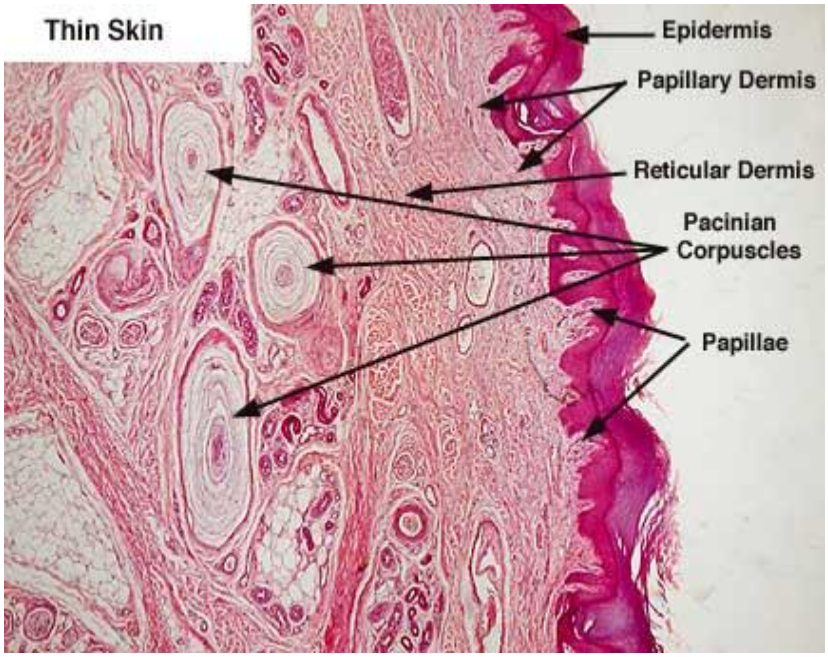

Figure 4: Layers of dermis **(Wheater, 2005).**

The surface of the dermis is very irregular and has many projections (dermal papillae) that interdigitate with projections (epidermal pegs or ridges) of the epidermis. A basal lamina is always found between the stratum germinativum and the papillary layer of the dermis and follow the contour of the interdigitations between these layers. Underlying the basal lamina is a delicate net of reticular fibers, the lamina reticularis. This composite structure is called the basement membrane and can be seen with

the light microscope. The dermis contains two layers with rather indistinct boundaries, the outermost papillary layer and the deeper reticular layer **(Schwartz, 2002).**

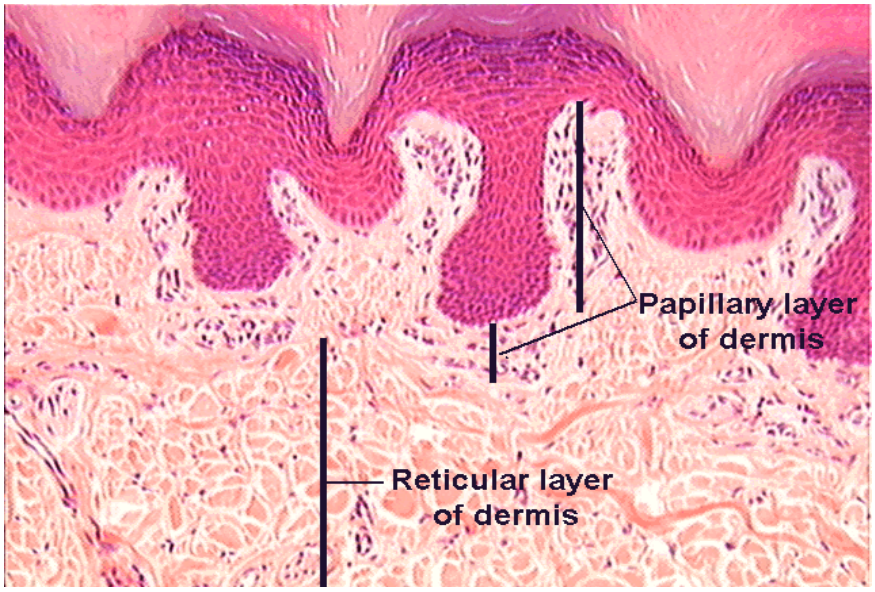

Figure 5: Papillary and reticular layers of dermis **(Wheater, 2005).**

The thin papillary layer is composed of loose connective tissue, fibroblast and other connective tissue cells, such as mast cells and macrophages, are present. Extravasated leukocytes are also seen.The papillary layer is so called because it constitutes the major part of dermal papillaea. From this layer, special collagen fibrils insert in the basal lamina and extend to the dermis .They Bind the dermis to the epidermis and are called anchoring fibril.

The reticular layer is thicker, composed of irregular dense connective tissue (mainly type 1 collagen), and therefore has more fibers and fewer cells than dose the papillary layer. The dermis contains a network of fibers of the elastic system, with the thicker fibers characteristically found in the reticular layer **(Wheater etal., 2005).**

Subcutaneous tissues:

It consists of loose connective tissue that bind the skin loosely to the subjacent organs, making it possible for the skin to slid over them. The hypodermis often contains fat cells that vary in number according to the area of the body and vary in size according to nutritional status. This layer is also referred to as superficial fascia and, where thick enough, the panniculus adipose. The connective tissue of the skin contains a rich network of blood and lymphatic vessels **(Lodish etal., 2003).**

Skin blood vessels system:

The arterial vessels that nourish the skin form two plexuses. One is located between the papillary and reticular layers; the other is located between the dermis and the subcutaneous tissue. Thin branches leave these plexuses and vascularize the dermal papillae. Each papilla has only one arterial ascending branch and one venous descending branch.

Veins are dispose in three plexuses, two in position described for arterial vessels and the third in the middle of the dermis. Arteriovenous anastomoses with glomera are frequent in the skin, participating on the regulation of body temperature.

Lymphatic vessels begin as closed sacs in the papillae of the dermis and converge to form two plexuses, as described for the arterial vessels **(Schwartz, 2002).**

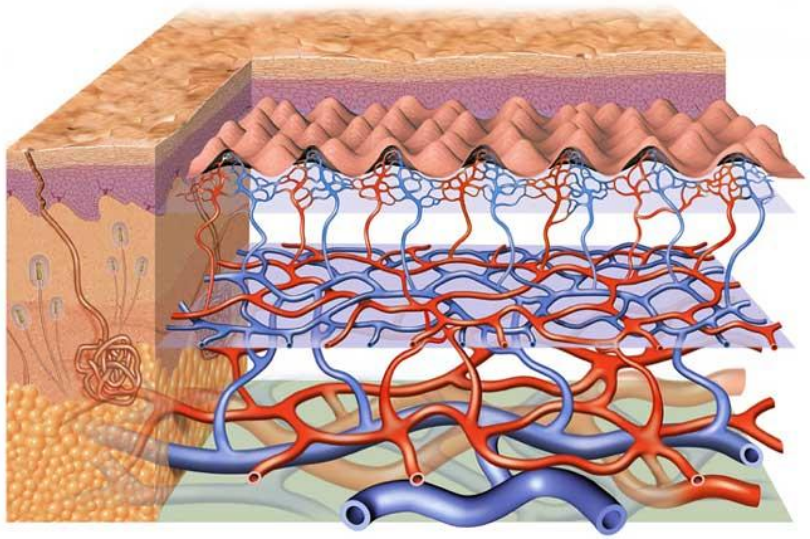

Diagram 5: Skin blood vessels network **(Wheater, 2005).**

Nerve supply of the skin:

There is a rich supply of nerve in the dermis, and the effectors nerves to the skin are postganglionic fibers of sympathetic ganglia of the para vertebral chain. No parasympathetic innervations are present. The afferent nerve ending form a superficial dermal network with free nerve endings, a hair follicle network, and the innervations of encapsulated sensory organ. Free nerve endings are sensitive to touch-pressure (pressure is sustained touch), tactile reception, high and low temperature, pain, itching, and other sensations. The expanding ending includes the Ruffini endings, and the encapsulating endings include the Vater-pacini, Meissner, and Krause corpuscles **(Lodish etal., 2003).**

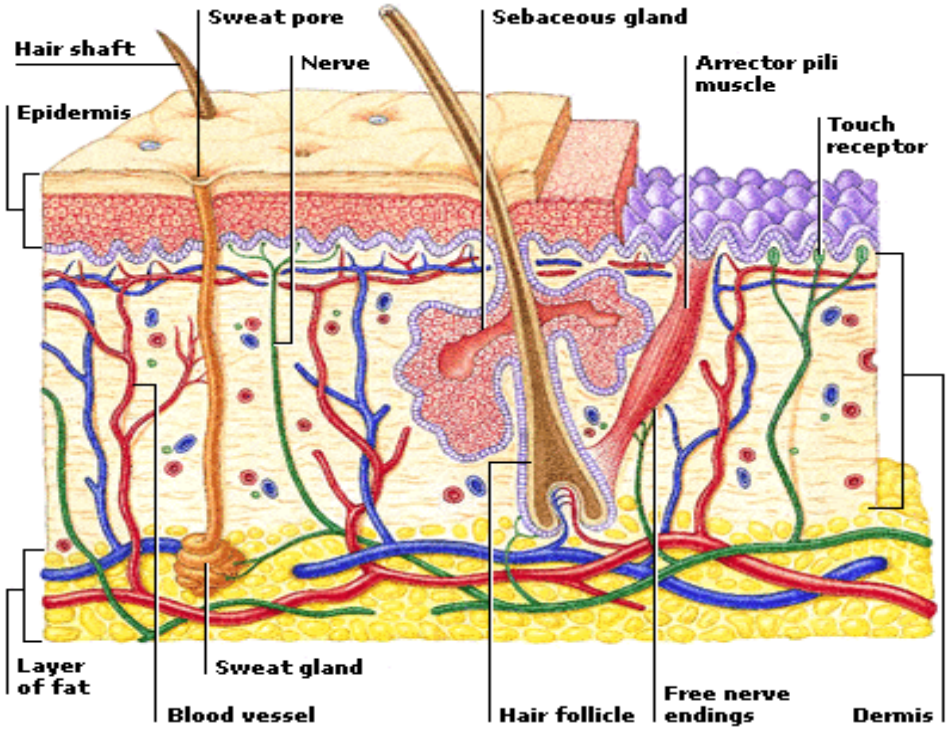

Diagram 6: Free nerve ending of the skin **(Wheater, 2005).**

Hairs:

Are elongated keratinized structures derived from invagination of dermal epithelium. Hair grows discontinuously and have periods of growth followed by periods of rest.

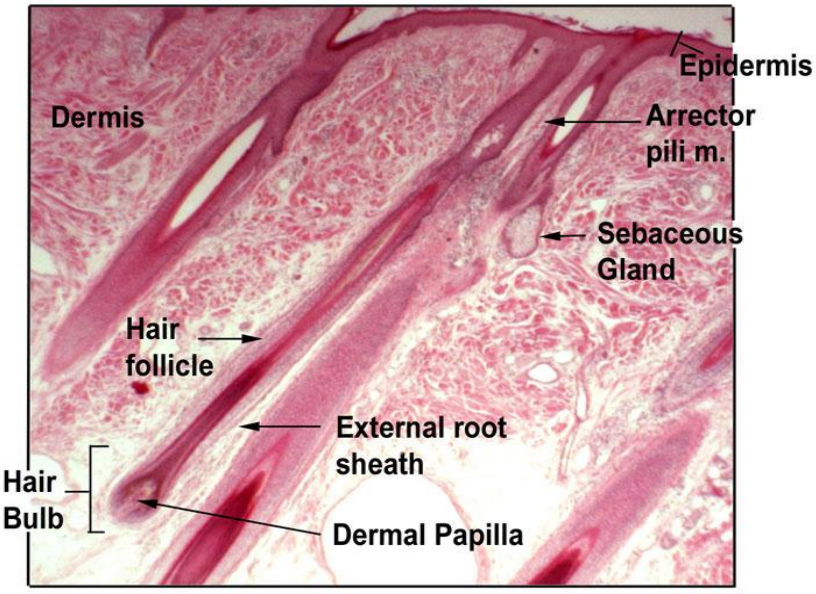

Figure 6: Hair follicle **(Wheater's, 2005).**

Each hair arises from an epidermal invagination, the hair follicle that during its growth period has a terminal dilatation called a hair bulb. At the base of the hair bulb, a dermal papilla can be observed. That contains a capillary network that is vital in sustaining the hair follicle. The epidermal cells covering this dermal papilla form the hair root that produces and is continuous with the hair shift, which protruded beyond the skin.

During periods of growth, the epithelial cells that make up the hair bulb are equivalent to those in the stratum germinativum of the skin. In certain types of thick hairs, the cells of the central region of the root at the apex of the dermal papillae produce large, vacuolated, and moderately keratinized cells that form the medulla of the hair. Root cells multiply and differentiate into heavily keratinized, compactly grouped fusiform cells that form the hair cortex.

The outermost cells give rise to the internal root sheath. The external root sheath is a continuous with epidermal cells and, near the surface, shows all the layers of epidermis. **(Wheater etal., 2005).**

Nails

Nails are plate of keratinized epithelial cells on the dorsal surface of each distal phalanx. The proximal part of the nail, hidden in the nail groove, is the nail root. The epithelium of the fold of skin covering the nail root consists of the usual layers of cells. The stratum corneum of this epithelium forms the eponychium, or cuticle. The nail plate, which corresponds to the stratum corneum of the skin, rests of the epidermis called the nail. Only the stratum basale and the stratum spinosum are present in the nail bed. Nail plate epithelium arises from the nail matrix. The proximal end of the matrix extended deep to the nail root. Cells of the matrix divide, move distally, and eventually cornify, forming the proximal part of the nail plate. The nail plate then slides forward over the nail bed (which forms no contribution to the formation of the plate). The distal end of the plate becomes free of the nail bed and is worn away or cut off **(Lodish etal., 2003).**

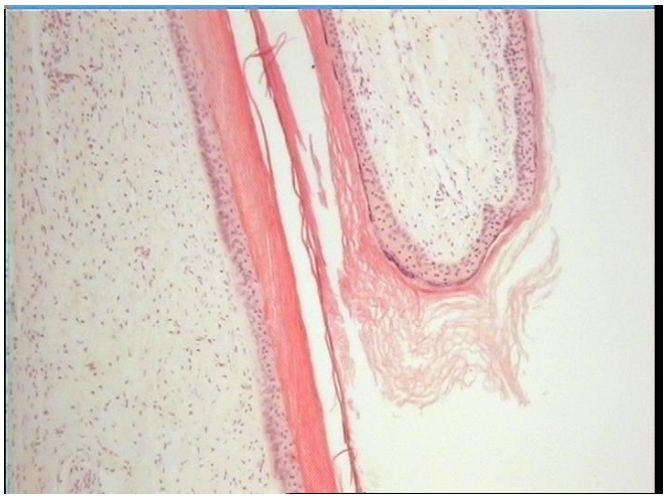

Figure 7: Nail eponychium **(Wheater, 2005).**

Glands of the skin:

Sebaceous gland:

Sebaceous glands, which not found in the glabrous skin in the palms and soles, are acinar glands that usually have several acini opening into a short duct. This duct is usually ends in the upper portion of the hair follicle. The acini consist of a basal layer of undifferentiated flattened epithelial cells that rests in the basal lamina. These cells are proliferating and differentiate, filling the acini with rounded cells containing increasing amounts of fat droplets in their cytoplasm. Their nuclei gradually shrink, and the cells simultaneously become filled with fat droplets and burst. The product of this process is sebum, the secretion of the sebaceous gland, which is gradually moved to the surface of the skin **(Wheater etal., 2002).**

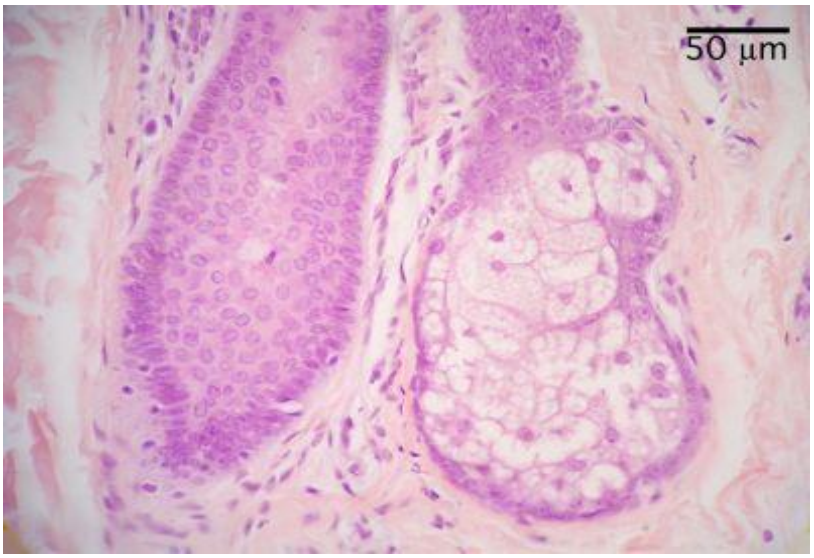

Figure 8: Sebaceous gland **(Wheater, 2005).**

Sweat gland:

Sweat glands are wildly distributed in the skin except certain regions, such as the glans penis. The merocrine sweat glands are simple, coiled tubular glands what ducts open. The secretory part of the gland is embedded in the dermis, it measure approximately 0.4mm in diameter and is surrounded by myoepithelial cells. Contraction of these cells helps to discharge the secretion.

Two types of cells have been described in the secretory portion of the sweat glands. Dark cells are pyramidal cells that line most of the luminal surface of this portion of the gland. Their basal surface does not touches the basal lamina. Secretory granules containing glycoproteins are abundant in their apical cytoplasm. Clear cells are devoid of secretory granules. Their basal plasmalemma has the numerous invaginations characteristic of cells involved in transepithelial salt and fluid transport. The ducts of these glands are lined with stratified cuboidal epithelium.

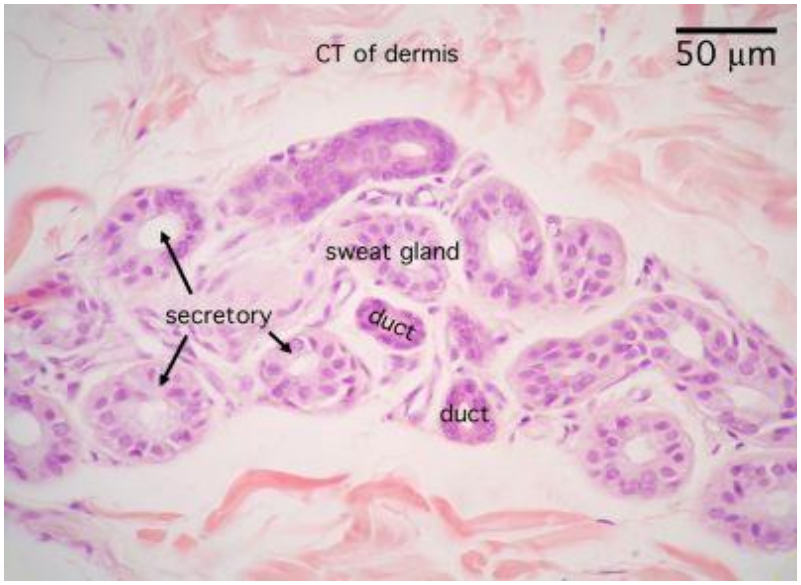

Figure 9: Merocrine sweat gland **(Wheater, 2005).**

In the additional of merocrine sweat glands, another type of sweat gland apocrine glands are present in the axillary, areolar, and anal regions.That are larger (3-5 mm in diameter) than merocrine sweat glands. They are embedded in the dermis and hypodermis, and their duct open into hair follicles. Apocrine glands are innervated by adrenergic nerve ending, whereas merocrine glands receive cholinergic fibers **(Lodish etal., 2003).**

Pathology Of Skin Lesions

The pathology of the skin lesions that diagnosed radio logically:

1- Psoriasis.

٢-Malignant melanoma.

3- Squamous cell carcinoma.

4- Basal cell carcinoma.

٥- Subcutaneous abscess.

٦-Seborrheic keratosis.

٧-Pigmented nevi.

Pathology of some skin lesions

Disorders affecting the skin are extremely common and range from the relatively innocuous viral warts to life threatening malignant melanomas. Many skin lesions are external manifestations of a systemic disease, such as systemic lupus erytheromatosus and acquired immunodeficiency syndrome (AIDS) (e.g., Kaposi's sarcoma).

Pathology of skin disease that can be diagnosed radiologically:

Psoriasis

Psoriasis is a common chronic inflammatory dermatosis that sometimes associated with arthritis, myopathy, enteropathy, spondylitic heart disease.

Figure 10: Downward elongation of the rete ridges **(Josef etal., 2003).**

Clinical picture:

The patient complains of scaly lesions that most frequently affects the skin of the elbows, knees, scalp, lumbosacral areas, intergluteal cleft, and glans penis **(Korte etal., 2004)**.

Macroscopic picture:

The most typical lesion a well demarcated, pink to salmon colored plaque covered by loosely adherent scales that are characteristically silver - white in color with underlying erythema. Nail changes occur in 30% of cases of psoriasis and consist of yellow brown discoloration (often linked to an oil slick), with pitting, separation of the nail plate from the underlying bed (onycholysis), thickening, and crumbling. In the rare variant called pustule arpsoriasis, multiple small pustules form an erythematous plaque **(Josef etal., 2003)**.

Figure 11: Macroscopic picture of psoriasis. Plaque psoriasis is raised, roughened, and covered with white or silver scale with underlying erythema **(Jason etal.,1998).**

Microscopic picture:

There is increase epidermal cell turnover resulting in marked epidermal thickening (acanthosis), with regular downward elongation of the rete ridges.

The stratum granulosum is thinned or absent, and extensive overlying parakeratotic scale is seen.

Typical of psoriatic plaques is the thinning of the portion of the epidermal cell layer that overlies the tips of dermal papillae (suprapapillary plates) and dilated, tortuous blood vessels within these papillae. These blood vessels bleed readily when the plaque is lifted, given rise to multiple minute bleeding points (**Auspitz's sign**). Neutrophils form small aggregates within slightly spongiotic foci of the superficial epidermis(**spongiform pustules**) and within the parakeratotic stratum corneum(Munro's microabcesses) **(Krueger and Bowcock, 2005).**

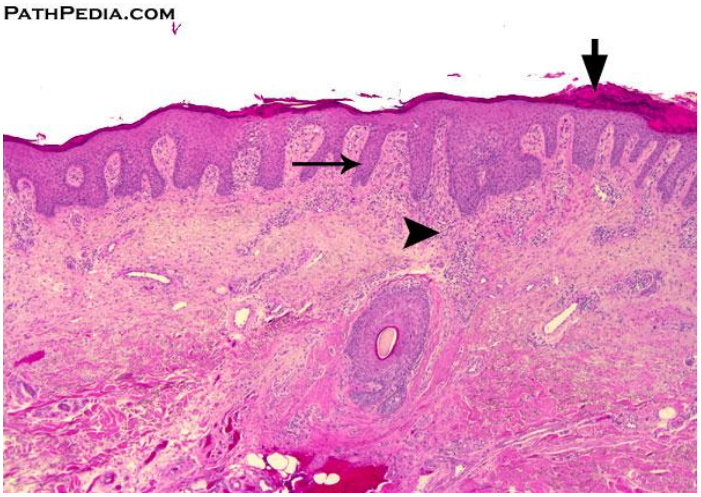

Figure 12: Downward elongation of the rete ridges **(Josef et al., 2003).**

Malignant Melanoma (MM):

Malignant melanoma is a neoplasm of melanocytes or of the cells that develop from melanocytes. Although melanoma was once considered an uncommon disease, the annual incidence has increased dramatically over the last few decades, as have deaths from melanoma. Prognosis of a melanoma lesion can be predicted based on the following: The depth of invasion, presence or absence of ulceration and to nodal status at diagnosis **(Kantor etal., 2009).**

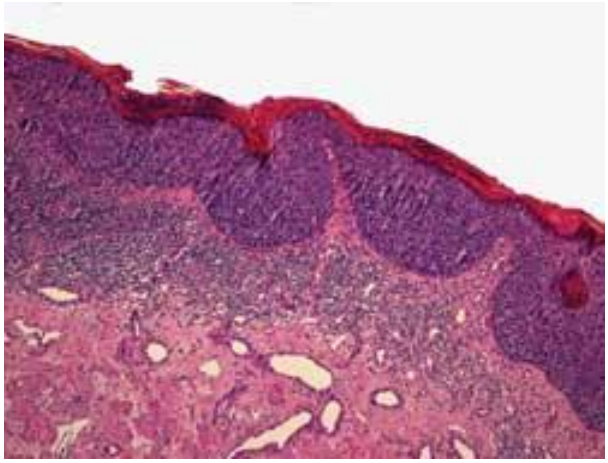

Figure 13: Malignant melanoma **(Josef etal., 2003).**

Clinical picture:

Malignant melanoma of the skin is usually asymptomatic**,** although itching may be an early manifestation. Reported skin lesions as many as eight or more in number with changes in its size, color, or symmetry with bleeding or ulceration **(Schuchter etal., 2000)**

Risk factors:

(1) History of previous sun exposure, including severe sunburns in childhood. Or exposure to ultraviolet radiation.

(2) Presence of family history of melanoma, skin cancer, or multiple nevus syndromes **(Gould Rothberg etal., 2009)**.

(3) Previous history of melanoma.

(4) Lightly pigmented individuals are at high risk for the development of melanoma than are darkly pigmented individuals **(Sabel and wong, 2009).**

Age

Melanoma may occur at any age, although children younger than 10 years rarely develop a de novo melanoma. The average age at diagnosis is 57 years, and up to 75% of patients are younger than 70 years. Melanoma is the most common malignancy in women aged 25-29 years and accounts for more than 7000 deaths annually. It is commonly found in patients younger than 55 years, and it accounts for the third highest number of lives lost across all cancers **(Kantor and Kantor, 2009).**

Macroscopic picture:

Melanoma lesion more likely to be asymmetric lesions, with irregular borders, very dark black or blue in color and more than 6 mm in diameter. Present sometime with ulceration. Melanomas may develop in or near a previously existing precursor lesion or in healthy-appearing skin. A malignant melanoma developing in healthy skin is said to arise de novo, without evidence of a precursor lesion **(Rigel and Carucci, 2000).**

Many of these melanomas are induced by solar irradiation. The greatest risk of sun exposure–induced melanoma is associated with acute, intense, and intermittent blistering sunburns. This risk is different than that of squamous and basal cell skin cancers, which are associated with prolonged, long-term sun exposure **(Schuchter etal., 2000).**

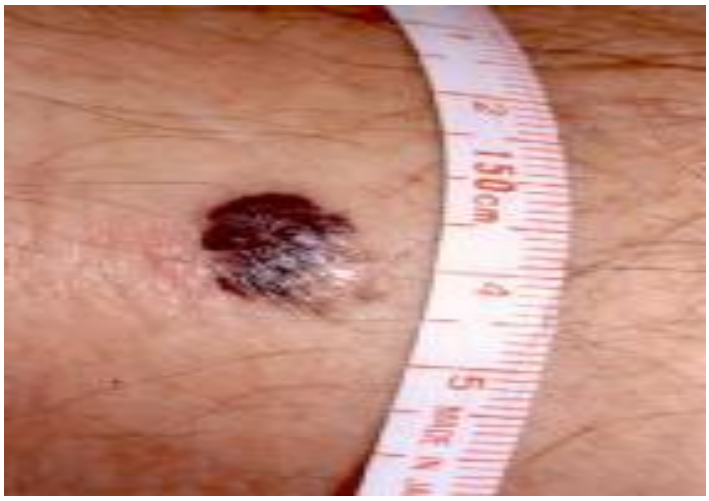

Figure 14: Macroscopic picture of malignant melanoma. A 1.5-cm melanoma with characteristic asymmetry, irregular borders, and color variation **(Bernard etal., 2008).**

Figure 15: Macroscopic picture of malignant melanoma **(Bernard etal., 2008).**

Figure 16: Macroscopic picture of lentigo malignant melanoma **(Bernard etal., 2008).**

Sites of melanoma:

Melanoma occurs in unexposed areas of the skin, including the palms, soles, and perineum. Certain lesions are considered to be precursor lesions of melanoma, including the common acquired nevus, dysplastic nevus, congenital nevus, and cellular blue nevus. Other sites include the eyes, mucosa, gastrointestinal tract, genitourinary tract and leptomeninges. Metastatic melanoma with an unknown primary site may be found in lymph nodes only **(Kantor and Kantor, 2009).**

Microscopic picture:

Melanomas originate from melanocytes, which arise from the neural crest and migrate to the epidermis, uvea, meninges, and ectodermal mucosa. The melanocytes, which reside in the skin and produce a protective melanin, are contained within the basal layer of the epidermis, at the junction of the dermis and epidermis.

Individual melanoma cells are usually considerably larger than the nevus cells. They contain large nuclei with irregular contours, having chromatin characteristically clumped at the periphery of the nuclear membrane and prominent red (eosinophilic) nucleoli. These cells proliferate as poorly formed nest or as individual cells at all levels of the epidermis. In the radial phase of growth and, in the dermis, as expansil, balloon-like nodules in the vertical phase of growth.

Melanomas have 2 growth phases, radial and vertical. During the radial growth phase, malignant cells grow in a radial fashion in the epidermis. With time, most melanomas progress to the vertical growth phase, in which the malignant cells invade the dermis and develop the ability to metastasize **(Anderson ,2000).**

Many genes are implicated in the development of melanoma, including ***CDKN2A (p16), CDK4, RB1, CDKN2A (p19), PTEN/MMAC1,*** **and** ***ras. CDKN2A (p16)*** appears to be especially important in both sporadic and hereditary melanomas. This tumor suppressor gene is located on band 9p21, and its mutation plays a role in various cancers **(Gould etal., 2009).**

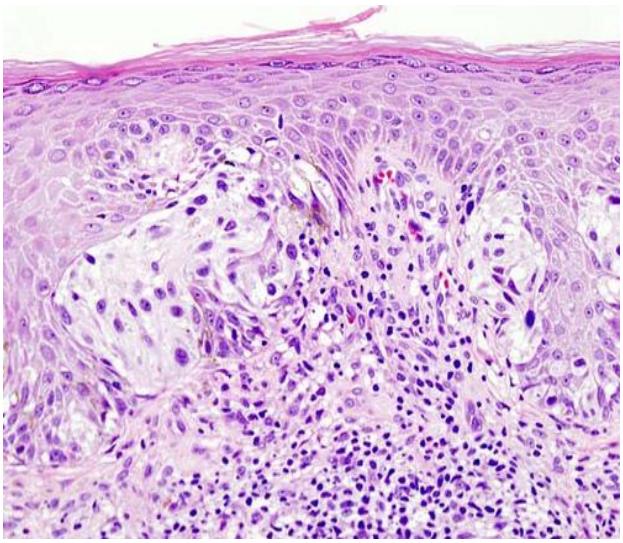

Figure 17: Dysplastic melanocytic cells **(Josef etal., 2003).**

Five different forms or histological types of melanoma exist, as follows:

Superficial spreading melanomas:

Approximately 70% of cutaneous malignant melanomas are the superficial spreading melanoma (SSMs) type and often arise from a pigmented dysplastic nevus. SSMs typically develop after a long-standing stable nevus changes; typical changes

include ulceration, enlargement, or color changes. A SSM may be found on any body surface, especially the head, neck, and trunk of males and the lower extremities of females.

Nodular melanomas:

Nodular melanomas (NMs) represent approximately 10-15% of melanomas and also are found commonly on all body surfaces, especially the trunk of males. These lesions are the most symmetrical and uniform of the melanomas and are dark brown or black in color. The radial growth phase may not be evident in NMs; however, if this phase is evident, it is short-lived because the tumor advances rapidly to the vertical growth phase, thus making the NM a high-risk lesion. Approximately 5% of all NMs are amelanotic melanomas.

Figure 18: Nodular melanoma **(Josef et al., 2003).**

Lentigo maligna melanomas:

Lentigo maligna melanomas (LMMs) also account for 10-15% of melanomas. They typically are found on sun-exposed areas (e.g., hand, neck). LMMs may have areas of hypopigmentation and often are quite large. LMMs arise from a lentigo maligna recursor lesion.

Acral lentiginous melanomas:

Acral lentiginous melanomas (ALMs) are the only melanomas that have an equal frequency among blacks and whites. They occur on the palms, soles, and subungual areas. Subungual melanomas often are mistaken for subungual hematomas (splinter hemorrhages). Like NM, ALM is extremely aggressive, with rapid progression from the radial to vertical growth phase.

Mucosal lentiginous melanomas:

Mucosal lentiginous melanomas (MLMs) develop from the mucosal epithelium that lines the respiratory, gastrointestinal, and genitourinary tracts. These lesions account for approximately 3% of the melanomas diagnosed annually and may occur on any

mucosal surface, including the conjunctiva, oral cavity, esophagus, vagina, female urethra, penis, and anus. Noncutaneous melanomas commonly are diagnosed in patients of advanced age. MLMs appear to have a more aggressive course than cutaneous melanomas, although this may be because they commonly are diagnosed at a later stage of disease than the more readily apparent cutaneous melanoma **(Balch etal., 2001).**

Stages of malignant melanoma:

Clinically, lesions are classified as thin if they are 1 mm or less in depth; moderate if 1-4 mm; and thick if less than 4 mm in depth. According to TNM classification **a**s T is the thickness of the lesion, N is the presence of lymph node and M is the presence of the metastasis.

StageIA

Lesions less than or equal to 1 mm thick with no evidence of ulceration or metastases (T1aN0M0) are associated with a 5-year survival rate of 95 %.

StageIB

Lesions less than or equal to 1 mm thick with ulceration noted but without lymph node involvement (T1bN0M0) or lesions 1.01-2 mm thick without ulceration or lymph node involvement (T2aN0M0) are associated with a 5-year survival rate of approximately 91%.

StageIIA

Melanomas greater than 1 mm but less than 2.01 mm in thickness with no evidence of metastases but with evidence of ulceration (T2bN0M0) or lesions 2.01-4.0 mm without ulceration or lymph node involvement (T3aN0M0) are associated with an overall 5-year survival rate of 77-79%.

StageIIB

Melanomas 2.01-4 mm thick with ulceration but no lymph node involvement (T3bN0M0) or lesions greater than 4 mm without ulceration or lymph node involvement (T4aN0M0) are associated with a 5-year survival rate of 63-67 %.

StageIIC

Lesions greater than 4 mm with ulceration but no lymph node involvements (T4bN0M0) are associated with a 5-year survival rate of 45 %.

StageIIIA

Patients with any depth lesion, no ulceration and 1 positive (micrometastatic) lymph node (T1-4a, N1a, M0) have a 5-year survival rate of 70%. T1-4a, N2a, M0

lesions (any depth lesion, no ulceration but 2-3 nodes positive for micrometastasis) are associated with a 5-year survival rate of 63%.

StageIIIB

Patients with any depth lesion, positive ulceration and 1 lymph node positive for micrometastasis (T1-4b,N1a,M0) or 2-3 nodes positive for micrometastasis (T1-4b,N2a,M0) have a 5-year survival rate of 50-53%. Patients with any depth lesion, no ulceration and 1 lymph node positive for macrometastasis (T1-4a,N1b,M0) or 2-3 nodes positive for macrometastasis (T1-4a,N2b,M0) have a 5-year survival rate of 46-59% .

StageIIIC

Patients with any depth lesion, positive ulceration and 1 lymph node positive for macrometastasis (T1-4b,N1b,M0) or 2-3 nodes positive for macrometastasis (T1-4b,N2b,M0) or 4 or more metastatic lymph nodes, matted lymph nodes, or in transit met(s)/satellite(s) have a 5-year survival rate of 24-29%.

StageIV

Melanoma metastatic to skin, subcutaneous tissue, or lymph nodes with normal LDH (M1a) is associated with a 5-year survival rate of 19%. M1b disease (metastatic disease to lungs with normal LDH) has a 5-year survival rate of 7%. M1c disease (metastatic disease to all other visceral organs and normal LDH or any distant disease with elevated LDH) is associated with a 5-year survival rate of 10 % **(Xing etal., 2010)**.

Squamous Cell Carcinoma (SCC):

It is the second most common tumor arising on sun-exposed sites in older people, exceeded only by basal cell carcinoma.

Clinical picture:

SCC that has not invaded through the basement membrane of the dermoepidermal junction termed (in situ carcinoma). Appear as sharply defined, red, scaling plaque.

Invasive lesions are nodular show keratin production appreciated clinically as hyperkeratosis, and may ulcerate. Well differentiated lesions may be indistinguishable

from keratoacanthoma.When the oral mucosa is involved, a zone of white thickening may be seen and referred clinically as leukoplakia **(Bale and Yu, 2000).**

Risk factor:

(1) Exposure to sunlight is the major predisposing factor. With subsequent DNA damage.

(2) Industrial carcinogens (tars and oil).

(3) Chronic ulcer and draining osteomylitis.

(4) Old burn scar.

(5) Ingestion of areseicals, and ionizing radiation.

Macroscopic picture:

It starts as a small nodule in the epithelium which grows and infiltrates the underlying tissue then takes one of the following patterns:

(A) Polypoid or fungating carcinoma: this form a large outward growth with an Infiltrating base.

(B) Infiltrating carcinoma: in which the malignant tissues infiltrates more to deeper structures.

(C) Ulcerative carcinoma: (malignant ulcer) it is the commonest type which either arises as such from the beginning or develops on top of one of the above two types.

It appears as a large ulcer with raised everted edges, fixed indurated base and a necrotic floor **(Josef etal., 2003).**

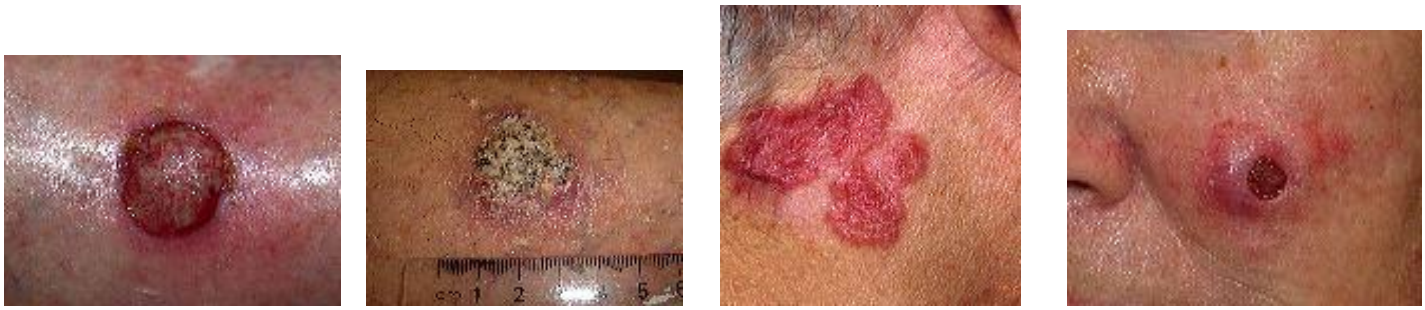

Figure 19: Macroscopic picture of different images of squamous cell carcinoma in different parts of the body **(Bernard etal., 2008).**

Microscopic picture:

There is infiltration of sub epithelial tissue by large polygonal cells arranged in solid masses of variable size and shape which are separated by dense fibrous stroma.The malignant cells have abundant esinophilic cytoplasm and large rounded darkly stained nuclei.In some masse, the cells in the central area are replaced by structure less lamellae of keratin stained brightly red with eosin. This occurs in differentiated groups and called (cell nest).

The degree of differentiation of SCC depends on the numbers of groups with the cell nest appearance. In less differentiated tumors, cell nests are few in numbers and the malignant cells show more marked anaplasia **(Bale etal., 2000).**

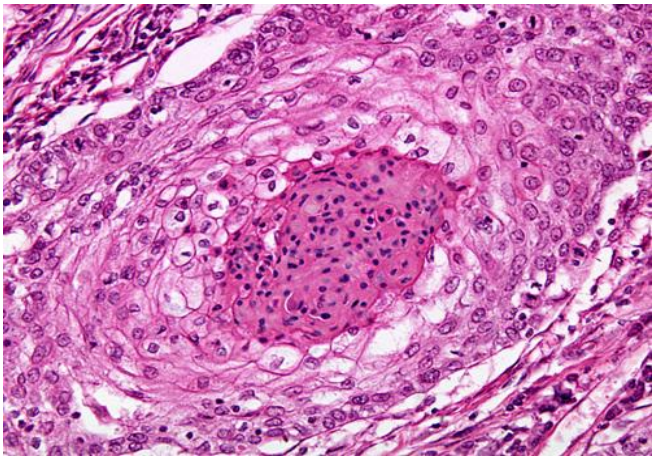

Figure 20 Squamous cell carcinoma **(Josef et al., 2003).**

Broder's classification is used in SCC and depends on the number of cell groups with the cell nest appearance:

Grad 1: 75-100% keratinized groups i.e. well differentiated SCC.

Grad 11: 50-75% keratinized groups.

Grad 111:25-50% keratinized groups.

Grad 1V:0-25% keratinized groups. i.e. undifferentiated SCC. **(Bale etal., 2000).**

Basal Cell Carcinoma (BCC):

Basal cell carcinomas are common, slow growing tumors that rarely metastasized. They have a tendency to occur at sites subject to chronic sun exposure (the face and the neck) and in lightly pigmented people.

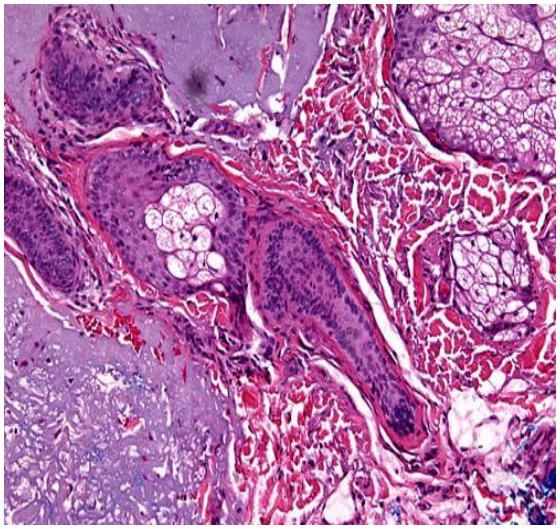

Figure 21: Basal cell carcinoma **(Josef etal., 2003).**

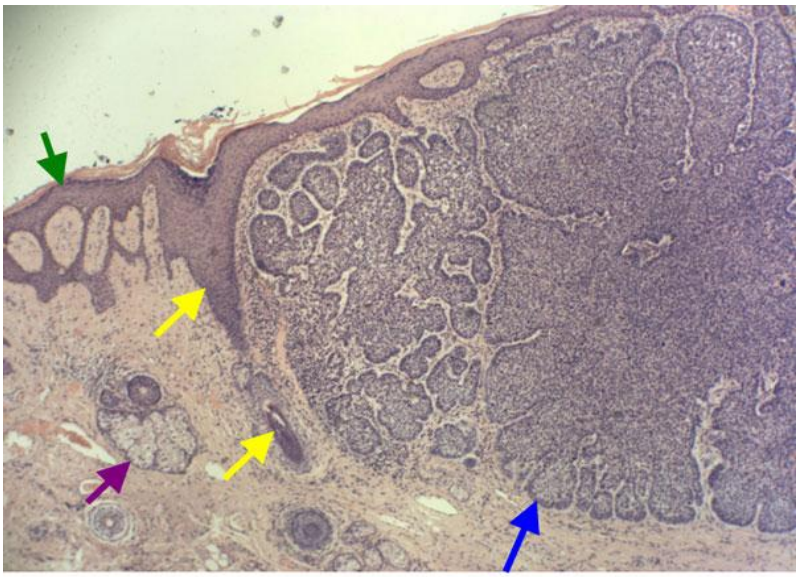

Normal Vs Cancerous skin.
The green arrow: Normal skin;
Yellow arrows: hair shaft (upper) and follicle (lower);
Purple arrow: Sweat gland near hair follicle;
Blue arrow: Basal cell skin cancer

Figure 22: Basal cell carcinoma

(Josef etal., 2003).

The incidence of BCC rises sharply with imunosupression and in patients with inherited defects in DNA repair **(e.g., xeroderma pigmentosum).**

Clinical picture:

These tumors present clinically as pearly papules often containing prominent, dilated sub epidermal blood vessels (telangiectasias). Nodule ulcerates latter forming (Rodent Ulcer).

Macroscopic picture:

It arises as small firm nodule, gradually increases in size and ulcerates forming an irregular ulcer with rolled- in beaded edges, fixed indurated base and necrotic floor.

The ulcer may show healing at one edge and extension and erosion at the other edge. Secondary pyogenic infection is common **(Rubin etal., 2005).**

Figure 23: Macroscopic picture of nodular basal cell carcinoma appearing as a waxy, translucent papule with central depression and a few small erosions **(Bernard etal., 2008).**

Figure 24: Macroscopic picture of superficial basal cell carcinoma .Scale, erythema, and a threadlike raised border are present in this superficial basal cell carcinoma on the trunk **(Bernard etal., 2008).**

-

Figure 25: Macroscopic picture of Large superficial basal cell carcinoma **(Bernard etal., 2008).**

Figure 26: Macroscopic picture of nodular basal cell carcinoma .This translucent pink papule has telangiectases and a crusted erosion, characteristic of nodular basal cell carcinoma **(Bernard etal., 2008).**

Microscopic picture:

The dermis is infiltrated by masses of malignant epithelial cells variable in size and shape. The cells take a blue Hematoxyline stain specially the outer cell layer where the cells are columnar and parallel "palisade arrangement".

The inner cells are polyhedral and rounded. The cells show malignant features with loose myoxiod stroma. Masses are retracted from surrounding stroma. The tumor may change to basosquamous or squamous cell carcinoma **(Betti etal., 2009).**

Subcutaneous Abscess:

A localized suppurative inflammation characterized by formation of cavity containing pus Caused by staphylococcus infection.

Clinical picture:

Swelling with fever, throbbing pain, loss of appetite and loss of function of the organ.

Macroscopic picture:

A swelling which is red, hot, painful with loss of the function. The pus is characterized by thick creamy fluid, alkaline in reaction, yellow in color, odorless, and don't clot on standing **(Stevens etal., 2005).**

Microscopic picture and pathogenesis:

Pyogenic bacterial and toxins cause central area of necrosis surrounded by acute inflammatory cells mainly polymorphs and dilated congested blood vessels. So, Abscess is formed now of two zones, central necrosis and peripheral acute inflammation which sometime called (pyogenic membrane) **(Ghoneim etal., 1998).**

Larger numbers of leucocytes are attracted by chemotactic substances to the inflamed area. Many PNL die and transformed to pus cells that secrete liquefying enzymes to liquefy the necrotic tissue which is at first separated from the surrounding tissue and is known as slough, then necrotic tissue become completely liquefied.

So, abscess now is formed of three zones (central necrosis, mid zone of pus and peripheral zone of acute inflammation).Osmotic pressure inside abscess increase due to digestion and liquefaction of necrotic materials which split larger particles to smaller one. So fluid is absorbed from the surrounding tissue, increase tension inside the abscess cavity causing throbbing pain **(Brook and Fraizer, 2000).**

Seborrheic Keratosis(SK):

Seborrheic keratoses are the most common benign tumor in older individuals. It have variety of clinical appearances, and they develop from the proliferation of epidermal cells. Although no specific etiologic factors have been identified, they occur more frequently in sunlight- exposed areas **(Ginarte etal., 2000).**

Clinical picture:

Seborrheic keratoses usually are asymptomatic, but they can be an annoyance. Lesions can itch and rub or catch on clothing, thereby becoming inflamed. Lesions often are unattractive and serve as negative psychological connotations daily reminders of aging **(Tindall and Smith, 1998).**

Patients are sometimes concerned that these enlarging lesions are malignant. Sometimes a person may have many seborrheic keratoses and not notice a dysplastic nevus or a malignant melanoma that develops among the seborrheic keratoses **(Nakagawa etal., 1996).**

A significant danger can arise if a person does not detect a malignant melanoma at an early stage. Although lesions may resolve on occasion, spontaneous resolution does not ordinarily occur **(Cascajo etal., 1996).**

The sign of Lesser-Trélat is the association of multiple eruptive seborrheic keratoses with internal malignancy. Most commonly, the sign is observed with adenocarcinoma, especially of the gastrointestinal tract; however, an eruption of seborrheic keratoses may develop after an inflammatory dermatosis (e.g. eczema, severe sunburn) **(Sperry and Wall, 1998).**

Macroscopic picture:

SK usually begins with the appearance of one or more sharply defined, light brown, flat macules. The lesions may be sparse or numerous. As they initially grow, they develop A velvety to finely verrucous surface, followed by an uneven warty surface with multiple plugged follicles and a dull or lackluster appearance. They typically have an appearance of being stuck on the skin surface.

The color of the lesions can vary from pale brown with pink tones to dark brown or black. Their natural history includes slow enlargement with increasing thickness and the gradual development of new lesions **(Verhagen etal., 1999).**

A familial trait exists for the development of multiple seborrheic keratoses in about half of the patients, with an autosomal dominant mode of inheritance **(Shimizu etal., 1996).**

Seborrheic keratoses can occur on almost any site of the body, with the exception of the palms and soles and mucous membranes **(Verhagen etal.,1999).**

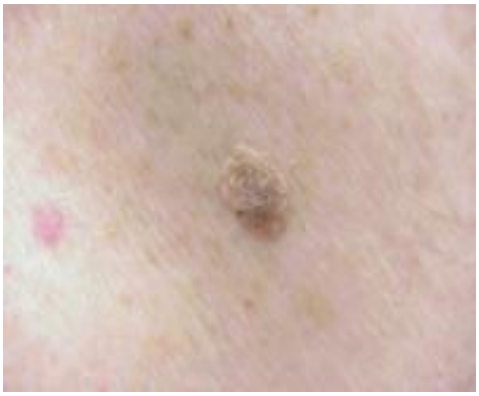

Figure 27: Macroscopic picture of Sharply circumscribed elevated seborrheic keratoses **(Jason etal.,1998).**

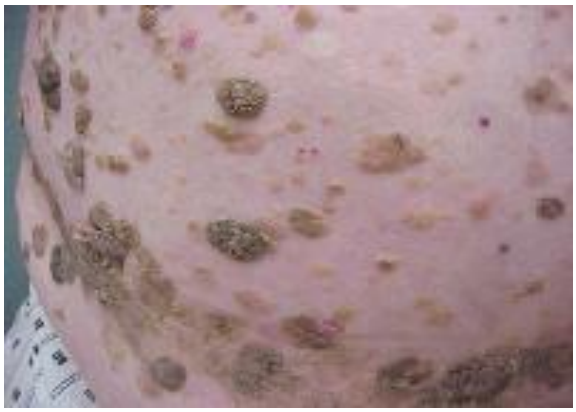

Figure 28: Macroscopic picture of multiple seborrheic keratoses in an autosomally dominant mode of inheritance **(Jason etal.,1998).**

Microscopic picture:

The etiology of the development of a seborrheic keratosis is not known. SK exhibit histologic evidence of proliferation. Increased cell replication has been demonstrated in SK with bromodeoxyuridine incorporation studies and immunohistochemistry for proliferation-associated antigens. A moderate increase is observed in the rates of apoptosis in all varieties of SK compared to normal skin **(Eads etal., 1997).**

Seborrheic keratoses are usually found on sun-exposed skin, and the reticulated type of seborrheic keratoses may develop from solar lentigines. Epidermal growth factors or their receptors have been implicated in the development of seborrheic keratoses **(Groves etal., 1998).**

No difference was observed in the expression of immunoreactive growth hormone receptors in keratinocytes from normal epidermis and keratinocytes from seborrheic keratoses. The expression of *BCL2*, an apoptosis-suppressing oncogene, is low in seborrheic keratosis in contrast to the high values in basal cell and squamous cell carcinoma **(Shimizu etal., 1996).**

No increase is observed in the sonic hedgehog signal transducers patched (ptc) and smoothened (smo) messenger RNA (mRNA) in seborrheic keratosis over normal skin **(Tojo etal.,1999).**

A high frequency of mutations in the gene encoding the tyrosine kinase receptor FGFR3 (fibroblast growth factor receptor 3) has been found in certain types of seborrheic keratoses. This may the first clue into the genetic basis for the pathogenesis of seborrheic keratoses.

FGFR3 belongs to a class of transmembrane tyrosine kinase receptors involved in signal transduction to regulate cell growth, differentiation, and migration, as well as wound healing and angiogenesis. Upon ligand binding, FGFR3 dimerizes, which, in turn, induces phosphorylation of the kinase domain.

Activating mutations in FGFR3 have been found in approximately 40% of hyperkeratotic seborrheic keratoses, 40% of acanthotic seborrheic keratoses, and 85% of adenoid seborrheic keratoses **(Hafner etal., 2007).**

Seborrheic keratoses have a varying degree of pigmentation. In pigmented seborrheic keratoses, the proliferating keratinocytes trigger the activation of neighboring melanocytes by secreting melanocyte-stimulating cytokines **(Nindl etal., 1997).**

Endothelin-1 has dual stimulatory effects on DNA synthesis and melanization of human melanocytes and has been implicated as playing a part in the hyperpigmentation observed in seborrheic keratoses **(Teraki etal., 1996).**

Immunohistochemically, the keratinocytes of seborrheic keratoses express low molecular weight keratin but often exhibit a partial lack of the high molecular weight forms of keratin **(Eads etal., 1997).**

Pigmented nevi (PN):

PN are benign neoplasm or hamartomas composed of melanocytes, the pigment-producing cells that constitutively colonize the epidermis.

Melanocytes are derived from the neural crest and migrate during embryogenesis to selected ectodermal sites (primarily the skin and the CNS), but also to the eyes and the ears. Octopi melanocytes have been identified at autopsy in the gastrointestinal and genitourinary tracts.

Congenital pigmented nevi are thought to represent an anomaly in embryogenesis and, as such, could be considered, at least in a sense, malformations or hamartomas. In contrast, most acquired melanocytic nevi are considered benign neoplasm **(DeDavid etal., 1997).**

Clinical picture:

PN are common lesions that can be found on the integument of almost all individuals. Some patients present with few lesions, while others have hundreds. The number on a given individual increases in rough proportion to the degree of skin pigmentation.

The lesions often asymptomatic, and when the lesion has become symptomatic (e.g. itchy, painful, irritated, or bleeding) is considered an important indicator of potential malignant change **(Palicka etal., 2010).**

Macroscopic picture:

PN can be broadly divided into congenital and acquired types. Determining if a lesion is congenital or acquired is generally easily accomplished by direct query of the patient, although, some small congenital PN are tardive and may be perceived by the patient as acquired **(Tran etal., 2008).**

Not all PN that change are malignant, especially if change is noted in a person younger than 40 years. However, change that is perceptible over a short time is an indicator of potential malignancy and designates a lesion deserving of biopsy. Acquired PN are typically less than a centimeter in diameter and evenly colored **(Mooi.1999).**

PN most commonly are tan to brown, but coloration can be variable, ranging from skin-colored (nonpigmented) to jet black. The deep pigmentation associated with dark PN often stems from associated intracorneal pigmentation. The spectrum of "hypermelanotic" melanocytic nevus includes lesions with heavy epidermal pigmentation **(Tran etal., 2008).**

Congenital pigmented nevi vary considerably in size and are commonly classified as small (<1 cm), intermediate (1-3 cm), or large/giant (>3 cm). Congenital pigmented nevi are generally relatively evenly pigmented and tan or brown, especially those that are thin.

In some congenital nevi, the cells extend from the level of the epidermis to the subcutaneous fat. These lesions can have an array of colors, and, at times, they cannot be easily distinguished from melanoma based solely on findings from the clinical evaluation.

Congenital pigmented nevi are hamartomalike; that is, they contain a predominance of melanocytes but also seem to have simultaneous accentuation of other cutaneous elements. Thus, an increase in the number of hair follicles, the presence of follicles of increased size, or an increase in other appendages may be observed **(DeDavid etal., 1997).**

Conventional or common acquired pigmented nevi are generally less than 1 cm in diameter and evenly pigmented. Some atypical melanocytic nevi (melanocytic nevus of the so-called Clark or dysplastic type) exceed 1 cm in size, especially when such lesions occur on the trunk **(Gallagher and Mclean, 1995).**

Junctional pigmented nevi are macular or thinly papular. Junctional lesions typically range from brown to brownish-black. The darker coloration of junctional pigmented nevi stems from the fact that the surface epidermis is often simultaneously hyperpigmented **(Sagebiel 1997).**

Compound and intradermal pigmented nevi display elevation relative to surrounding uninvolved skin. Compound pigmented nevi are often lighter in color than junctional nevi and range from tan to light brown. Some compound pigmented nevi have areas of dark pigmentation, particularly those that have been recently irritated or

traumatized. Many wholly intradermal pigmented nevi display no significant pigmentation **(Ackerman and Milde, 1998).**

The development of a new area of pigmentation within a long-standing non pigmented or lightly pigmented compound or intradermal pigmented nevus, is a cause for concern. While pigmentary changes could be due to incidental inflammation or recent irritation or trauma, the possibility of evolving melanoma is also a consideration in the differential diagnosis. Generally, a biopsy for microscopic examination is warranted in this conte **(Shea and Prieto, 1999).**

Dysplastic or atypical nevi (also known as Clark nevi) are acquired variants that are relatively flat, thinly papular, and relatively broad. Often, such lesions exhibit target-like or fried egg–like morphology, as noted above, with a central papular zone and a macular surrounding area with differing pigmentation **(Ko etal., 2009).**

Dysplastic nevi often occur in a familial fashion. Affected individuals may present with dozens or hundreds of such lesions. Almost invariably, individuals with dysplastic nevi are of northern European ancestry from the United Kingdom, the Netherlands, Germany, or, occasionally, Poland or RussMost of these individuals have fair skin and other Celtic features. Some individuals have only a few atypical nevi, and their risk of melanoma may not be much higher than persons without such nevi **(Ackerman etal., 1998).**

Persons with large numbers of nevi (>100) have a high lifetime risk of melanoma that approaches unity. Persons with large numbers of nevi and a familial history of melanoma (consisting of $\geq$2 members of the primary family with melanoma) have an extremely high risk of developing melanoma and deserve vigilant clinical monitoring **(Harrison etal., 1999).**

Dysplastic nevi generally grow through lateral extension of the intraepiderm component of the lesion; therefore, these lesions often assume the clinical configuration of a fried egg, with a central papular zone and a surrounding macular area of differing pigmentation. The peripheral border is often perceived as blurred or fuzzy because of this lateral extension of superficial melanocytes.

Some authorities have postulated that Clark (dysplastic) nevi are sufficient or common precursors to melanoma. The designation dysplastic was chosen to suggest

that these lesions represent an intermediate (unstable) form between conventional nevi and melanoma **(Ackerman etal., 1998).**

This concept remains controversial. They may represent precursor lesions, markers for an increased risk of de novo melanoma, or both. Some data suggest that most melanomas in patients with the dysplastic nevus syndrome occurs de novo **(James etal., 2005**).

While the removal of all dysplastic nevi from an individual with melanoma is generally not indicated, removal of lesions with a highly atypical appearance is indicated to be certain that melanoma is not present **(Lazova etal., 2000).**

Spitz nevi vary considerably in size, but they generally are smaller than 1 cm in diameter. Many Spitz nevi have a keratosis like quality because of associated epidermal hyperplasia and hyperkeratosis, and some have an angiomalike appearance because of associated vascular ectasia.

The degree of pigmentation of Spitz nevi also varies; a heavily pigmented, small, spindle cell variant on the legs of women has been referred to as "pigmented spindle cell nevus" or "Reed nevus" because the pigmented spindle cell variant was described by Richard Reed **(Cesinaro etal., 2005).**

Blue nevi are not always blue, and they are not even always pigmented. The designation blue nevus, although flawed, has been preserved for historical reasons. Blue nevi are sometimes larger than other melanocytic nevi, occasionally measuring

2 cm or greater in diameter. This is particularly true of cellular lesions (cellular blue nevi) that occur at sun-protected sites, such as the buttocks.

Blue nevi are often firm because of associated stromal sclerosis, and they often have a nodular quality, a reflection of their deeper position within the skin. Heavily pigmented blue nevi manifest clinically as blue, black, or gray lesions, whereas blue nevi with lesser degrees of pigmentation may be tan or brown or strictly the color of surrounding healthy skin.

Hypocellular blue nevi that cover an extensive clinical distribution have been referred to as "dermal melanocytic hamartomas" by some authors. This spectrum includes the entities nevus of Ito, nevus of Ota, and nevus of Sun **(Murali etal., 2009)**.

Figure 29: Macroscopic picture of A Clark (dysplastic) nevus with modest variation in pigmentation and irregular borders. Biopsy of the lesion proved no evidence of melanoma **(Jason etal.,1998).**

Figure 30: Macroscopic picture of A compound Clark (dysplastic) nevus with fried egg–like clinical morphology, with a central dark papule flanked by an eccentric more lightly pigmented macular zone **(Jason etal.,1998).**

Figure 31: Macroscopic picture of a heavily pigmented junctional Spitz nevus, also known as pigmented spindle cell nevus. Note that many Spitz nevi are nonpigmented and may have an angioma like clinical appearance **(Jason etal.,1998).**

Microscopic picture:

Melanocytes are present in the basal layer of the epidermis and exhibit a certain degree of territoriality. Non-neoplastic melanocytes typically exhibit contact inhibition to each other, and thus pigment cells are usually not found as contiguous cells. With certain forms of stimulation, such as the exogenous administration of ultraviolet irradiation, the density of melanocytes in normal epithelium may increase. Normal melanocytes may also involve adnexal epithelium, most notably the bulbs of follicular papillae.

PN represent proliferations of melanocytes that are in contact with each other, forming small collections of cells known as nests **(Shea etal., 1999).**

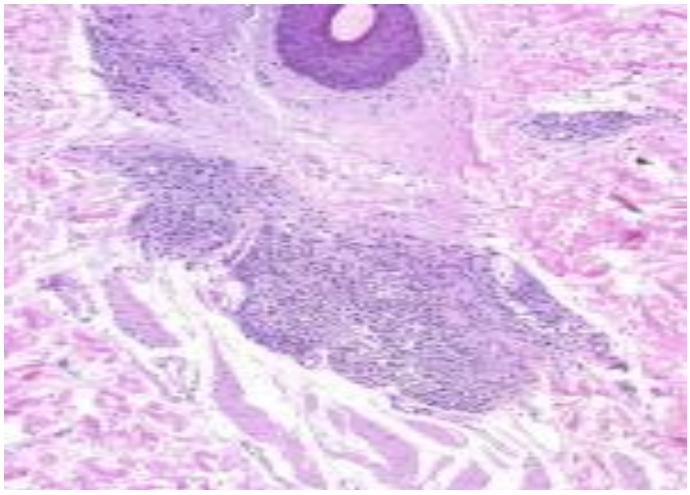

Figure 32: Congenital nevus **(Josef etal., 2003).**

Histopathologically, a congenital nevus differs from an acquired pigmented nevus in that melanocytes are often distributed deeply within the reticular dermis, within the adventitial dermis around adnexal elements, and sometimes within the subcutis. This congenital nevus shows a folliculocentric array of melanocytes **(DeDavid etal., 1997).**

Conventional (ordinary or common acquired) pigmented nevi develop as a proliferation of single melanocytes along the dermoepidermal junction. As the melanocytes proliferate, small nests of cells develop in the lower-most part of the

epidermis, and the resultant Lesion is termed a junctional pigmented nevus. With continued proliferation, nests persevere along the junction, but they can also be found within the superficial dermis, a configuration termed compound pigmented nevus. As a nevus ages, the junctional component often diminishes or entirely involutes. The resultant nevus is termed an intradermal pigmented nevus **(Sagebiel, 1997).**

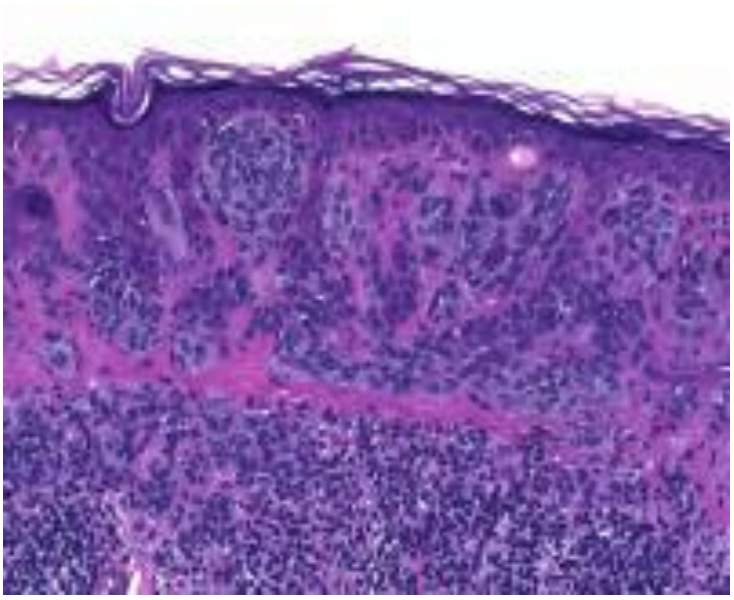

Figure 33: Conventional compound pigmented nevus **(Josef etal., 2003).**

A conventional compound pigmented nevus. Note the presence of melanocytes with small nuclei in nests along the dermoepidermal junction and the presence of similar melanocytes in nests and syncytia in the subjacent dermis **(Ackerman etal., 1999).**

Congenital pigmented nevi are similar to their acquired counterparts in that junctional, compound, and intradermal patterns can be seen. Most congenital nevi extend well into the dermis, with melanocytes positioned in the interstitial dermis between collagen bundles **(DeDavid etal., 1997).**

The depth of extension into the dermis is variable. Some large congenital nevi exhibit cells that extend into subcutaneous septa. Congenital pigmented nevi with melanocytes. Confined to the upper half of the reticular dermis has been termed superficial congenital

nevi. Lesions of this type are typically smaller than 2 cm in overall diameter **(Lazova etal., 2000).**

Spitz nevi, shown below, are virtually always acquired pigmented nevi, and they can exhibit a microscopic pattern that is junctional, compound, or wholly intradermal. Like all benign nevi, Spitz nevi tend to be relatively small and symmetrical and laterally demarcated, but Spitz nevi differ from conventional nevi in that nucleomegalic cells are common and predominate in some lesions. Such nucleomegalic Spitz nevus cells may be aneuploid, tetraploid, or octoploid. The explanation as to why Spitz nevi are commonly nondiploid while lacking other attributes of malignancy has not yet been forthcoming. Clearly, anomalies in ploidy alone are not sufficient for full malignant transformation **(Ferrara etal., 2005).**

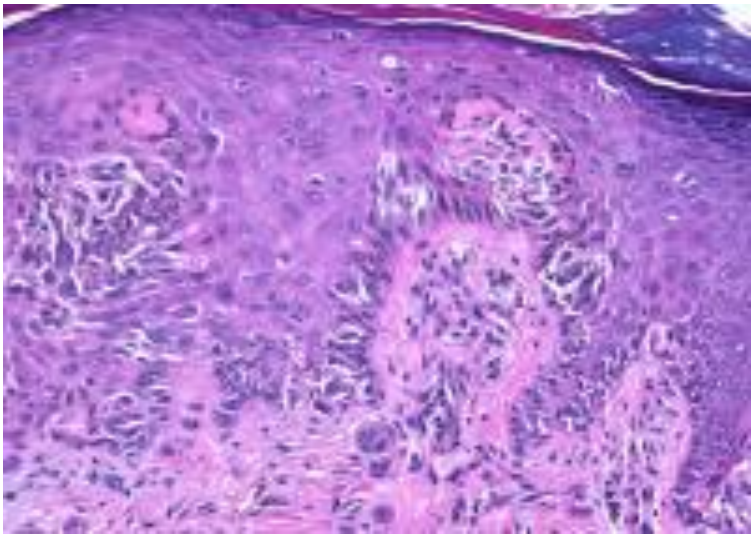

Figure 34: Spitz nevus **(Josef etal., 2003).**

This Spitz nevus shows large melanocytes with spindled and epithelioid cytomorphology arrayed along the junctional zone of an acanthotic and hyperkeratotic epithelium.

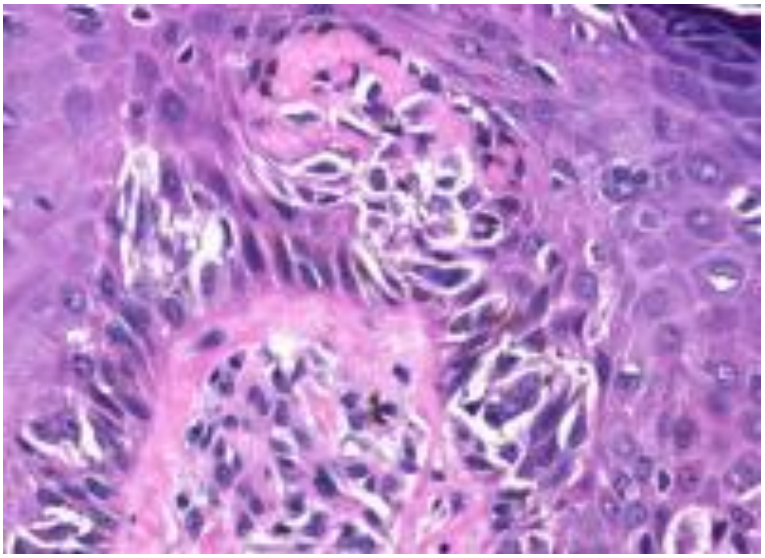

Figure 35: Spitz nevus **(Josef etal., 2003).**

At higher magnification, this Spitz nevus also demonstrates large, dull-pink globules along the junctional zone. These structures are known as Kamino bodies. Kamino bodies are most commonly observed in association with Spitz nevi but are occasionally observed in pigmented nevi of other types. Well-formed Kamino bodies are almost never (if ever) found in association with melanoma **(Ackerman etal., 1998).**

Overlap in the morphology of pigmented nevi can occur. For example, occasional pigmented nevi can display overlap between the morphology of Spitz nevus and dysplastic nevus. Overlap between blue and Spitz nevi can also be seen. Such lesions have been humorously referred to as "Sparks" (Spitz + Clarks) or "blitz" (blue + Spitz) nevi. When more than one type of cellular morphology occurs in a pigmented nevus, the lesion is referred to as a combined pigmented nevus. Conventional pigmented nevi are commonly combined with Spitz or blue nevi **(Ko etal., 2009).**

Blue nevi, shown below, are typically largely or entirely dermal melanocytic neoplasms composed of spindled and/or dendritic melanocytes with heavy cytoplasmic pigmentation. Some blue nevi are composed of epithelioid melanocytes, especially the deeply extending variant designated deep penetrating nevus, and many exhibit considerable associated sclerosis. The designation blue is far from the truth in many, if not most, instances because pigmented nevi with spindled and dendritic melanocytes can be tan, brown, black, gray, or even skin-colored; however, despite its inaccuracy, the designation blue nevus remains the universal standard for this category of lesions.

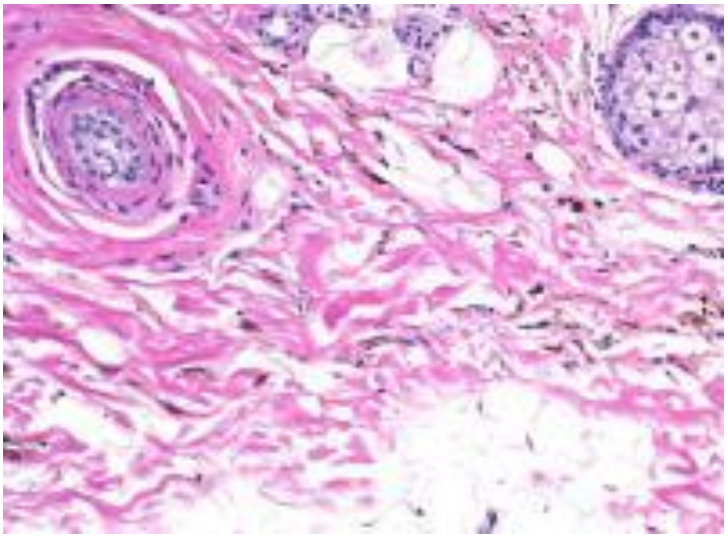

Figure 36: Blue nevus **(Josef etal., 2003).**

This blue nevus is composed of small dendritic melanocytes. This type of cytomorphology can be seen in so-called common blue nevi and in topographically restricted lesions such as nevus of Ito or nevus of Ota **(Murali etal., 2009).**

Some authorities have promoted the use an eponymic approach to the classification of pigmented nevi. The merit of this proposal derives from the fact that eponymic naming avoids the semantic misdeeds of the past. For example, the benign entity formerly (and incorrectly) known as juvenile melanoma becomes a Spitz nevus in the eponymic system. Dysplastic nevi are eponymically known as Clark nevi, in memory of Wallace Clark. The designation Miescher nevus can be used to designate dome-shaped, superficial congenital nevi that are commonly expressed on the face and the upper part of the trunk, whereas the designation Unna nevus can be used to refer to acrochordon like lesions that commonly develop near skin folds.

Despite the enthusiasm for eponymic naming in some areas, the usage of such designations can impede communication with the uninitiated. The author sees no difficulty in the usage of eponyms (and uses eponyms sporadically in his own practice), as long as the exact nature of the lesion in question is clearly stated in the language of the pathology report **(Ackerman etal.,1998).**

Chapter 2

Technique

The technique of recent modalities used in the diagnosis of some skin lesions:

1- Positron Emission Tomography / Computed Tomography (PET/CT).

2- Raman spectroscopy.

3- Elastography.

Technique of PET /CT:

PET is a tomographic scintigraphic technique in which a computer-generated image of local radioactive tracer distribution in tissues is produced through the detection of annihilation photons that are emitted when radionuclide introduced into the body decay and release positrons **(Habibian ,1999).**

PET is a tomographic imaging technique that uses a radiolabeled analog of glucose, 18F-FDG, to image relative glucose use rates in various tissues. Because glucose use is increased in many malignancies, as glucose and 18FDG uptake into malignant cells is facilitated by increase expression of the glucose transporter in tumor cells.18FDG does not enter the Krebs cycle after phosphorylation through hexokinase into 18FDG-6 phosphate) and therefore it is effectively trapped in the cells, allowing the measurement of glucose metabolism. The metabolic rate of glucose can be calculated from the time course of radiotracer concentration in tissue and in arterial blood where Cglc is the circulating glucose level **(Delbeke etal., 2002).**

Hybrid PET/CT scanners are composed of two distinct imaging systems integrated into a single gantry with near simultaneous imaging acquisition. PET provides functional, molecular information fused with anatomic location provide by CT. CT data are reconstructed using filtered back projection, whereas PET data are reconstructed using iterative algorithms.

CT images can be obtained after injection of a PET radiopharmaceutical because CT detectors are insensitive to annihilation radiation.

Combined PET/CT devices provide both the metabolic information from PET and the anatomic information from CT in a single examination. PET is a sensitive method for detecting, staging, and monitoring the effects of therapy of many malignancies **(Wieler etal., 2000).**

As shown in some clinical scenarios, the information obtained by PET/CT appears to be more accurate in evaluating patients with known or suspected malignancies than does the information obtained from either PET or CT alone or the results obtained from PET and CT separately but interpreted side by side. PET and CT are proven diagnostic procedures **(Delbeke etal., 2002).**

Technique of Raman spectroscopy:

In Raman spectroscopy a sample is irradiated with laser light, which results in light scattering. The majority of scattered light has unchanged frequency (so-called Rayleigh line) whereas the rest is shifted in frequency (Raman effect). The frequency shifts can be analyzed and presented as a Raman spectrum. The Raman effect is caused by molecular vibrations in the irradiated sample and thus gives information about the structure of the molecules. Molecular vibrations can be divided into deformational vibrations where the angles between the bonds change, and stretching vibrations where the lengths of the bonds change but the angle between them remains constant.

Optical spectroscopy has been around for many years and traditionally has been applied to a number of diverse fields, including analytical chemistry, geology, and even art history. Over the past 20–25 years, the use of optical spectroscopy for biomedical applications has grown significantly.

Its attractiveness comes from its ability to provide quantitative information about the biochemical and morphological states of tissue in a minimally invasive or noninvasive manner.

Spectra typically are collected with fiber-optic probes and charge-coupled device (CCD) cameras, and diagnostic algorithms have been developed to discriminate between different categories of tissue. Of the many optical spectroscopic techniques, fluorescence spectroscopy was one of the first to be developed as a diagnostic tool for a variety of diseases including cancers and plaques, as well as other conditions such as burns. However, although fluorescence spectroscopy can differentiate between normal tissue and disease (cancer) successfully, it suffers from a lack of specificity when differentiating between multiple non normal groups.

Diffuse reflectance spectroscopy provides valuable structural information by determining tissue optical properties. The lack of information regarding tissue biochemistry makes this method generally insufficient by itself for tissue diagnosis.

In recent years, Raman spectroscopy has garnered a great deal of interest in disease diagnosis, particularly cancer, because of its ability to provide molecular specific information about tissues **(Mahadevan-Jansen 2003).**

Raman Spectroscopy:

Raman scattering is an inelastic scattering process that occurs when an electron enters a virtual excited state due to an incident photon, then falls back to a higher or lower vibrational energy level with accompanying release of a new photon.

The energy transfer is proportional to a specific vibrational mode of the molecule, so Raman spectra are independent of excitation wavelength, and the change in energy between the incident and released photon is displayed as relative wave numbers (1/wavelength). Raman spectral peaks tend to be narrow, particularly in the fingerprint region of about 700–2000 cm, and each peak can be associated with specific vibrations in molecular bonds.

Thus, this technique provides biochemical information about a sample, including conformations and concentrations of constituents with the level of detail that is determined by the instrumentation and the need of the application.

Over the years, different forms of Raman spectroscopy have been developed and used for biological applications. The earliest of these is Fourier transform (FT)–Raman spectroscopy, a method that measures Raman spectra with high signal-tonoise ratio (S/N) and minimal fluorescence interference and has been used for many in vitro applications.

The typically long integration times and bulky instrumentation negate this technique for in vivo use. Ultraviolet resonance Raman (UVRR) spectroscopy can be used to target specific molecules by selecting excitation wavelength at their resonance, Thus yielding strong Raman signals.

The high excitation intensities and mutagenicity of UV light prevent the application of this technique for in vivo use. Surface-enhanced Raman spectroscopy (SERS) is an excellent technique that can detect molecular signatures in trace amounts and has been pursued for such applications as biochips. However, the use of silver and other such elements for enhancement prevents its implementation in vivo. Thus, near-infrared (NIR) dispersive Raman spectroscopy, in which NIR excitation minimizes fluorescence and absorption by tissue, has been the technique of choice for in vivo applications **(Utzinger etal., 2003).**

Instrumentation for Tissue Raman:

A typical system for measuring macroscopic Raman spectra of tissue, particularly in vivo, consists of a laser source for illumination, a fiber-optic probe to deliver the laser light

and collect the Raman-scattered light while rejecting the laser line and Rayleigh-scattered light, and a spectrograph and CCD to record the spectra.

Early attempts at measuring Raman spectra of tissue were difficult because of the fluorescent nature of tissue and limitations of sources and detectors.

Over the last several years, powerful, stable diode lasers emitting NIR light have become prevalent. These sources are ideal for clinical use because they are easily portable and are available at wavelengths in the "optical window" of tissue, such as785 nm and 830 nm, at which they generate minimal background fluorescence while penetrating fairly deeply into tissue.

On the detection end, high throughput spectrographs designed specifically for NIR-Raman spectroscopy are now readily available. Silicon-based CCD detectors have made great strides as well. Back-illuminated, deep-depletion CCDs that avoid etaloning allow high-resolution Raman spectra to be gathered with short (<5 s) integration times.

Recent developments in cooling technology have led to the development of thermoelectrically cooled detectors that can be operated at temperatures below _80 °C rather than using liquid nitrogen — again aiding portability. With the rise in the availability of handheld spectrometers, the Raman industry also has seen the development of handheld Raman spectrometers.

While successful in manufacturing and industrial applications, these systems still suffer from high noise characteristics and lack of cooling, preventing their use for in vivo tissue applications. Most in vivo Raman applications rely on fused silica–based optical fibers for remote sensing. However, the fibers themselves have a Raman signal, so this signal must be minimized using appropriate filters.

A band pass filter between the delivery fiber and sample prevents Raman-scattered light from illuminating the sample, while a long pass or notch filter between the sample and collection fibers prevents reflected laser light and Ray Leigh-scattered light from entering the collection leg and generating additional Raman signal **(Matousek etal., 2005)**.

Based upon this fundamental concept, a number of different fiber-optic probe designs have been implemented for in vivo Raman studies. Each of these designs is optimized for

increased S/N, target interrogation, and minimal background signal from within the probe. Some of these designs include obliquely polished fiber tips to increase the area of excitation and collection overlap, attaching a ball lens to the tip of the fibers to increase overlap or change the depth of focus, and side-firing fibers to get 360° of coverage. Some of these probes were developed by academic institutions **(Matousek etal., 2005).**

There also exist numerous commercial Raman fiber probes. However, these probes typically are designed for industrial applications and are not suitable for use on tissue. Thus, most in vivo probes are custom designed and built in-house or special ordered. Much of the discussion to this point has been focused on macroscopic or volumetric measurement of Raman signals rom tissue. Recently, there has been much interest in obtaining depth resolved Raman signals from tissues where discrimination could be improved by filtering out signatures from above or below the lesion. One way to obtain depth resolution is with a confocal setup, in which a pinhole (or a fiber) is used to reject out-of-focus light, allowing for depth separation.

In fact, confocality for Raman spectroscopy typically is incorporated in a microscope setting. These systems provide excellent spatial resolution and are used for biochemical mapping and spectral characterization of tissues.

Although some of these systems have been used to obtain tissue spectra from easily accessible areas of the skin, there is a need for compact handheld confocal probes for routine clinical use **(Smith etal., 2005)**

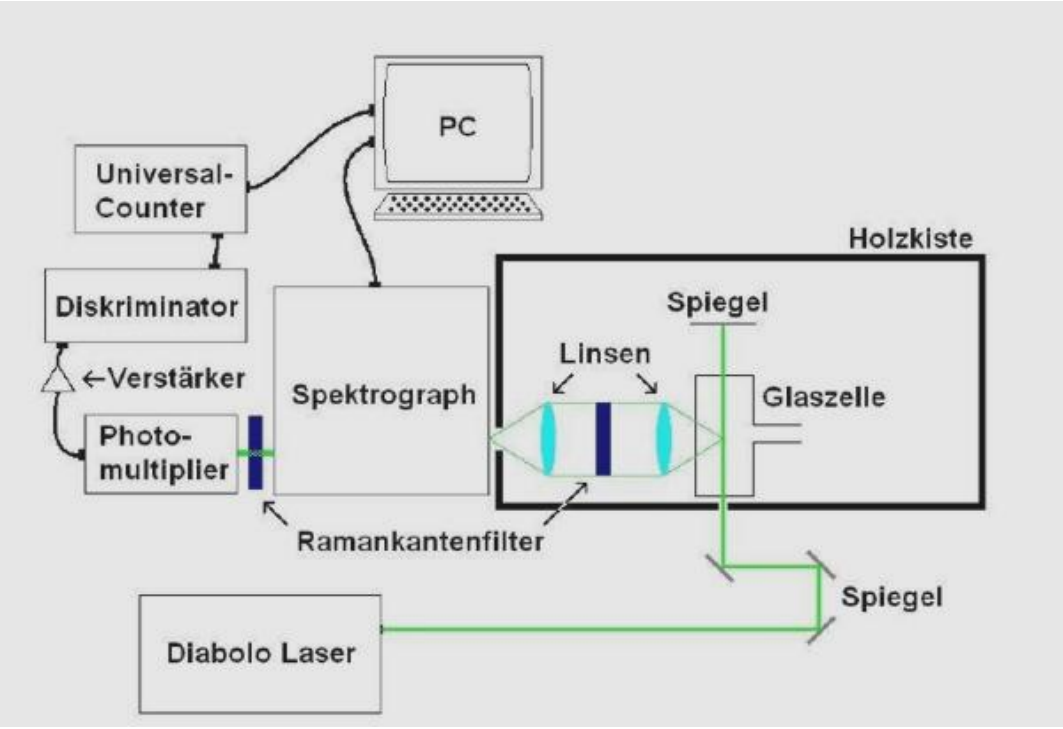

Diagram 7: The principle of Raman spectroscope **(Utzinger etal., 2003).**

Recent studies have demonstrated other methods for depth resolution such as Kerr-gated, spatially offset, and polarized Raman spectroscopy. These methods show much promise for biomedical applications and will be worth tracking in coming years. In all tissue Raman applications, various data processing steps must be followed to extract the tissue Raman signal from the raw measured spectra.

These include system calibration, fluorescence background subtraction, and noise smoothing. Perhaps the most challenging of these is the problem of fluorescence, the primary reason that most researchers in the field have moved to the NIR wavelengths. Current methods rely on mathematical techniques such as the use of second derivatives, Fourier filtering, and polynomial fitting to remove the fluorescence background.

Once Raman spectra are extracted, classification algorithms are developed using variety of multivariate statistical methods such as linear and nonlinear discrimination analysis, neural networks, genetic algorithms, and cluster analysis. The goal in each case is to obtain high sensitivity and specificity in the recognition of a target condition amidst a variety of tissue categories depending upon the application at hand **(Smith etal., 2005).**

Technique of Elastography:

Elastography, which is based on principal of physical elasticity, consists of applying a pressure on the examined medium and in estimating the induced strain distribution by tracking the tissue motion. In practical terms, RF ultrasonic data before and after the applied compression are acquired and speckle tracking techniques, e.g., cross correlation methods, are employed in order to calculate the resulting strain. The resulting strain image is called elastogram **(Brusseau etal., 2002).**

Theory

(1)Important quantities

Young's modulus (E) describes longitudinal deformation in terms of strain (fractional change in length) in response to longitudinal stress (force per unit area). **The shear modulus *G*** relates transverse strain to transverse stress and is related to shear wave propagation in isotropic homogeneous media. **The bulk modulus *K*** of elasticity describes the change in volume of a material to external stress. Another physical property of isotropic in homogeneous solids is the **Poisson ratio V**, which is a ratio of transverse contraction per unit breadth divided by longitudinal extension per unit length **(Greenleaf etal., 2003).**

One may ask the question, "Which physical parameter corresponds most closely to the characteristics felt by palpation?" In general, Poisson's ratio of tissue has a value of

between 0.49 and 0.499, which means tissue is nearly incompressible. (liquid - incompressible medium has 0.5) . This leads to a simple result that Young's modulus and the shear modulus of tissue are related by a scaling factor of three, that is, *E=3G.*

The bulk moduli K of most soft tissues differ by less than 15% from that of water, even though the shear modulus varies over a huge range. Thus, shear and Young's moduli, which have the widest dynamic range, are the most suitable elasticity parameters to measure and are probably the most closely associated with what is felt in palpation. The high water content of biological tissues means that they change shape easily when compressed but the volume is conserved. Consequently, K >> G, n ˜ 0.5 and E = 3G. **(Greenleaf etal., 2003).**

(2) The stress excitation methods:

The excitation methods can be divided based on their **temporal characteristics** into two general groups: static methods and dynamic methods. In static methods, tissue is compressed slowly and the distribution of its displacement is measured in some way [e.g., with MR, ultrasound, or optically].The difficulty with the static method is that it requires knowledge of boundary condition outside of the region under investigation.

On the other hand, dynamic methods rely on the wave equation, which in its differential form is local in character. The excitation methods may also be grouped based on the **spatial characteristics** of the excitation. External methods apply a stress, or a compression force, on the skin to deform the tissue beneath. This is often done by a simple mechanical means, such as pressing and holding a plate on the skin (in static approach) or vibrating the skin using a vibratory device (in dynamic approach). Internal excitation methods apply the excitation internally and directly on the region of interest within tissue.

Both static and dynamic excitations are possible with the radiation force of ultrasound. Biological sources, such as breathing or cardiovascular pulsation, are other means for internal excitation of tissue. Ultrasound displacement methods are based on either Doppler measurements or simple displacement measurement using pulse-echo methods **(Konofagou etal., 2003).**

(3)Principle of elastography

Application of 1D ultrasound signals before and after compression and consequently changes of reflected signal are clear from diagram 8.

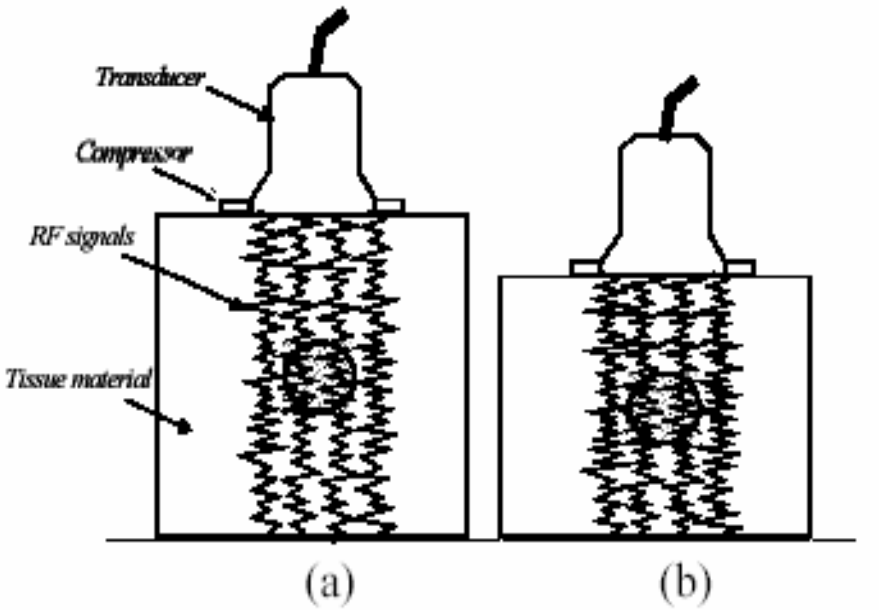

Diagram 8: The principle of Elastography: The tissue is insonified a) before and b) after a small uniformcompression. In the harder tissues (e.g. the circular lesion depicted) the echoes will be less distorted than in the surrounding tissues, denoting thus smaller strain **(Konofagou etal., 2003).**

If one or more of the tissue elements has a different stiffness parameter than the others, the level of strain in that element will generally be higher or lower; a stiffer tissue element will generally experience less strain than a softer one **(Ophir et al., 2002).**

Diagram 9 shows a schematic representation of the time delay and strain computation process. The windows are usually translated in small overlapping steps along the temporal axis of the echo line, and the calculation is repeated for all depths.

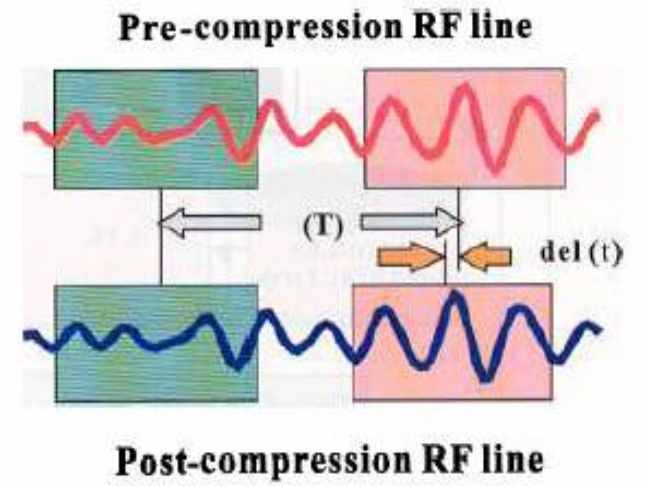

Diagram 9: A schematic showing the process of computing the strain in a tissue segment. Congruent windowed segments of the pre-compression and post-compression signals are compared by cross correlation. While the early windowed segments exhibit virtually no delay, a finite delay (designated Del (t)) is detected between the later segments **(Ophir etal., 2002).**

The strain is computed as the gradient of the time delay (or displacement), i.e. Strain = del (t) /T, where T is the initial (pre-compression) separation between the windowed segments **(Ophir etal., 2002).**

Radiological diagnosis of skin lesions

Radiological diagnosis of some skin diseases:

1-Malignant melanoma.

2- Squamous cell carcinoma.

3- Basal cell carcinoma.

4- Pigmented nevi.

5- Seborrheic keratosis.

6- Subcutaneous abscess.

7- Psoriasis.

Radiological diagnosis of Malignant Melanoma (MM):

Diagnosis by Raman spectroscopy:

Melanoma is the most aggressive skin cancer. The specificity and sensitivity of clinical diagnosis varies from around 40% to 80%. The chemical changes in the melanoma tissue detected by Raman spectroscopy and neural networks can be used for diagnostic purposes **(MacKie, 2000).**

MM removal at early stages is almost always curative and therefore early detection is essential. Difficulties in diagnosis of cutaneous MM arise because benign lesions like pigmented nevi (PN), seborrheic keratosis (SK), and other types of skin cancer such as basal cell carcinoma (BCC) may resemble melanoma **(Kanzler etal., 2001).**

Raman spectroscopy is a technique that provides information about the molecular structure of the investigated sample and has been widely used for the past 70 y for nondestructive chemical analysis **(Puppels , 2001).**

Spectra evaluation

To analyze alterations in protein and lipid structure, the positions, shape, and intensity of spectral bands for proteins, lipids, and water were studied in the region 1200–1750 cm^{-1}. This area comprises the major protein and lipid vibrations. Among seven important protein vibrations, the amide I and amide III vibrations are clearly represented in Raman spectra of the skin.

The amide I band (around 1650 cm^{-1}) reflects mainly C=O stretching vibrations, whereas the amide III band (around 1270 cm^{-1}) is a more complex mode involving several chemical bonds. Combined maximum intensity frequencies of the amide I and III bands reflect protein secondary structure (-helix conformation, -sheet, random coil). Moreover, a C-C stretch band at approximately 935 cm^{-1} is typical for an -helix. Lipid-specific vibrations are found around 1300 cm^{-1} (twisting and wagging vibrations) and in the region extending to 1340 cm^{-1} **(Edwards etal., 1998).**

The intensities of the described spectral bands were calculated using Matlab software (The MathWorks, USA). To demonstrate spectral changes for proteins, the ratio between the amide I band and (CH_2) (CH_3) in proteins and lipids ($I_{1650\ cm^{-1}}/I_{1450\ cm^{-1}}$) and the ratio

between the amide III and lipids at around 1320 cm^{-1} were calculated ($I_{1270\ cm^{-1}}/I_{1320\ cm^{-1}}$) (Table II, Table III).

Spectra of normal skin

Peaks originating from vibrations within protein molecules and lipids were clearly resolved (diagram 10, Table II). In normal skin the positions of the amide I and III bands (1650 cm^{-1} and 1270 cm^{-1}) and the presence of a well-developed band around 935 cm^{-1} suggested a helical protein structure **(Miura etal., 2001).**

Pigmentation increased the background level of the spectra, which was most pronounced in the region 1800–2500 cm^{-1} as previously described for normal skin diagram11. This region does not contain protein and lipid band **(Knudsen etal., 2002).**

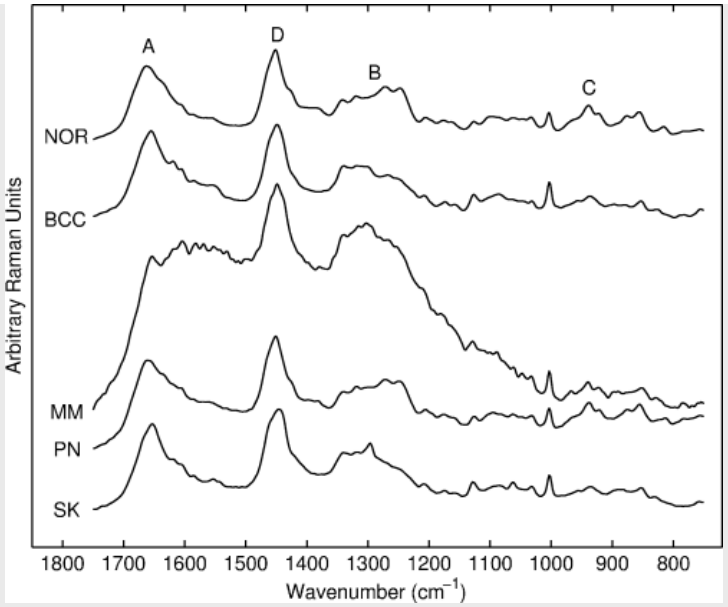

Diagram 10:NIR-FT Raman spectra of normal skin (NOR), PN, MM, BCC, and SK. Spectral alterations of the following major spectral bands are shown: (*A*) a major decrease in intensity of the amide I band of proteins in MM, a slight decrease of the right wing of the band in PN; (*B*) the amide III band region around 1270 cm^{-1} and an increase in the lipid-specific region 1300–1340 cm^{-1} in MM, BCC, and SK; (*C*) a decrease of the (C-C) band around 940 cm^{-1} in proteins in MM, BCC, and SK; (*D*) a widening of the (CH_2)(CH_3) in proteins and lipids in MM, BCC, and SK. For intensity comparison all spectra were normalized to the 1450 cm^{-1} band **(Miura etal., 2001).**

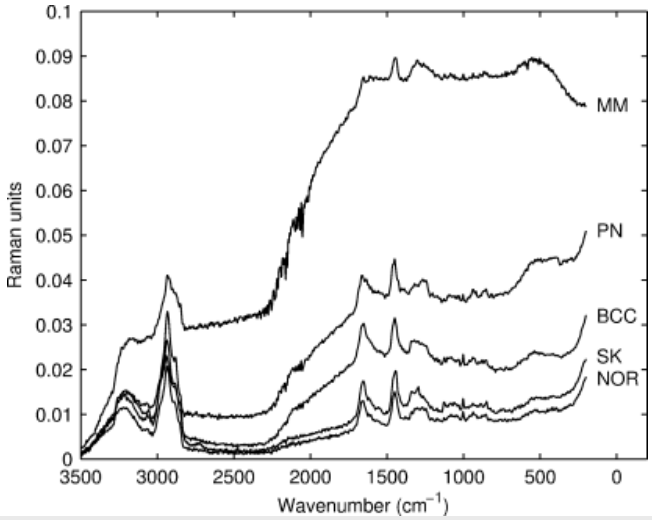

Diagram 11: NIR-FT Raman spectra of normal skin (NOR), PN, MM, BCC, and SK. Note the influence of the pigmentation on the 1800–2500 cm^{-1} region **(Miura etal., 2001).**

Table II - Major protein and lipid band positions of NIR-FT Raman spectra of normal skin (NOR), PN, MM, BCC, and SK.

	Amide I in proteins	Amide III in proteins	$(CH_2)(CH_3)$ in proteins and lipids
NOR	1662 (1656–1668)	1264 (1241–1287)	1451 (1449–1453)
PN	1660 (1652–1668)[a]	1264 (1242–1286)	1451 (1448–1454)
MM	1655 (1647–1663)[a]	1272 (1258–1286)	1449 (1443–1455)[a]
BCC	1655 (1651–1659)[a]	1268 (1253–1283)[b]	1449 (1445–1453)[a]
SK	1653 (1649–1657)[a]	1276 (1266–1286)[a]	1446 (1441–1451)[a]

Values represent means with 95% confidence intervals.

[a] Significant compared to NOR.

[b] Significant compared to BCC.

Skin tumor spectra reveal protein and lipid alterations

Spectra revealed clear-cut changes between the investigated types of tumors allowing differentiation of MM from other investigated lesions (diagram10, Table II, Table III).

MM presented with a decrease in the amide I band intensity resulting in flattening of the spectral area between 1500 cm^{-1} and 1800 cm^{-1} (diagram 10 a, Table II). This suggested a change in molecular composition of proteins. Moreover, an increase in

intensity of the band at 1300 cm^{-1} of the CH twisting and wagging in lipids and the band around 1310–1330 cm^{-1} was seen with a relative decrease in the amide III regions of proteins (diagram 10 b, Table II) **(Hintz-Madsen etal., 2001).**

Table III - Major band ratios in NIR-FT Raman spectra of normal skin (NOR), PN, MM, BCC, and SK.

	Amide I in proteins, $I_{1650\ cm^{-1}}/I_{1450\ cm^{-1}}$	**Amide III in proteins,** $I_{1270\ cm^{-1}}/I_{1320\ cm^{-1}}$	**C–C in proteins,** $I_{930\ cm^{-1}}/I_{1000\ cm^{-1}}$
NOR	0.69 (0.54–0.84)	1.15 (0.96–1.34)	2.49 (1.24–3.74)
PN	0.62 (0.39–0.85)[a]	1.05 (0.98–1.12)[a]	2.24 (0.64–3.84)[a]
MM	0.29 (-0.27–0.85)[a,b]	0.99 (0.93–1.05)[a,b]	0.77 (-0.29–1.83)[a]
BCC	0.86 (0.51–1.21)[a]	0.94 (0.86–1.02)[a]	0.82 (0.10–1.54)[a]
SK	0.81 (0.33–1.29)[a]	0.95 (0.82–1.08)[a]	0.85 (0.14–1.56)[a]

Values represent means with 95% confidence intervals

[a] Significant compared to NOR.

[b] Significant compared to BCC.

MM spectra showed a decrease in protein band intensity around 940 cm^{-1} diagram 10 c. With decrease in intensity of the amide I band diagram 10 a.

Neural network analysis of Raman spectra achieved a diagnostic sensitivity of 85% and specificity of 99% for the diagnosis of MM **(Zurada etal., 2000).**

Presenting wrongly classified skin lesions is presented in Table IV. MM had a tendency to be misdiagnosed as BCC and PN, whereas PN were confused with normal skin.

Table IV - Specificity and sensitivity of neural network analysis of Raman spectra for classification of normal skin (NOR), PN, MM, BCC, and SK.

	Sensitivity	Specificity
NOR	96%±3	94%±3
PN	78%±6	97%±2
MM	85%±5	99%±1
BCC	98%±2	98%±2
SK	96%±3	100%±0

Sensitivity and specificity are defined as in Altman (1991) and are shown±twice the SD of the approximated normal distribution to the binomial distribution **(Zurada J etal., 2000)**.

The sensitivity map for MM in diagram 12 showed important spectral intensities at 1620–1670 cm^{-1}, 1230–1300 cm^{-1}, and 1430–1450 cm^{-1}, which matched the spectral differentiation marked A, B, and D in diagram12.

Moreover, the sensitivity map pointed out new frequencies not used for visual inspection of the spectra: 2840–3000 cm^{-1}, 2000–2350 cm^{-1}, and 1000 cm^{-1}, marked E, F, and G respectively in diagram11. Vibrations reflected at these spectral regions are most probably characteristic for (E) CH stretching in proteins and lipids, (F) skin fluorescence, and (G) ring vibrations in aromatic amino acid residues **(Gniadecka etal ., 2001).**

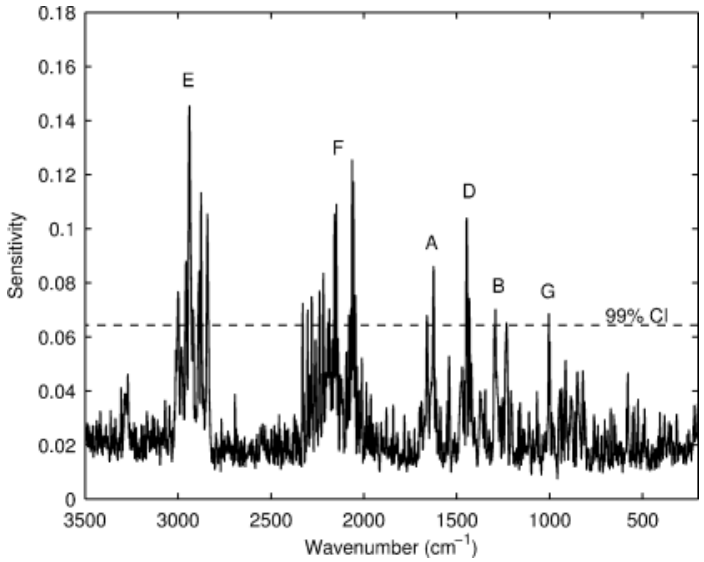

Diagram 12: The sensitivity map of neural network weighting of spectral frequencies, used for MM classification. The *dashed line* indicates the 99% confidence interval. Spectral bands marked (*A*), (*B*), (*D*) correspond to the description from Diagram 10 showing differences detected on visual classification of the spectra. (*E*) CH_3 stretching vibrations in proteins and lipids (around 2940 cm^{-1}); (*F*) vibration caused by skin fluorescence (2000–2350 cm^{-1}); (*G*) ring vibrations in amino acids (around 1000 cm^{-1}) **(Zurada etal., 2000).**

It is demonstrated that it is possible to differentiate MM from PN, BCC, and SK by neural network analysis of the near-infrared Fourier transform (NIR-FT) Raman spectra.

The neural network analysis used spectral alterations reflecting changes in composition and structure of proteins and lipids. MM and BCC spectra showed similar patterns but were distinctive. Intensities in the amide III regions of proteins decreased relative to the lipid-specific bands.

An emergence of the lipid component of the $(CH_2)(CH_3)$ accounting for shifting of the 1450 cm^{-1} band occurred both in BCC and MM spectra **(Hintz-Madsen etal., 2001).**

The first Raman spectroscopy study on cancer recognition was performed on skin cancer where the decrease in intensity of the amide III region was reported **(Liu etal., 1999).**

The peak around 1320 cm^{-1} can be attributed to both collagen and nucleic acids (DNA), more specifically to the purine bases guanine and adenine **(Stone et al., 2000).**

Raman spectra obtained from MM and BCC show alterations in the 1310–1340 cm^{-1} region. Therefore it is most probable that malignant transformation triggers similar molecular changes independently of the tissue involved. Alterations of the amide bands in Raman spectra are attributed to the conformational changes of proteins. Collagen contributes predominantly to Raman spectra of the skin **(Johansson etal., 2000).**

Therefore changes in its structure or its degradation could explain the decrease in the amide band intensities. Collagen degradation is influenced by matrix metalloproteinase **(Yoshizaki etal., 2002).**

Upregulation of metalloproteinases was found in invasive skin tumors like MM and BCC **(Hofmann etal., 2000).**

Neural network analysis based only on the spectral information allowed to diagnose MM with a sensitivity of 85% and a specificity was 99%. This is comparable to the diagnostic accuracy for MM achieved by trained specialists in dermatology **(Chen etal., 2001).**

Diagnosis by ultrasound and Elastography:

High-frequency ultrasound with elastography can help differentiate between cancerous and benign skin conditions, allows for accurate characterization of the extent and depth of the lesion below the surface, which can aid physicians in treatment.

Elastography non invasively estimates the axial tissue strain, or elastic properties of tissue. Cystic lesions demonstrate high levels of elasticity, while malignant lesions are relatively "hard" with a very low level of elasticity. Ultrasound with elastography, more so than optical or light images, is unique in its ability to provide the proper depth at which to analyze lesions around 5 mm below the surface **(Schmid-Wendtner etal., 2005).**

This may be useful in the early detection of melanoma before the classic signs such as or changes in border are present on the skin's surface. In addition, elastography "This also could guide the surgeon as the surgeon is doing an excision or biopsy to not just look at the tip of the iceberg that they can see at the skin surface, but actually to be able to look deeper, so they can see exactly which areas they can cut out safely and still remove the entire without unnecessarily removing more than that **(Harland etal., 2003).**

Malignant lesions had higher strain ratios (minimum 5.3; maximum 32.2), none of the malignant lesions violated a strain-ratio cutoff of 3-5, although preliminary, the data suggest that strain ratios may also be useful in distinguishing between malignant lesions.

Melanomas are characterized by their homogeneous lesion, which is very hypoechogenic spindle-shaped appearance being clearly separated from the surrounding tissue. The lesion extends laterally, and may include a vertical extension zone. The entry echo is low-grade **(Schmid-Wendtner etal., 2005).**

There is a significant correlation between the preoperative, sonographically assessed thickness of the tumour and the one assessed by postoperative, histological morphometry offering some guidance in the preoperative assessment **(Pellacani etal., 2003).**

A still unsolved problem, however, is the difficulty of distinguishing between tumors parenchyma and subtumoral inflammatory infiltrate, or pigmented nevi. Consequently, some tumors are sonographically overestimated with a precise measurement of the tumor thickness sometimes being impossible **(Harland etal., 2003).**

Recently, Ulrich *et al.* have shown that the correlation between sonometry and histometry increases appreciably if tumors with significant inflammatory infiltrate or nevus-associated melanomas were excluded from the analysis **(Krahn etal., 2001).**

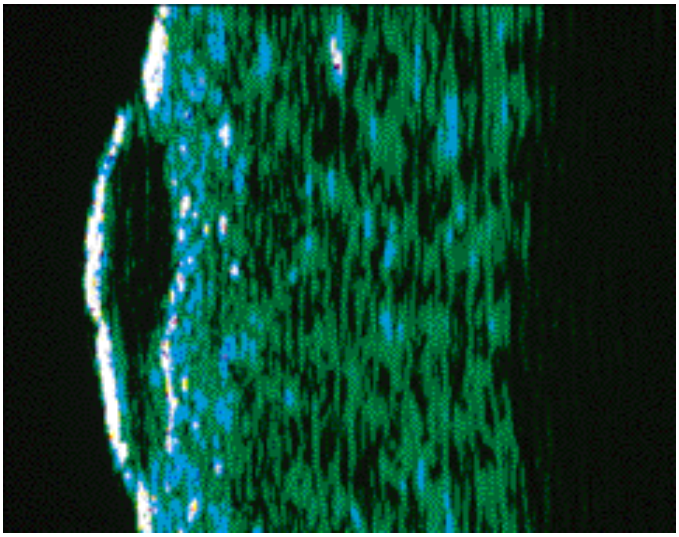

Figure 37: Ultrasound image of superficial spreading melanoma on back. Sonographical tumor thickness 1.20 mm. Histological tumor thickness 1.15 mm **(Lassau etal., 2002).**

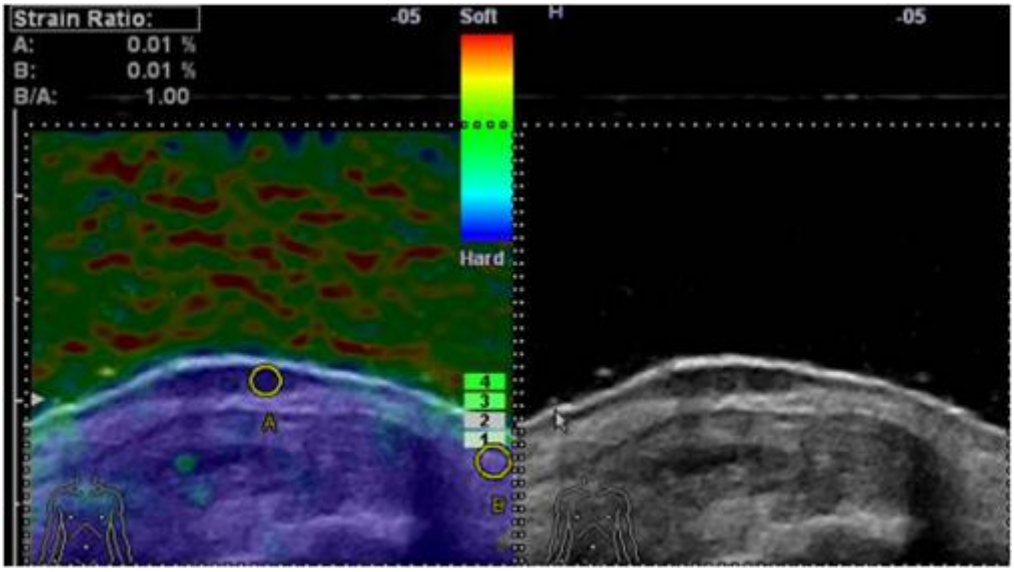

Figure 38: An elastogram (left) and ultrasound image (right) showing malignant melanoma of the skin **(Lassau etal., 2002).**

Diagnosis by PET/ CT:

The role of PET /CT in diagnosis of malignant skin lesions as follow:

(1)To assess extent of disease.
(2)To detect malignant melanoma in whom a sentinel node biopsy was not or can not be performed in stage II.
(3)To exclude systemic involvement in skin lymphomas.

(4)To exclude primary malignancy in skin conditions that may be paraneoplastic phenomena e.g. dermatomyositis **(Prichard etal., 2001).**

Radiological diagnosis of Squamous Cell Carcinoma (SCC):

It is frequent tumors most commonly localized on skin areas exposed to chronic sun exposure, occurring either de novo or actinic keratoses. The occurrence of metastases ganglion and visceral is possible wherever the tumor is large or its dermal invasion is deep **(Grossman etal 2001).**

Diagnosis by MRI:

The application of MRI in dermatology can give a detailed picture of a tumor and its depth of invasion in relation to adjacent anatomic structures. It has reported as well as delineates pathways of tumor invasion. Confirmation of the glomus tumor of the nail by MRI. MR spectroscopy has been used to differentiate the diseased skin from the normal skin **(Song etal, 1999).**

MRI is more advantageous over other radiological techniques in analyzing some tissues. It gives better contrast (by about 25%) than computed tomography. And it is dependent on a number of parameters of protons, e.g., density, T1 and T2 relaxation times, bulk motion, diffusion, magnetic susceptibility, and so forth **(Bond etal 2000).**

The cellular distribution of water with or without increase in global tissue water is different in cancerous tissue than that of normal skin. The increase in total proton density associated with changes in water structure alters free mobile protons in epidermis, dermis, and subcutaneous tissue.

These changes reflect as contrast and brightness in MRIs. Quick pulse repetition times and short data collection times (echo times) are known as spin-echo times, Because of the small paramagnetic properties of skin tissue, the lesions and metastasis appear hypointense on T1 **(Schwinghofer, 1999).**

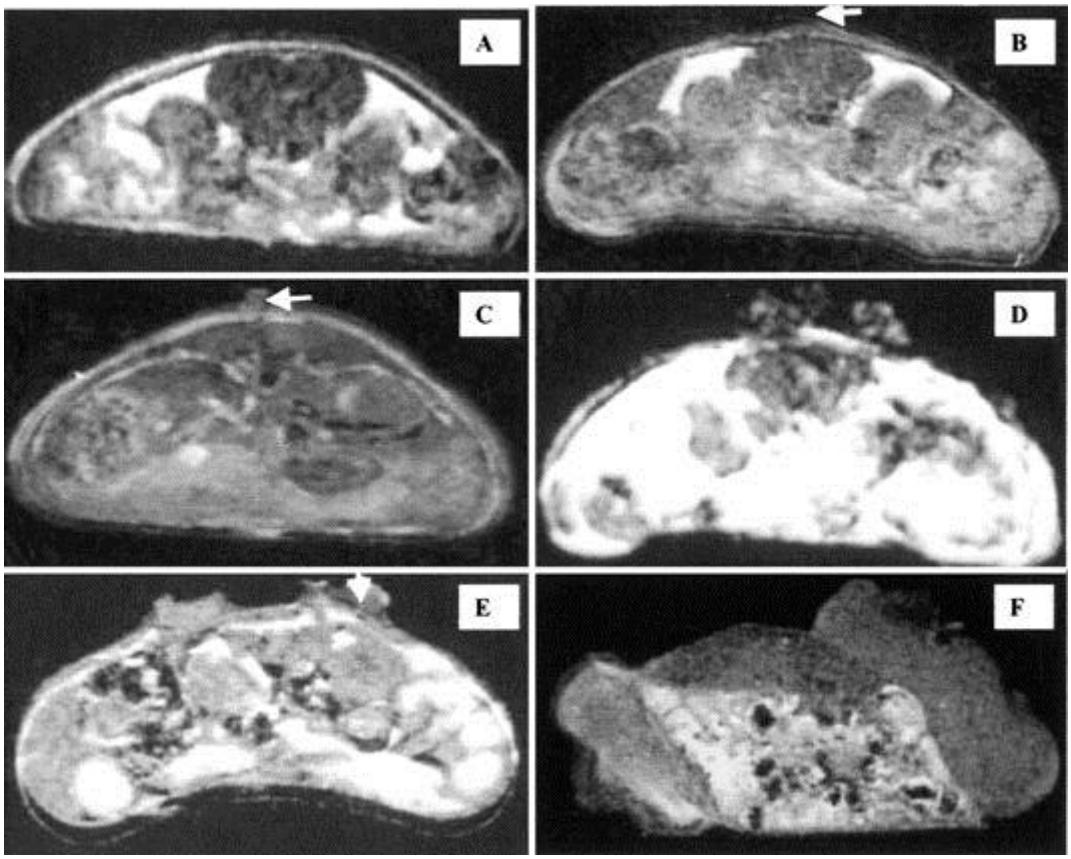

Figure 39: Trans-axial multi spin-echo MRIs (echo-time [TE] = 15 msec, repetition time [TR] = 600 msec) of normal skin (A) and tumor on different stages of growth Tumors are indicated by arrows (from B to F) **(Schwinghofer, 1999).**

To demonstrate the tumor invasion in the internal structure, it is necessary to view the tumor regions, at a high resolution and sections of smaller thickness.

The images given in Figure 39 A to F correspond to the view of the normal skin (A) and tumor (B to F), respectively. The tumor-to-fat contrast is very considerably significant as the tumor shows considerably less signal intensity than fat in the T1-weighted images (average about 20%). As explained earlier malignant tumors appear as hypointense on T1-weighted images.

The changes seen in Figure 40, B to F are accompanied by the disappearance of dermal-epidermal interphase and spreading of tumor deeper inside and are quite obvious. However, in the benign tumors, the dermal-epidermal interphase was not totally lost **(Maurer etal., 2002).**

1. 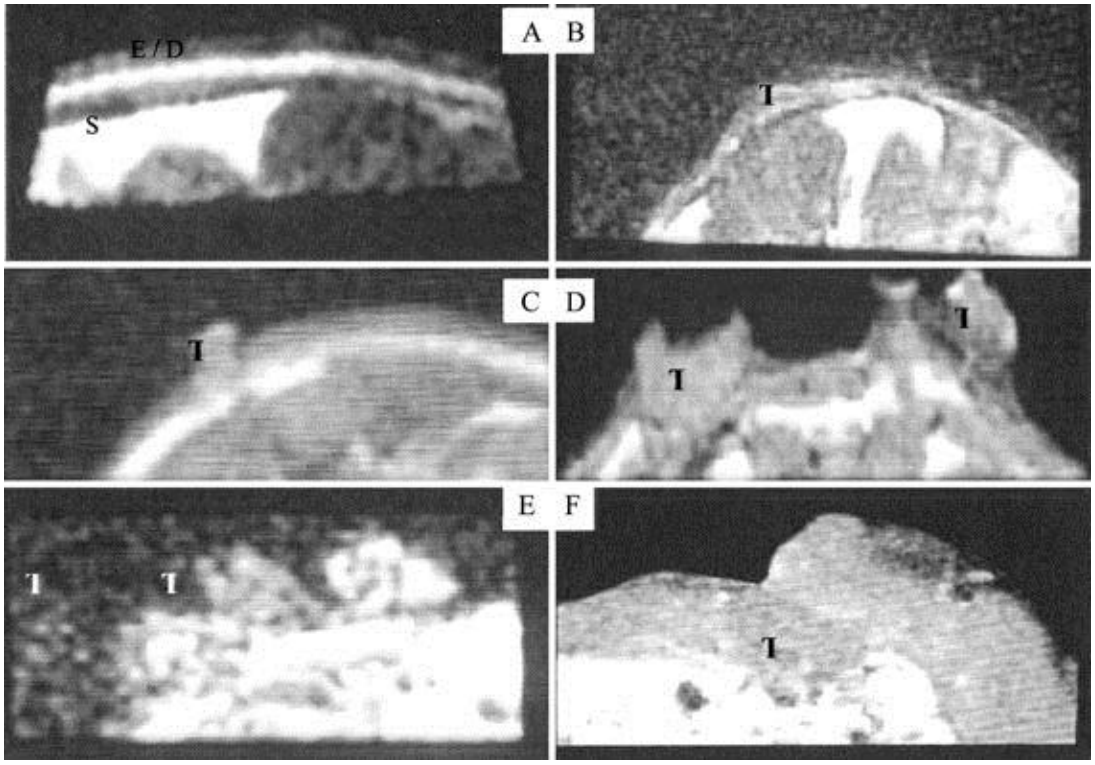

Figure 40: T = tumor area, E = epidermis, D = dermis, and S = subcutis. The loss of dermis and epidermis interphase accompanied by the invasion of tumor area **(Maurer etal., 2002).**

Diagnosis by ultrasound and Elastography:

Ultrasonographic study almost always shows a significant hyperechogenic of superficial part related to Hyperkeratosis . This can lead to the formation of a shadow cone which prevents the visualization of the tumor depth and its extension **(Harland etal., 2003)**.

It must then strip Hyperkeratosis, to better visualize the tumor which is hypoechogenic.

Elastograghy has the same role as in malignant melanoma but with different on strain ratio as a squamous cell carcinoma with a strain ratio of 13.273. Squamous cell carcinomas had a higher ratio overall as more invasive cells were present **(Rallan etal., 2003).**

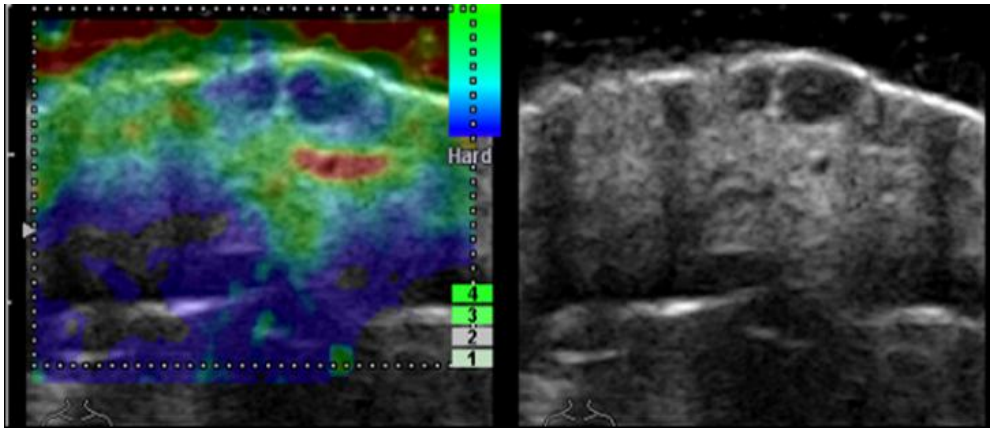

Figure 41 An elastogram (left) and ultrasound image (right) showing squamous cell carcinoma of the skin **(Harland etal., 2003)**.

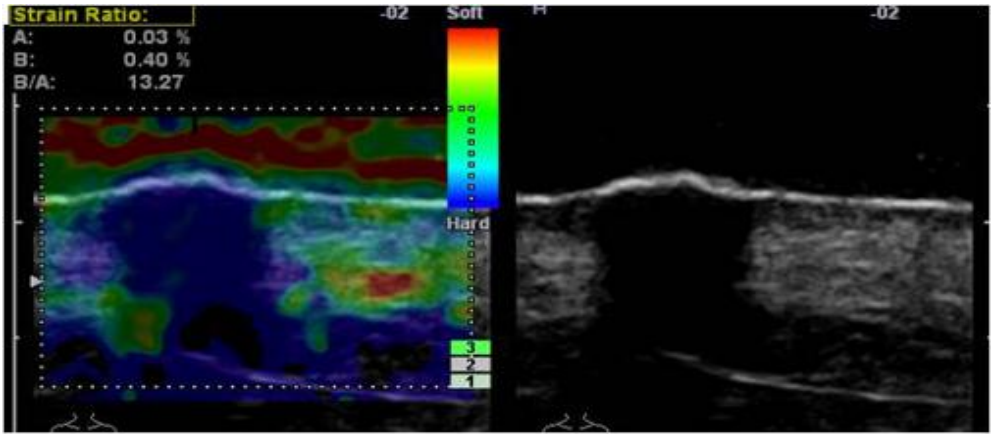

Figure 42: An elastogram (left) and ultrasound (right) showing squamous cell carcinoma of the skin **(Harland etal., 2003)**.

.

Radiological diagnosis of Basal Cell Carcinoma (BCC):

This is the most common cancer most often located on skin areas exposed to chronic sun exposure which incidence increases regularly due to the aging population and sun exposure habits. First-line treatment is surgery.

Diagnosis by Raman spectroscopy:

Basal cell carcinoma BCC showed similar spectral changes in the region 1300–1340 cm^{-1} (diagram10b, Table II). As in melanoma. The emerging bands in this region were found around 1300 cm^{-1} and 1330 cm^{-1}.

BCC spectra showed a decrease in protein band intensity around 940 cm^{-1} diagram10 c. In contrast to MM, BCC spectra did not show any decrease in intensity of the amide I band diagram10 a **(Nijssen etal., 2002)**.

BCC diagnosis was 97% and 98%, respectively. The confusion map, established by the neural network **(Zurada etal., 2000).**

Diagnosis by ultrasound and Elastography:

Depending on size and histological type of basal cell carcinoma. They generally present as bizarely formed low echogenic foci often causing an enhancement of dorsal echoes **(Coulomb, 2004).**

Ultrasonographic appearance is often stereotyped and almost pathognomonic image overall anechogene, with film–sized large dense echoes. Boundaries with surrounding dermis are the most often well marked, but in some cases, Ultrasound shows homes more remotely clinical lesion, limits which may be a help in the choice of treatment.

Similarly, invasion in depth towards the hypodermis, cartilage, muscle or bone is easily viewable (within the limits of the appliance, between 5 and 7 mm deep, which is usually the case in the face).The character anfractuous of some common locations of face basal cell carcinoma requires a sufficiently small and handy probe to assess tumor (internal canthus, ear shell) extension **(Berson etal., 2005).**

The role of elastography is the same as that of squamous cell carcinoma.

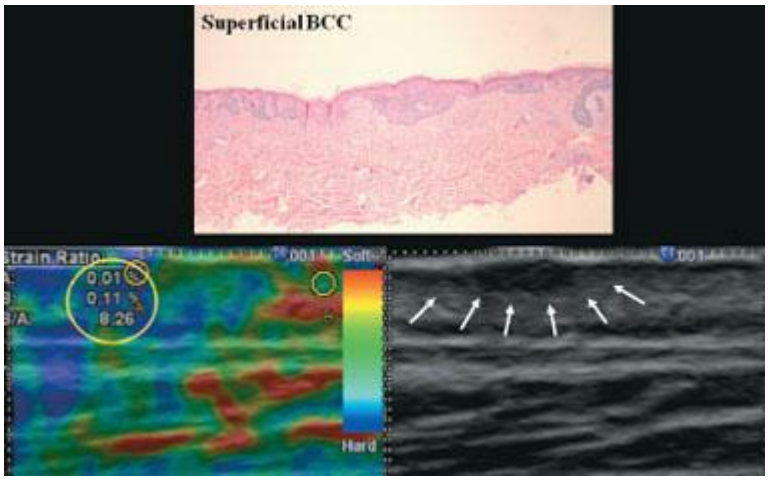

Figure 43: Top, histopathology slide demonstrates proliferation of basal cells in the epidermis with palisading cells at the periphery and adjacent early stromal changes, but without the dermal invasion characteristic of basal cell carcinoma (BCC). Bottom left, ultrasound elastography demonstrates blue area of decreased elasticity associated with BCC. The ratio of this abnormal region to adjacent epidermis was greater than 5.0 (elastic ratio of 8.26) suggesting malignancy. Bottom right, high-resolution (16 mHz) ultrasound demonstrates corresponding area of decreased echogenicity (darker) with a well-demarcated border and an intact basement membrane **(Harland etal., 2003).**

Radiological diagnosis of pigmented nevi:

PN are benign neoplasms or hamartomas composed of melanocytes, the pigment-producing cells that constitutively colonize the epidermis.

Diagnosis by Raman spectroscopy:

Spectra of pigmented nevi (PN) were almost identical to those of normal skin but consistently showed a decrease in intensity in the right wing of the amide I band (diagram 10 a, Table II). This suggested minor changes in composition or conformational alterations in the proteins. Moreover, in the region from 1800 cm^{-1} to 2500 cm^{-1}, an increase in intensity of the otherwise flat spectral region was observed diagram 10. This phenomenon occurred most probably due to an increase in pigmentation of the lesional skin, similar to that of highly pigmented skin and in MM spectra **(Nijssen etal., 2002)**.

PN were diagnosed with 78% sensitivity by Raman spectroscopy **(Zurada etal., 2000)**.

Diagnosis by ultrasound and Elastography:

Upon sonography, pigmented nevi present as spindle-shaped structures with low echogenic material, thus being hard to distinguish from malignant melanomas. Current technology is therefore better suited to quantification of pigmented skin lesion size than diagnosis. Elastograghy has the main role to differentiate it from malignant melanoma. As it has a strain ratio of (min. 0.01; max. 3) **(Zymanska etal., 2000).**

Radiological diagnosis of seborrheic keratoses (SK):
Diagnosis by Raman spectroscopy:

Seborrheaic keratoses (SK) were diagnosed with 96% sensitivity and was most frequently confused with BCC **(Zurada etal., 2000).**

For SK, a major increase in intensity of the 1300 cm^{-1} band of twisting and wagging vibrations of lipids reflected lipid accumulation in the horny cysts of SK **(Nijssen etal., 2002).**

Diagnosis by ultrasound:

It present with the phenomenon of attenuation or total extinction of reflected echoes. In the sonographic image they are characterized by a sound shadow and can, therefore, easily be distinguished from other tumors. **(Zymanska etal., 2000).**

Radiological diagnosis of subcutaneous abscess:
Diagnosis by ultrasound and Elastography:

Soft tissue infections are common conditions and range from superficial cellulitis to deeper soft tissue infections with abscess collections requiring surgery. Inadequately treated superficial soft tissue infections can progress to deeper tissue infections requiring more invasive surgery or bacteremia requiring hospitalization and intravenous antibiotics.

Increasingly prevalent antibiotic-resistant bacteria in soft tissue infections have changed current therapy, but primary therapy for a skin abscess remains surgical drainage, Therefore, it is even more important now to accurately identify skin abscesses **(Pallin etal., 2008).**

Differentiation of superficial cellulitis from a soft tissue abscess can be challenging but relies mostly on physical examination, with additional imaging by computed tomography or ultrasound if needed **(Tayal VS etal., 2006).**

The natural progression of an abscess from induration to fluid collection should provide a useful diagnostic signature when imaged with elastography, but to our knowledge, no studies to date have been performed using elastography on soft tissue infection **(Arslan etal., 1998).**

A

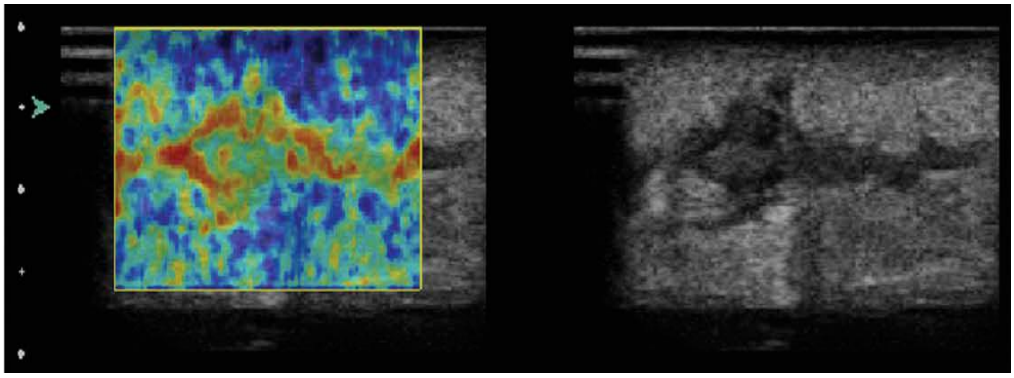

B

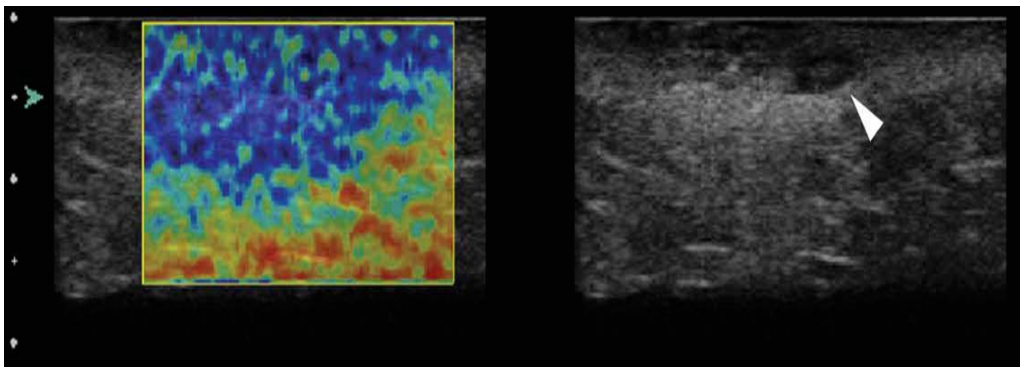

Figure 44: Abscess cavity visualized with B-mode imaging and elastography.
A, The elastographic color overlies the gray scale image (left), with the abscess cavity visualized as a soft (red) rim on a less soft (yellow and aqua) background. The surrounding induration is visualized as stiff (deep blue on aqua). The image on the right is identical but without the elastographic overlay. **B**, The abscess cavity (arrowhead) is visualized with gray scale imaging (right image) but not with elastography. The surrounding induration is clearly visible as stiff (dark blue with aquaspeckling) **(Squire etal., 2006).**

A

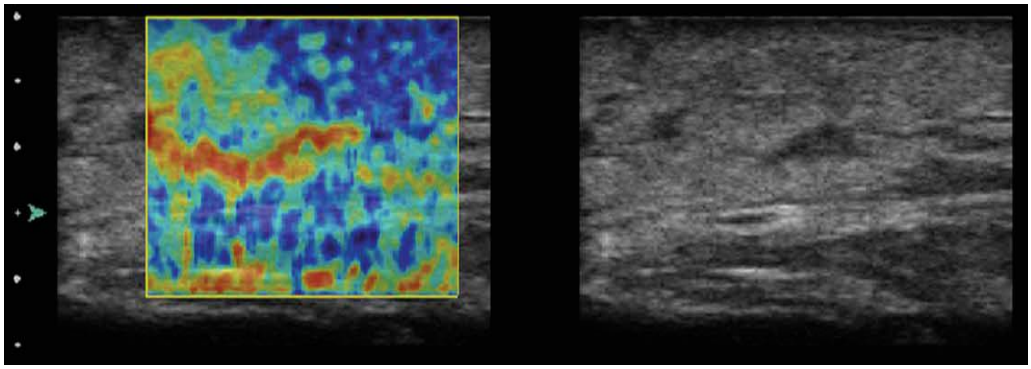

B

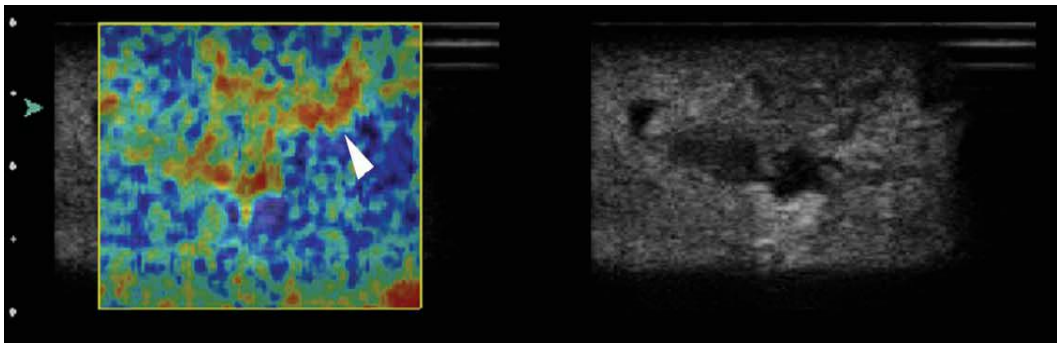

Figure 45: Elastographic imaging of isoechoic abscesses. **A**, An isoechoic abscess that is difficult to visualize with gray scale imaging (left) is visible on elastography, with a soft (red) signal on a background of middle stiffness (aqua and green). **B**, An abscess with mixed isoechoic and hypoechoic signals shows additional extensions of the abscess cavity (arrowhead) on elastography (red on yellow) that is not visible on gray scale imaging **(Squire etal., 2006)**.

A

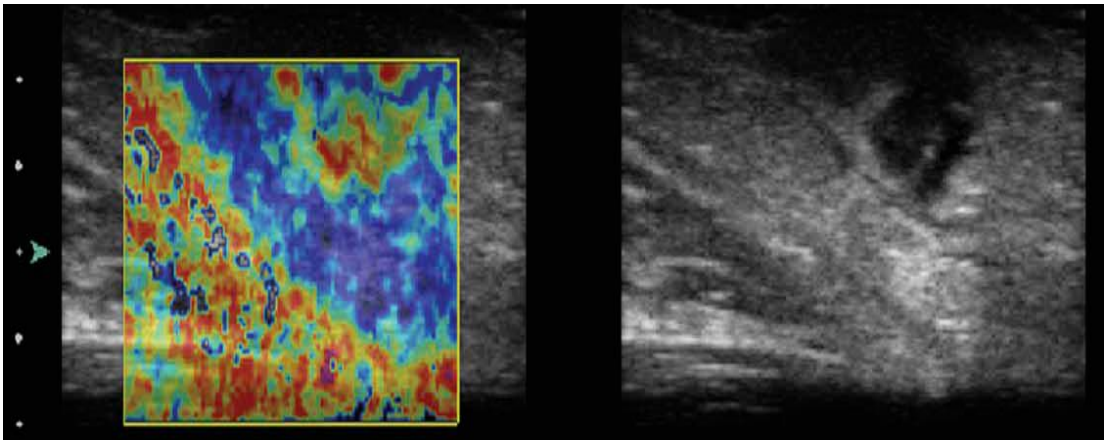

B

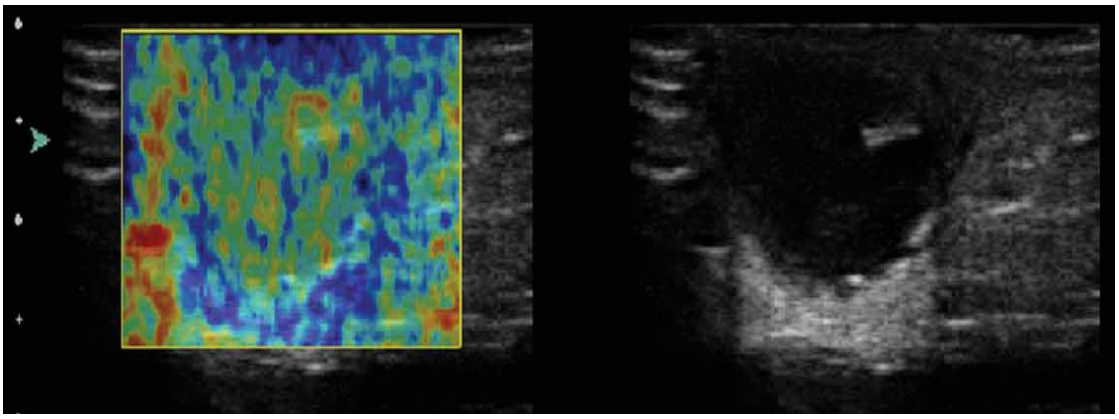

Figure 46: Elastographic color spectrum of skin abscesses. Softer abscess cavities with purulent material are visualized with elastography as larger spots of soft (**A**, red) on a less soft (**A**, yellow and green) background or smaller spots of soft (**B**, red and yellow) on a background of middle stiffness (**B**, green). The stiff blue of the surrounding induration accentuates the softer abscess cavity **(Struk etal., 2001)**.

A

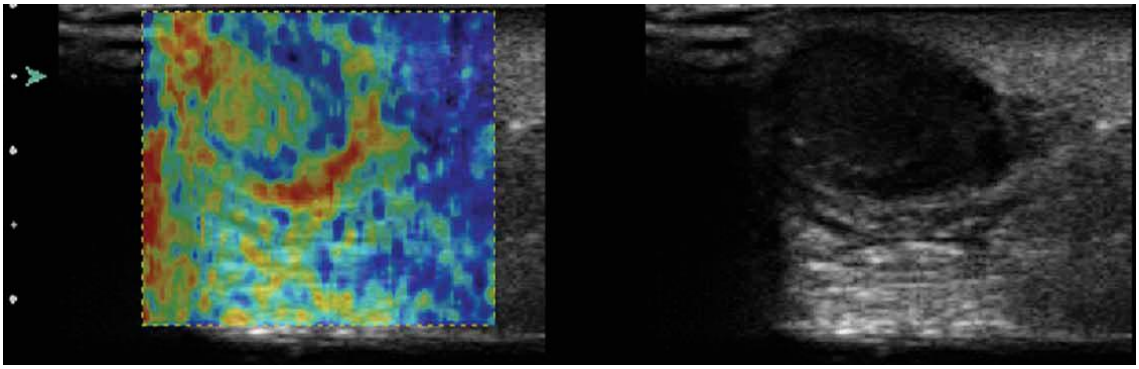

B

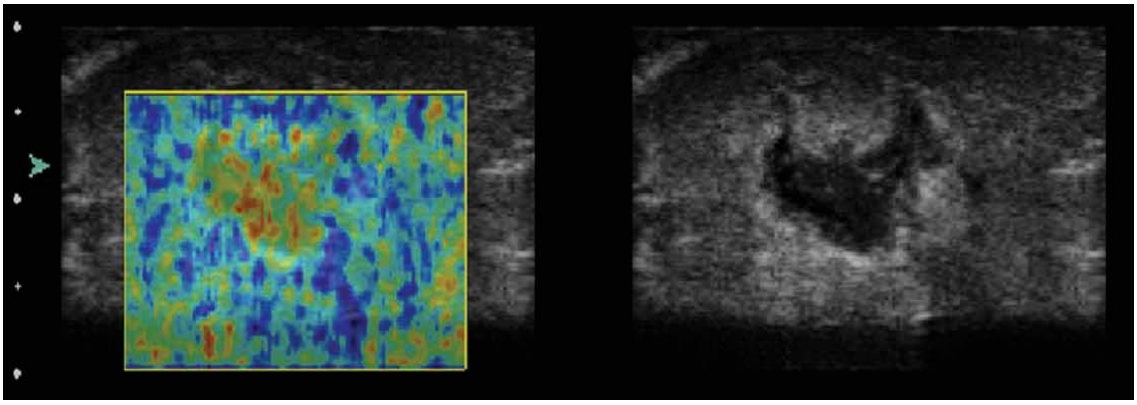

C

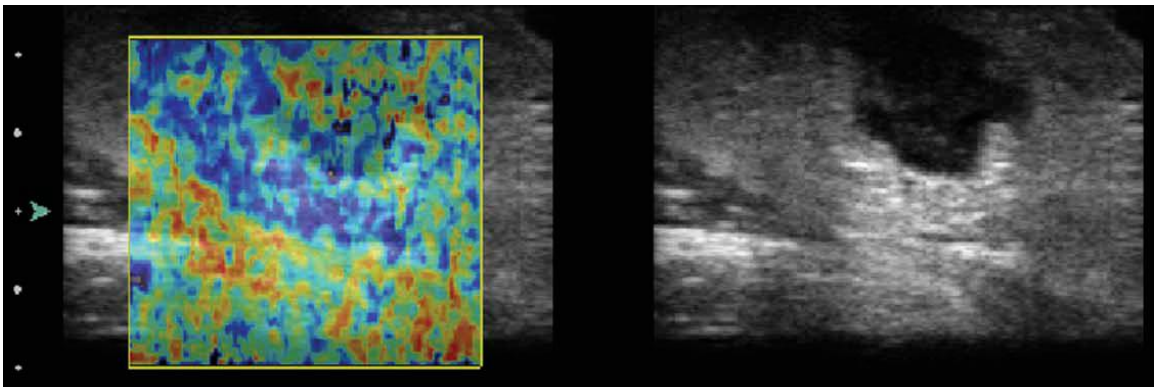

Figure 47: Elastographic color pattern of skin abscesses. The variable consistency of the abscess cavity is visualized with elastography as bands of color (**A**), larger spots of softer color on a background of medium stiffness (**B**, green and yellow), or smaller speckling of softer colors (**C**, red and yellow) surrounded by a range of stiffer colors **(Struk etal., 2001).**

A

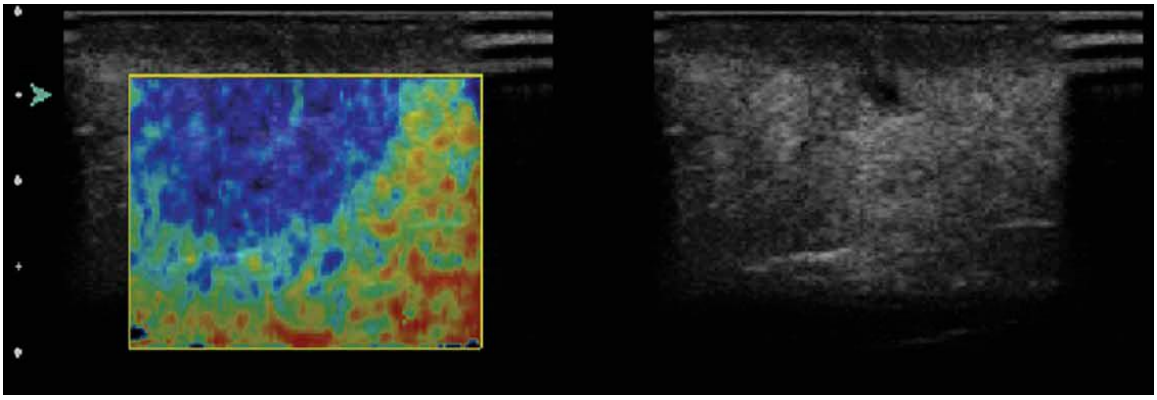

B

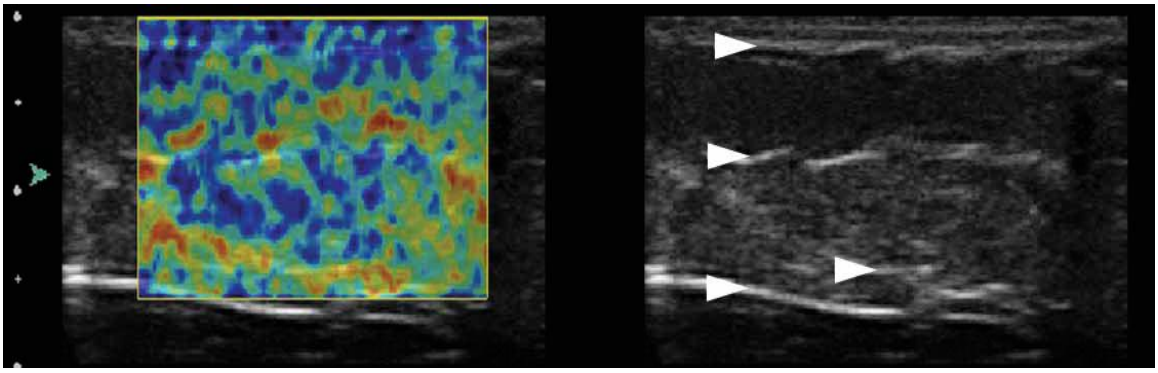

Figure 48: Elastographic imaging of soft tissue induration. **A**, Hard indurated tissue surrounding the abscess cavity is visualized with elastography as stiff regions (blue) surrounding the abscess cavity. **B**, A comparison view of the contralateral (side without infection shows no localized stiff tissue (speckled mixed colors) and retention of the normal tissue planes (arrowheads) **(Struk etal., 2001).**

A

B

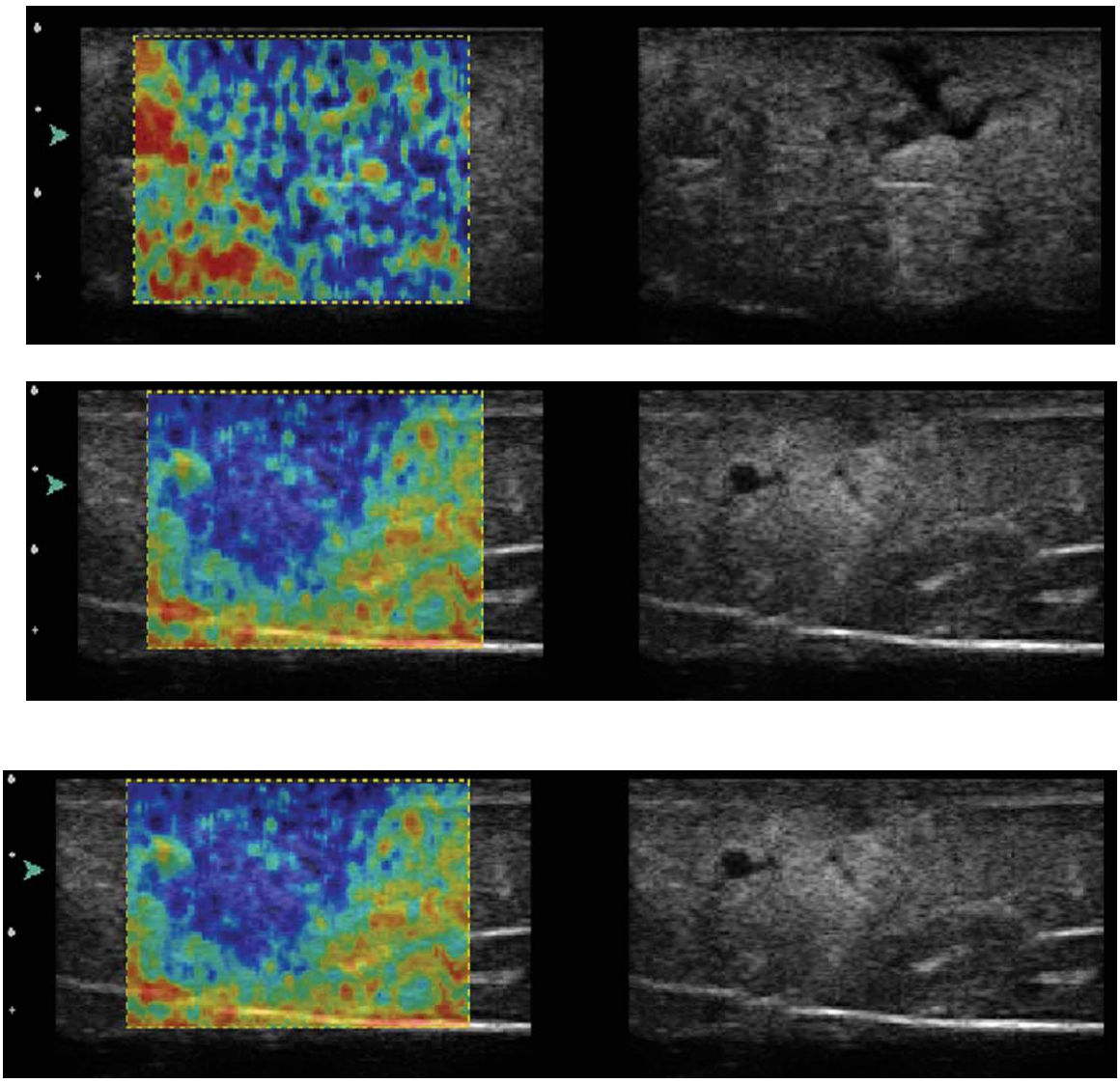

Figure 49: Elastographic pattern of skin infection induration. Firm indurated tissue surrounding the soft abscess cavity is visualized with elastography as a range of patterns from speckled stiff coloring (**A**, blue) on a less soft (**A**, aqua) background to larger stiff spots (**B**, blue) on a background of middle stiffness (**B**, green and Aqua) to almost solid stiff coloring (**C**, blue). The stiff induration (blue) is accentuated by the softer normal tissue (mixed colors) **(Struk etal., 2001).**

A

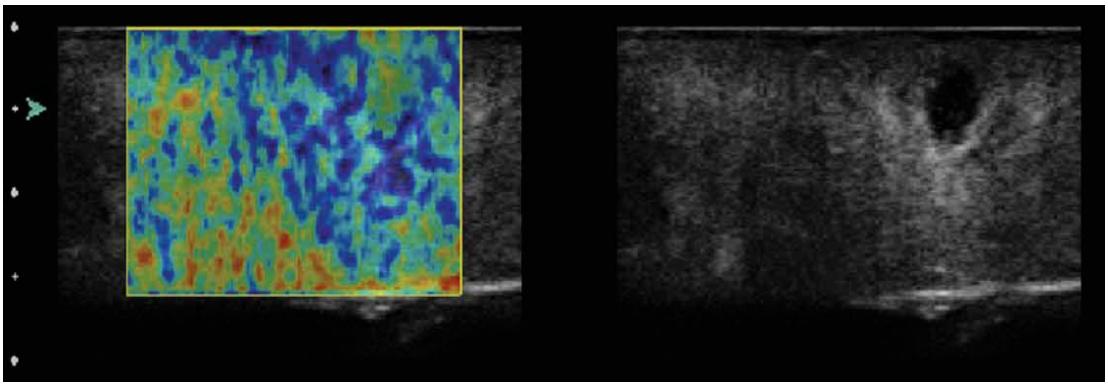

B

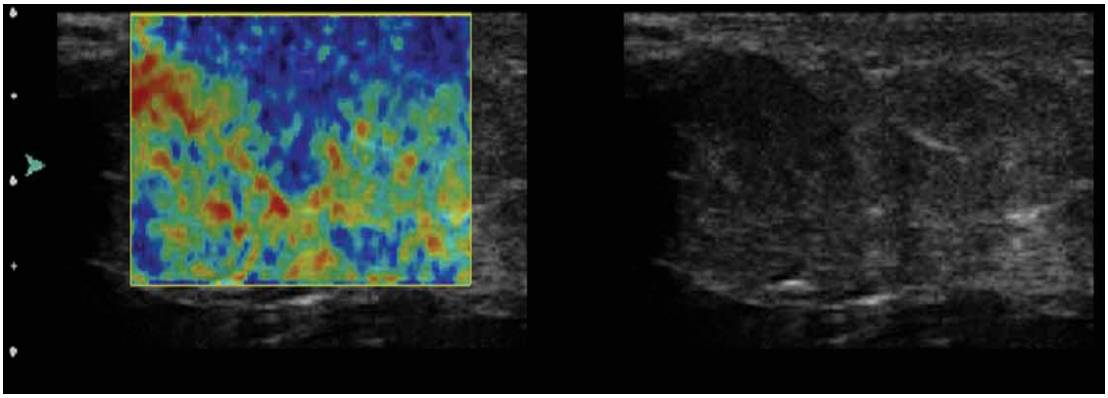

Figure 50: Elastographic color spectrum of skin infection induration.The surrounding induration is visualized with elastography as either speckled (**A**) or almost solid (**B**) stiff coloring (deep blue and aqua) **(Squire etal., 2006).**

Radiological diagnosis of psoriasis:

Diagnosis by ultrasound:

It is a lesion which has echographiquement Hyperkeratosis (big echo of entry), epidermal thickening and histologically a hypervascularisation and a dermal infiltrate, which explains the hypoechogenicite of the superficial Dermis. These quantifiable data allow evaluating the effectiveness of the treatment **(Berson etal., 2000).**

The using of high-frequency, B-mode, 40-MHz ultrasound scanning to image plaques of psoriasis show, In early studies, 15-MHz ultrasound A-scans or amplitude-mode scans demonstrated that the thickness of psoriatic plaques is increased compared with normal skin **(Hoffmann etal., 1999).**

When plaques of psoriasis are viewed using ultrasound imaging, bands of varying echogenicity have been observed. At 40MHz, ultrasound images of psoriasis exhibit a

three-layer structure (1) band A corresponds to the scaly parakeratotic cell layers and the suprapapillary epidermis; (2) band B represents the edematous and congested papillary dermis in the elongated epidermal rete ridges; and (3) band C is associated with the underlying reticular dermis (diagram 13 and figure 51) **(Overgaard etal., 2000).**

It has been suggested that the data from ultrasound images may reflect the severity of the psoriasis. Sonograms obtained at the lower ultrasound frequencies may not be of high enough quality to accurately assess the thickness of the echogenic bands. It is only recently that the development of higher-frequency systems has produced pictures with improved resolution, thereby enabling to image skin in greater detail. The 40-MHz high-frequency ultrasound machine, with its higher resolution, has ability to determine the size of the bands in a psoriatic plaque more precisely than previously able to do with the lower-frequency systems **(Querleux etal., 2001).**

The width of band B correlates best with the severity of psoriasis of a plaque as measured by the SET score. Also, the change in disease activity of a psoriatic plaque as measured by ASET correlates best with the change in the thickness of the non echogenic band B (Figure 51) **(Serup 1999).**

The thickness of band B correlates with the clinical severity of a psoriatic plaque as assessed by the degree of SET. (Degree of desquamation, erythema and thickness) **(Marks etal., 1999).**

The observation that band B corresponds to the major portion of the acanthotic epidermis and the superficial dermis, The width of band B is not a direct measure of thickness of a plaque of psoriasis; however, it reflects the thickness of the papillary dermis, which varies with the degree of vascularity, edema, and inflammation **(El-Gammal etal., 2002).**

The normalization of the epidermis and dermis that occurs with clinical improvement of a plaque of psoriasis may be responsible for the corresponding decrease in the width of the non echogenic band B (Figure 52) **(Vaillant etal., 2001).**

The use of high-frequency, real-time ultrasound scanning has enabled the generation of high-resolution images of psoriatic plaques. Ultrasound imaging has the advantage of being a noninvasive, relatively inexpensive technology that is quick and quite easy to perform **(Berson etal., 2000).**

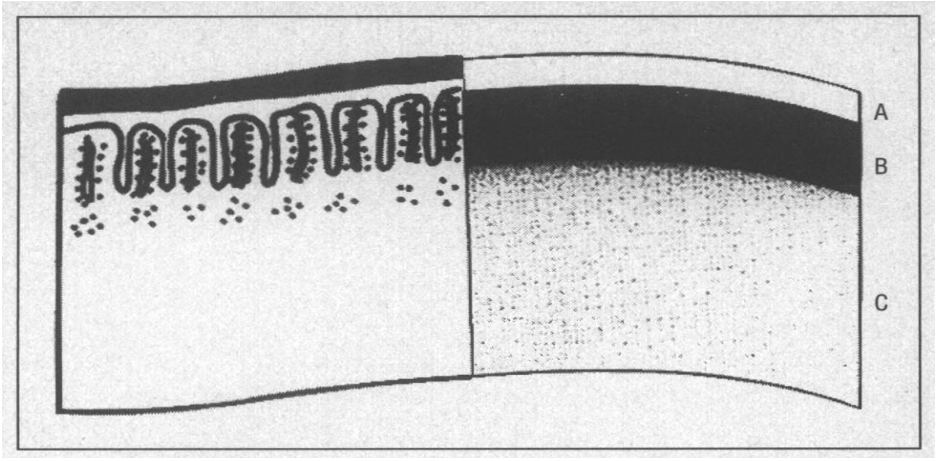

Diagram 13: Line diagram depicting location of bands A, B, and C in a high-frequency ultrasound image of a plaque of psoriasis

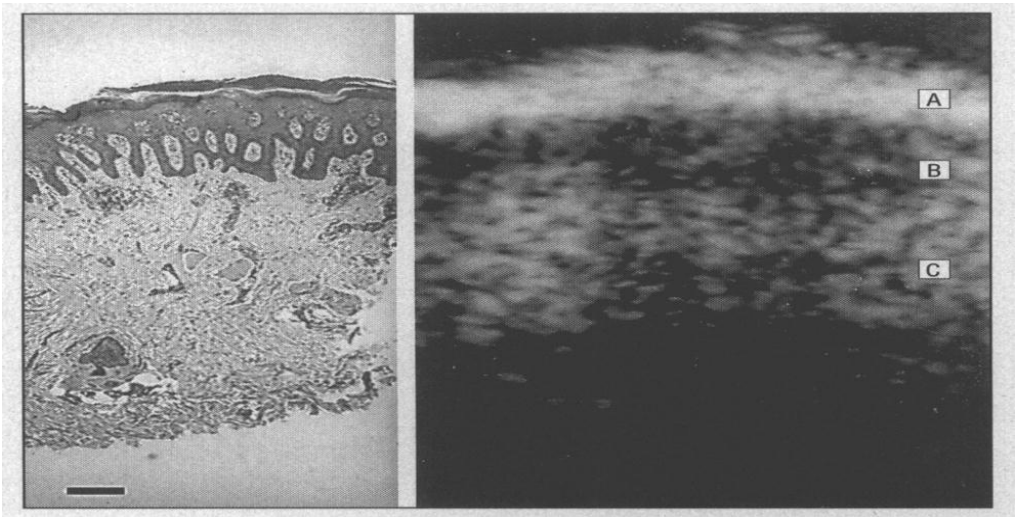

Figure 51: Comparison between histological section and high-frequency ultrasound image of a plaque of psoriasis showing bands A, B, and C both views are at the same magnification Bar indicates 200 fim. **(Hoffmann etal., 2001)**.

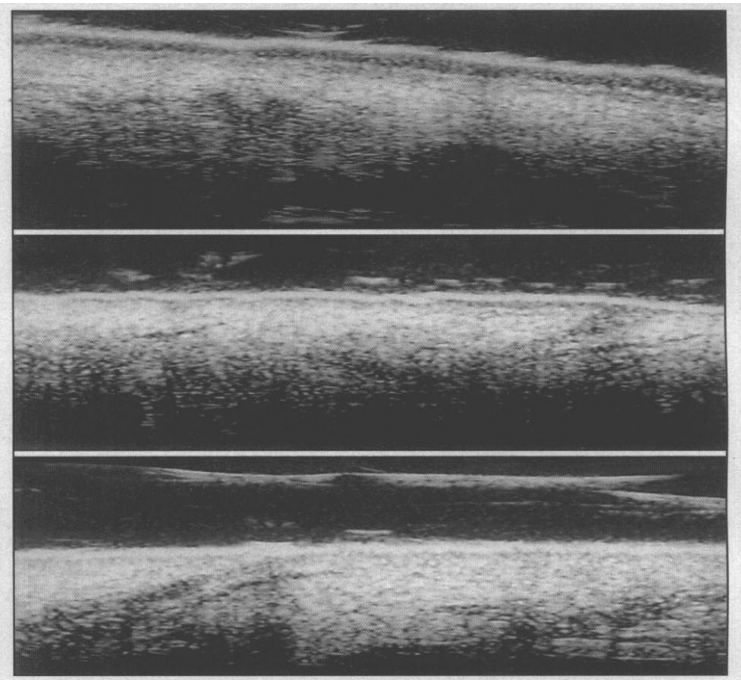

Figure 52: Top, Ultrasound image of a psoriatic plaque before treatment. Note the thickness of band B. Center, Ultrasound image when there has been moderate, but not complete, clinical improvement of the psoriasis Band B is still visible, although of decreased width compared with width before therapy. Bottom, Ultrasound image of a nearby clinically uninvolved area of skin. One small division on the scale equals 100 p.m. (**Hoffmann etal., 2001).**

Summary

Summary

Diagnosis of benign and malignant skin lesions is currently mostly relying on visual assessment and frequent biopsies performed by dermatologists. As the timely and correct diagnosis of these skin lesions is one of the most important factors in the therapeutic outcome.

As skin cancer is one of the most common cancer types in humans and its incidence is on the rise, especially in countries where the ozone layer is thinning. The correct and timely diagnosis of suspicious skin lesions is one of the most important factors in the therapeutical outcome. At present most dermatologists rely on their experience of visual assessment to distinguish benign and malignant skin lesions like pigmented nevi, seborrhoeic keratosis or basal cell carcinoma and malignant melanoma, as well as requiring biopsies of the affected skin.

New technologies to assist in identifying and diagnosing skin lesion and to minimize invasive biopsies have been developed, like hand-held magnification devices and computer-aided image analysis. Colored image processing methods were introduced for melanoma which focused on non-constant visual information of skin lesions. Neural network diagnosis of skin lesion has previously been applied by classifying extracted features from digitized dermoscopy images of lesions.

The extracted features are based on geometry, colors, and texture of the lesions, involving complex image processing techniques. Recently with Raman spectroscopy the molecular structure of skin lesions are exploited. Optical spectroscopy is another technology that is being established to aid in skin lesion diagnosis, as the multi-spectral nature of this imaging method allows detecting and classifying multiple physiological changes like those associated with increased vasculature, cellular structure, oxygen consumption or edema in tumors.

The application of MRI in dermatology can give a detailed picture of a tumor and its depth of invasion in relation to adjacent anatomic structures. It has reported as well as delineates pathways of tumor invasion

High frequency ultrasound can be usefully correlated with clinical tests to study focal skin lesions. The diagnosis of most benign skin cancers is usually made on clinical bases. Ultrasound examinations are performed preoperatively in questionable cases.

Malignant neoplasm appear at ultrasound as hypoechoic focal lesions, generally with no specific features in relation to the histological type; nevertheless, preoperative ultrasound may play an important role in that it measures the thickness of cutaneous melanoma, which is a very important prognostic factor.

In particular, 20 MHz probes permit to assess the depth of melanoma invasion. The sonographic evaluation of melanoma thickness is usually in agreement with histological findings ‘Satellite’. Neoplastic lesions growing near the main tumor can also be revealed .

Color and power Doppler studies may be combined with gray-scale imaging: the identification of abnormal intra- or peritumoral low-resistance pulsatile flow signals suggests the malignant nature of the cutaneous lesion.

High frequency ultrasound can also be used to study diffuse cutaneous conditions. Among them, ultrasound can provide a valid morphologic representation of psoriatic skin lesions and it is also a noninvasive and accurate method for evaluating the therapeutic efficacy of treatment.

High-frequency ultrasound with elastography can help differentiate between cancerous and benign skin conditions, allows for accurate characterization of the extent and depth of the lesion below the surface, which can aid physicians in treatment.

Elastography non invasively estimates the axial tissue strain, or elastic properties of tissue. Cystic lesions demonstrate high levels of elasticity, while malignant lesions are relatively “hard” with a very low level of elasticity.

This may be useful in the early detection of melanoma before the classic signs or changes in border are present on the skin’s surface.

Soft tissue infections are common conditions and range from superficial cellulitis to deeper soft tissue infections with abscess collections requiring surgery. Inadequately treated superficial soft tissue infections can progress to deeper tissue infections requiring more invasive surgery or bacteremia requiring hospitalization and intravenous antibiotic.

Ultrasound with elastography has been shown to be a useful adjunct to the physical examination in patients with suspected soft tissue fluid collections allows identification

of tissue “stiffness” by measuring the degree of distortion under the application of external force provided by the ultrasound probe.

PET provides functional, molecular information about the tumor fused with anatomic location provide by CT, PET is a sensitive method for detecting, staging, and monitoring the effects of therapy of many malignancies.

There is a limited role of both x-ray and CT in diagnosis of skin lesions as:
x-ray imaging using the mammography has a role in the diagnosis of arteriolar calcification of patients with calcific uremic arteriolopathy.

(CT) has been useful in staging mycosis fungoidesand which is uncommon primary malignant T cell lymphoma of the skin. And in defining the extent of adenopathy. Typical finding include focal skin thickening due to dermal and epidermal infiltration.

References

References

1) Ackerman AB, Magana-Garcia M. Naming acquired pigmented nevi. Unna 's, Miescher's, Spitz's Clark's. Am J Dermatopathol. ;12 (2):193-209. Apr 1999.

2) Ackerman AB, Milde P. Naming acquired pigmented nevi. Common and dysplastic, normal and atypical, or Unna, Miescher, Spitz, and Clark. Am. J.Dermato pathol ;14(5):447-53. Oct 1998.

3) Anderson CM. The changing prognosis of melanoma. Curr Oncol Rep. ; 2(4):322-8. Jul 2000.

4) Arslan H, Sakarya ME, Bozkurt M, Unal O, Dilek ON, Harman M. The role of power Doppler sonography in the evaluation of superficial soft tissue abscesses. Eur J Ultrasound; 8:101–106. 1998.

5) Ashbaugh DR. Quantitative-Qualitative Friction Ridge Analysis: An Introduction to Basic and Advanced Ridgeology. 1st. CRC; 1999.

6) A. Mahadevan-Jansen, in BiomedicalPhotonics Handbook, T. Vo-Dinh, Ed.*2003*

7) Balch CM, Buzaid AC, Soong SJ, et al. Final version of the American Joint Committee on Cancer staging system for cutaneous melanoma. J Clin Oncol. ;19(16):3635-48. Aug 15 2001.

8) Bale AE, Yu KP. The hedgehog pathway and squamous cell carcinomas. Hum Mol Genet. ;10(7):757 62. Apr 2000.

9) Baumann L. Skin ageing and its treatment. J Pathol. ;211(2):241-51. Jan 2007.

10) Bernard A. Cohen,MD, Christoph U . Lehmann, MD, Dernard A. Cohen, MD, Christoph U. Lehmann, MD. Derm Atlas, micrograph of basal cell carcinoma, p 144, figure 101. 2008.

11) Bernard A. Cohen,MD, Christoph U . Lehmann, MD, Dernard A. Cohen, MD, Christoph U. Lehmann, MD. Derm Atlas, micrograph of squamous cell carcinoma, p 154 a,b,c and d, figure 119.

2008.

12) Bernard A. Cohen,MD, Christoph U . Lehmann, MD, Dernard A. Cohen, MD, Christoph U. Lehmann, MD. Derm Atlas, micrograph of malignant melanoma, p 158, figure 123. 2008.

13) Berson M, Gregoire JM, Gens F, Rateau J, Jamet F, Vaillant L, Tranquart F, Pourcelot L. High frequency (20 MHz) ultrasonic devices: advantages and applications. Eur J Ultrasound;10:53-63. 2005.

14) Berson M, Vaillant L, Patat F, Pourcelot L. High-resolution real-time ultrasonic scanner. Ultrasound Med Biol;18:471-8. 2003.

15) Berson M, Vaillant L, Patat F, Pourcelot L. High-resolution real-time ultrasonic r. Ultrasound Med Biol.;18:471-478. 2000.

16) Betti R, Radaelli G, Mussino F, Menni S, Crosti C. Anatomic location and histopathologic subtype of basal cell carcinomas in adults younger than 40 or 90 and older: any difference?. Dermatol Surg. ;35(2):201-6. Feb 2009.

17) Bond JB, Haik BG, Futosh M, and Gupta KL. Magnetic resonance imaging of malignant melanoma with and without gadolinium contrast enhancement. Ophthalmol 98*:* 459–466. 2000.

18) Brook I, Frazier EH. Pathogenesis of wounds and cutaneous abscesses. Arch Surg; 125:1445. 2000.

19) Brusseau E., et al. Local Estimation of RF Ultrasound Signal Compression for Axial Strain Imaging : Theoretical Developments and Experimental Results, IEEE Engineering in Medicine and Biology Magazine – 21(4), , p. 86-94. July/August 2002.

20) Burns DA, Breathnach SM, Cox N, Griffiths CE, eds. Rook's Textbook of Dermatology. 7th ed. Wiley-Blackwell; 2004.

21) Canpolat Murat; AKMAN Ayse; AKIF CIFTCIOGLUM ALPSOYErkan; Department of biophysics, Akdeniz university, Antalya, Turquie.2007.

22) Carlson BM. Integumentary, skeletal, and muscular systems. In: Human Embryology and Developmental Biology. :153-81. 1st. 1998.

23) Cascajo CD, Reichel M, Sanchez JL. Malignant neoplasms associated with seborrheic keratoses. An analysis of 54 cases. Am J Dermatopathol. Jun 1996.

24) Cesinaro AM, Foroni M, Sighinolfi P, Migaldi M, Trentini GP. Spitz nevus is relatively frequent in adults: a clinico-pathologic study of 247 cases related to patient's age. Am J Dermatopathol. ;27(6):469-75. Dec 2005.

25) Chen SC, Bravata DM, Weil E & Olkin I. A comparison of dermatologists' and primary care physician accuracy in diagnosing melanoma: A systemic review. Arch Dermatol 137: 1627–1634. Clinical Exp Dermatol;28:632-8. 2001.

26) Coulomb A, Agence Nationale d'Accreditation et d'Évaluation (ANAES). Recommandations pour la prise en charge et le traitement des carcinomes basocellulaires. Ann Dermatol Venereol;131:661-756. 2004.

27) Crockett DJ. Lymphatic anatomy and lymphoedema. Br J Plast Surg. ;18:12-25. Jan 1998.

28) DeDavid M, Orlow SJ, Provost N, et al. A study of large congenital pigmented nevi and associated malignant melanomas: review of cases in the New York University Registry and the world literature. J Am Acad Dermatol. ;36(3 Pt 1):409-16. Mar 1997.

29) Delbeke D. mMartin WH, Patton JA, et al: Practical FDG imaaging. New York, Springer Verlag, 2002.

30) Eads TJ, Hood AF, Chuang TY, Faust HB, Farmer ER. The diagnostic yield of histologic examination of seborrheic keratoses. Arch Dermatol. ;133(11):1417-20. Nov 1997.

31) Edelson RL, Fink JM:The immunological function of the skin. Sci Am;256:48. 1999.

32) Edwards HGM, Williams AC & Barry BW. Pot.ential applications of FT-Raman Spectroscopy for dermatological diagnosis. J Mol Struct **347**: 379–388. 1998.

33) El- Gammal S, Auer T, Popp C, et al. Psoriasis vulgaris in 50-MHz B-scan ultrasound: characteristic features of stratum corneum, epidermis and dermis. Acta Derm Venereol (Stockh).;74:173-176. 2002.

34) Ferrara G, Argenziano G, Soyer HP, et al. The spectrum of Spitz nevi: a clinicopathologic study of 83 cases. Arch Der.matol. ;141(11):1381-7. Nov 2005.

35) Fongo A, Ferraris E, Bocca M. Skin tension lines and wrinkles. Anatomoclinical observations. Minerva Chir. ;21(13):627-30. 1999.

36) Gallagher RP, McLean DI. The epidemiology of acquired pigmented nevi. A brief review. Dermatol Clin. ;13(3):595-603. Jul 1995.

37) Ghoneim AT, McGoldrick J, Blick PW, et al. Aerobic and anaerobic bacteriology of subcutaneous abscesses. Br J Surg; 68:498. 1998.

38) Ginarte M, Garcia-Caballero T, Fernandez-Redondo V, Beiras A, Toribio J. Expression of growth hormone receptor in benign and malignant cutaneous proliferative entities. J Cutan Pathol. ;27(6):276-82. Jul 2000.

39) Giovagnorio F, etal. Color Doppler Sonography of focal lesions of the sku\in and subcutaneous tissue. J ultrasound Med; 18:89-93. 1999.
1999
40) Gniadecka M, Nielsen OF & Wulf H.C. Water content and protein structure in malignant and benign skin. J Mol Struct 662: 405–410. 2001.

41) Goldman MP. Shiffman MA, Mirrafati SJ, Lam SM, Cueteaux CG. Simplified Facial Rejuvenation. 2. Springer Berlin Heidelberg; 47-50. 2007.

42) Goldsmith LA. Biochemistry and physiology of the skin. Vol 5 and 6. oxford university Press, 1999.

43) Gould Rothberg BE, Berger AJ, Molinaro AM, Subtil A, Krauthammer MO, Camp RL, et al. Melanoma prognostic model using tissue microarrays and genetic algorithms. J Clin Oncol. ;27(34):5772-80. Dec 1 2009.

44) Greenleaf, J.F., et al, Selected Methods for Imaging Elastic Properties of Biological tissues, Annual Reviews of Biomedical Engineering, 2003.

45) Grossman D and Leffell DJ. Squamous cell carcinoma and its precursors: Clinical biology and molecular basis. In: Chu AC, and Edelson RL, editors. Malignant tumors of the skin. London: Arnold, Holder Head Line Group, 19–23. 2001.

46) Groves RW, Allen MH, MacDonald DM. Abnormal expression of epidermal growth factor receptor in cutaneous epithelial tumours. J Cutan Pathol. ;19(1):66-72. Feb 1998.

47) Habibian RM:Necular medicine imaging: A Teaching file. Philadilphia, Lippincott Williams& Wilkins, 1999.

48) Hafner C, Hartmann A, Vogt T. FGFR3 mutations in epidermal nevi and seborrheic keratoses: lessons from urothelium and skin. *J* Invest Dermatol. ;127(7):1572-3. Jul 2007.

49) Harland CC, Kale SG, Jackson P, Mortimer PS, Bamber JC. Differentiation of common benign pigmented skin lesions from melanoma by high-resolution ultrasound. Br J Dermatol .143:281-9. 2003

50) Harrison SL, Buettner PG, MacLennan R. Body-site distribution of pigmented nevi in young Australian children. Arch Dermatol. ;135(1):47-52. Jan 1999.

51) Hintz-Madsen M, Hansen L, Larsen J & Drzewiecki K. A probabilistic neural network framework for detection of malignant melanoma. In: Naguib RNG, Sherbet GV (eds)Artificial Neural Networks in Cancer Diagnosis, Prognosis and Patient Management Boca Raton: CRC Press ISBN 0-8493-9692-1, Chap 13, p 141–183. 2001.

52)Hoffmann K, el-Gammal S, Schwarze H, Dirschka T, Altmeyer P. Examination of psoriasis vulgaris using 20-MHz B-scan ultrasound. In: Altmeyer P, el\x=req-\ Gammal S, Hoffmann K, eds. Ultrasound in Dermatology. New York, NY: Springer\x=req-\ Verlag NY Inc; 244-249. 2000.

53) Hofmann UB, Westphal JR, Van Muijen GN & Ruiter DJ. Matrix metalloproteinases in human melanoma. J Invest Dermatol 115: 337–344. 1999.

54) James MR, Roth RB, Shi MM, et al. BRAF polymorphisms and risk of pigmented neoplasia. J Invest Dermatol. ;125(6):1252-8. Dec 2005.

55) Jason R Swanson and Jeffreyl. Melton MD, Dermatology atlas. Micrograph of pigmented nevi, p 133, figure 88a,b,c. 1998.

56) Jason R Swanson and Jeffreyl. Melton MD, Dermatology atlas. Micrograph of psoriasis, p 67, figure 43. 1998.

57) Jason R Swanson and Jeffreyl. Melton MD, Dermatology atlas. Micrograph of seborrheic keratoses, p 130, figure 81a,b. 1998.

58) Johansson CK, Gniadecka M, Ullman S, Halberg P, Kobayasi T & Wulf HC. Alterations in collagen structure in hypermobility and Ehlers–Danlos syndromes detected by Raman spectroscopy in vivo. Optical biopsy and tissue optics. Prog Biomed Optics Imaging 1: 138–143. 2000.

59) Josef Feit, Hana Jedličková, Zdeněk Vlašín, Günter Burg, Werner Kempf, Leo Schärer, Luděk Matyska . Basic and atlas of dermatopathology.2003.

60) Kantor J, Kantor DE. Routine dermatologist-performed full-body skin examination and early melanoma detection. Arch Dermatol. ;145(8):873-6. Aug 2009.

61) Kanzler MH & Mraz-Genrnhard S. Primary cutaneous malignant melanoma and its precursor lesions: Diagnostic and therapeutic overview. J Am Acad Dermatol 45: 260–276. 2001.

62) Kenneth A, Katz, Basic of dermatology, Department of dermatology, univerity of Pennsylvania.;105:24-30 .2001.

63) Ko CJ, McNiff JM, Glusac EJ. Pigmented nevi with features of Spitz nevi and Clark's/dysplastic nevi ("Spark's" nevi). J Cutan Pathol. ;36(10):1063-8. Oct 2009.

64) Konofagou E. E., et al, Elastography: From theory to clinical applications, Summer Bioengineering Conference, June 25-29, Florida, 2003.

65) Korte J, Sprangers MA, Mombers FM, et al. Quality of life in patients with psoriasis: a systematic literature review. J Investig Dermatol Symp Proc;9(2):140-7. Mar 2004.

66) Knudsen L, Johansson CK, Philipsen PA, Gniadecka M & Wulf HC. Natural variations and reproducibility of in vivo near-infrared Fourier transform Raman spectroscopy of normal human skin. J Raman Spectroscopy ,33: 574–579. 2003.|

67) Krahn G, Gottlober P, Sander C, Peter RU. Dermatoscopy and high frequency sonography: two useful non-invasive methods to increase preoperative diagnostic accuracy in pigmented skin lesions. Pigment Cell Res;11:151-4. 2001.

68) Krueger JG, Bowcock A. Psoriasis pathophysiology: current concepts of pathogenesis. Ann Rheum Dis. 64 Supple 2:ii30-6, Mar 2005.

69) Lamberty BG, Cormack GC. Fasciocutaneous flaps. Clin Plast Surg. ;17(4):713-26. Oct 1999.

70) Lassau N, Spatz A, Avril MF et al. Value of high-frequency US for preoperative assessment of skin tumors. Radiographics;17: 1559-65. 2002.

71) Lazova R, McNiff JM, Glusac EJ. Under the microscope. Surgeons, pathologists, and pigmented nevi. Clin Plast Surg. ;27(3):323-9, vii. Jul 2000.

72) Lilian de Oliveira Nune, Airton Abrahao Martin, Landulfo Silveira Jr., laboratory of biomedical vibrational spectroscopy, IP&D- institute of research and development, UNIVAP- University of vale do paraiba.2003.

73) Liu CH, Das BB & ShaGlassman WL *et al*. Raman, fluorescence, and time-resolved light scattering as optical diagnostic techniques to separate diseased and normal biomedical media. J Photochem Photobiol B - Biol 16: 187–209. 1999.

74) Lodish, Berk, Zipursky, Matsudaira, Baltimore &Darnell, eds. sixth edition. W.H. Freeman & Co. Molecular Cell Biology 2003.

75) MacKie RM. Malignant melanoma: Clinical variants and prognostic indicators. Clin Exp Dermatol 25: 471–475. 2002.

76) Maize JC, Snider RL. Nonmelanoma skin cancers in association with seborrheic keratoses. Clinicopathologic correlations. *Dermatol Surg*;21(11):960-2. Nov 1995 .

77) Malloy PC, Fishman EK, Magid D, Russel H, Morgan. Department of radiology and radiological science, Johns Hopkins hospital.1998.

78) Marks R, Barton SP, Shuttleworth D, Finlay AY. Assessment of disease progress in psoriasis. Arch Dermatol.;125:235-240. 1999.

79) Maurer J, Knolhmann FD, Schhms D, Garbe C, Vogl JJ, Bier I, and Felix R .Role of high resolution magnetic resonance imaging for differentiating melanin containing skin tumors. J Invest Radiol 30: 638–643.2000.

80) Maurer J, Strauss A, Ebert W, Bauer H, and Felix R .Contrast-enhanced high resolution magnetic resonance imaging of squamous cell carcinoma, Mn-TPPS4 and Gd-DTPA: Experimental results. Melanoma Res 10: 40–46. 2002.

81) Miura T & Thomas G, Jr. Raman spectroscopy of proteins and their assemblies. In: Biswas BB, Siddhartha R, (eds)Subcellular Biochemistry, Vol. 24, Proteins. Structure, Function and Engineering New York: Plenum Press p 55–99. 2001.

82) Moganty R Rajeswair,Aklank Jain, Ahok Sharma,Dineh Singh, N R Jagannathan, department of biochemistry and nuclear magnatic resonance, all India institute of medical science, Anari Nagar, New Delhi, india.2003.

83) Mooi WJ. Cutaneous pigmented naevus versus melanoma: pitfalls, surprises, dilemmas. Eur J Surg Oncol. ;25(6):622-7. Dec 1999.

84) Moore KL, Persuad TVN. The integumentary system. In: Before We Are Born: Essentials of Embryology and Birth Defects. 5th ed. :481-96. 1998.

85) Morris JL, Gibbins IL. Autonomic Innervation of the Skin. 1st. Informa Healthcare; 1997.

86) Murali R, McCarthy SW, Scolyer RA. Blue nevi and related lesions: a review highlighting atypical and newly described variants, distinguishing features and diagnostic pitfalls. Adv Anat Pathol. ;16(6):365-82. Nov 2009.

87) Nakagawa K, Yamamura K, Maeda S, Ichihashi M. bcl-2 expression in epidermal keratinocytic diseases. Cancer. ;74(6):1720-4. Sep 15 1996.

88) Nijssen A, Bakker Schut TC, Heule F, Caspers PJ, Hayes DP, Neumann MHA & Puppels GJ. Discriminating basal cell carcinoma from its surrounding tissue by Raman spectroscopy. J Invest Dermatol 119: 64–69. 2002.

89) Nindl M, Nakagawa H, Furue M, Ishibashi Y. Simple epithelial cytokeratin-expression in seborrheic keratosis. J Cutan Pathol. ;19(5):415-22. Oct 1997.

90) Ophir J., et al. Elastography: Imaging the Elastic Properties of Soft Tissues with Ultrasound. Journal of Medical Ultrasonics, Vol.29, 2002.

91) Overgaard Olsen L, Serup J. High-frequency ultrasound scan for non-invasive cross-sectional imaging of psoriasis. Acta Derm Venereol (Stockh).;73: 185-187.2000.

92) P. Matousek, I.P. Clark, E.R. Draper,M.D. Morris, A.E. Goodship, N. Everall, M. Towrie, W.F. Finney, and A.W. Parker, Appl. Spectrosc. 59, 393–400 .2005.

93) Palicka GA, Rhodes AR. Acral pigmented nevi: prevalence and distribution of gross morphologic features in white and black adults. Arch Dermatol. ;146(10):1085-94. Oct 2010.

94) Pallin DJ, Egan DJ, Pelletier AJ, Espinola JA, Hooper DC, Camargo CA Jr. Increased US emergency department visits for skin and soft tissue infections, and changes in antibiotic choices, during the emergence of community associated methicillin-resistant Staphylococcus aureus. Ann Emerg Med; 51:291–298.2008.

95) Pellacani G, Seidenari S. Preoperative melanoma thickness determination by 20-MHz .sonography and digital videomicroscopy in combination. Arch Dermatol 2003;139:293-8
Poblet E, Jiménez F, Ortega F. The contribution of the arrector pili muscle and sebaceous glands to the follicular unit structure. J Am Acad Dermatol. ;51(2):217-22. Aug 2004.

96) Poblet E, Jiménez F, Ortega F. The contribution of the arrector pili muscle and sebaceous glands to the follicular unit structure. J Am Aca Dermatol. ;51(2):217-22. Aug 2004.

97) Puppels GJ. Medical applications of Raman spectroscopy: From proof of principle to clinical implementation. Biopolymers (2001) 67: 1–9.

98) Prost-Squarcioni C. [Histology of skin and hair follicle]. Med Sci(Paris*)*. ;22(2):131-7. Feb 2006.

99) Prichard RS, Hill AD, Skehan SJ & O'Higgins NJ. Positron emission tomography for staging and management of malignant melanoma. Br J Surg 89: 389–396. 2000.

100) Querleux B, Leqeque JL, de Rigal J. echographie ultrasonore. Ann Dermatol Venereol.;115:980. Abstract.2001.

101) Rabe JH, Mamelak AJ, McElgunn PJ, Morison WL, Sauder DN. Photoaging: mechanisms and repair. J Am Acad Dermatol. ;55(1):1-19. Jul 2007.

102) Rallan D, Harland CC. Ultrasound in dermatology--basic principles and applications.2003.

103) Rigel DS, Carucci JA. Malignant melanoma: prevention, early detection, and treatment in the 21st century. CA Cancer J Clin. ;50(4):215-36; quiz 237-40. Jul-Aug 2000.

104) Rubin AI, Chen EH, Ratner D. Basal-cell carcinoma. *N Engl J Med*. Nov 24, ;353(21):2262-9.2005.

105) Sabel MS, Wong SL. Review of evidence-based support for pretreatment imaging in melanoma. J Natl Compr Canc Netw;7(3):281-9. . Mar 2009.

106) Sagebiel RW. Pigmented lesion pathology: the specimen and its report. A personal and probably biased approach. Pathology (Phila). \;2(2):281-98. 1997.

107) Schmid-Wendtner MH, Burgdorf W. Ultrasound scanning in dermatology. Arch Dermatol;141:217-24.2005.

108) Schuchter LM, Haluska F, Fraker D. Skin: malignant melanoma. In: Abeloff MD, et al, eds. Clinical Oncology. 2nd ed. New York: Churchill Livingstone; 1317-50.2000.

109) Schwartz, Shires, Spencer, Daly, Fischer & Galloway, eds. Eighth edition. McGraw-Hill. Principles of Surgery 2002.

110) Schwinghofer BW, Fruchwald FXI, Pohl-Markl H, Neuhold A, Wicke L, and Landrum WL. MRI evaluation of pigmented skin tumors. J Invest Radiol 24: 289–293.1999.

111) Serup J. Non-invasive quantification of psoriasis plaques: measurement of skin thickness with 15-mHz pulsed ultrasound. Clin Exp Dermatol.;9:502\x=req-\ 508.1999.

112) Shea CR, Prieto VG. Recent developments in the pathology of pigmented neoplasia. Dermatol Clin. ;17(3):615-30, ix. Jul 1999.

113) Shimizu N, Ito M, Tazawa T, Sato Y. Immunohistochemical study on keratin expression in certain cutaneous epithelial neoplasms. Basal cell carcinoma, pilomatricoma, and seborrheic keratosis. Am J Dermatopathol. ;11(6):534-40. Dec 1996.

114) Song HK, Wehrli Fw, and Ma J. MR microscopy of the human skin. Magn Reson Med 37: 185–191. 1999.

115) Sperry K, Wall J. Adenocarcinoma of the stomach with eruptive seborrheic keratoses: the sign of Leserp-Trelat. Cancer. ;45(9):2434-7. May 1 1998.

116) Squire BT, Fox JC, Anderson C. ABSCESS: applied bedside sonography for convenient evaluation of superficial soft tissue infections. Acad Emerg Med; 12:601–606.2006.

117) Stevens DL, Bisno AL, Chambers HF, et al. Practice guidelines for the diagnosis and management of skin and soft-tissue infections. Clin Infect Dis; 41:1373.2005.

118) Stone N, Tavroulaki P, Kendall C, Birchall M & Barr H. Raman spectroscopy for early detection of laryngeal malignancy: Preliminary results. Laryngoscope 110: 1756–1763.2000.

119) Struk DW, Munk PL, Lee MJ, Ho SG, Worsley DF. Imaging of soft tissue infections. Radiol Clin North Am; 39:2001.

120) Tayal VS, Hasan N, Norton HJ, Tomaszewski CA. The effect of soft-tissue ultrasound on the management of cellulitis in the emergency department. Acad Emerg; 13:384–388. Med 2006.

121) Taylor GI, Pan WR. Angiosomes of the leg: anatomic study and clinical implications. *Plast Reconstr Surg*. ;102(3):599-616; discussion 617-8. Sep 1998.

122) Teraki E, Tajima S, Manaka I, Kawashima M, Miyagishi M, Imokawa G. Role of endothelin-1 in hyperpigmentation in seborrhoeic keratosis. *Br J Dermatol*. ;135(6):918-23. Dec 1996

123) Tindall JP, Smith JG Jr. Skin lesions of the aged and their association with internal changes. JAMA. ;186:1039-42. Dec 21 1998.

124)Tojo M, Mori T, Kiyosawa H, Honma Y, Tanno Y, Kanazawa KY, et al. Expression of sonic hedgehog signal transducers, patched and smoothened, in human basal cell carcinoma. Pathol Int. ;49(8):687-94. Aug 1999.

125) Tran KT, Wright NA, Cockerell CJ. Biopsy of the pigmented lesion--when and how. *J* Am Acad Dermatol. ;59(5):852-71. Nov 2008.

126) U. Utzinger and R.R. Richards-Kortum, J. Biomed. Opt. 8, 121–147 (2003).

127) Vaillant L, Berson M, Machet L, Collens IA, Pourcelot L, Lorette G. Ultrasound imaging of psoriatic skin: a noninvasive technique to evaluate treatment of psoriasis. Int J Dermatol.;33:786-790.2001.

128) Verhagen AR, Koten JW, Chaddah VK, Patel RI. Skin diseases in Kenya. A clinical and histopathological study of 3,168 patients. Arch Dermatol;98(6):577-86. . Dec 1999.

129) Wheater, Burkitt, Stevens & Lowe, eds. fourth edition. Churchill Livingstone, Basic Histopathology 2005.

130) Wheater's Functional histology, a text and colour atlas, micrographs of the sebaceous glands. p. 168, Figure 9.14a &c.2005.

131) WHeater's Functional histology, a text and colour atlas, micrographs of the layers of the dermis. p. 165, Figure 9.11a.2005.

132) Wheater's Functional Histology, a text and atlas, Micrographs of merocrine sweat glands, p. 169, Figure 9.15.2005.

133) Wheater's Functional Histology, a text and colour atlas ,micrograph of the layers of skin, p. 159, Figure 9.4c.2005.

134) Wheater's Functional Histology, a text and colour atlas, micrograph of the melanocyte, 2005 p. 160, Figure 9.7a.

135) Wheater's Functional Histology, a text and colour atlas, micrograph of the langerhans cell, p. 161, Figure 9.8.2005.

136) Wheater's Functional Histology, a text and colour atlas, Micrograph of nail eponychium, p. 171, Figure 9.17.2005.

137) Wheater's Functional Histology, a text and colour atlas, Schematic diagram of layers of epidermis p. 159, Figure 9.5. 2005.

138) Wheater's Functional Histology, a text and colour atlas, Schematic micrograph of skin blood vessesls network, p. 173, Figure 9.19.2005.

139) Wheater's Functional Histology, a text and colour atlas, Schematic micrograph of free nerve ending of the skin, p. 174, Figure 9.21.2005.

140) Wiassm Bleibel D, Bora Hazar MD and Richard Herman MD, departments of internal medicine, nephrology and radiology, Carita Carney hospital university school of medicine, Boston, MA.2006.

141) Wieler HJ, Coleman RE: PET in clinical oncology. New York, Springer Verlag, 2000.

142) Winklelmann RK: the Merkel cell system and a comparison between it and the neurosecretory or APUD cell system. J Invest dermatol;88;56.1999.

143) Xing Y, Bronstein Y, Ross MI, Askew RL, Lee JE, Gershenwald JE, et al. Contemporary Diagnostic Imaging Modalities for the Staging and Surveillance of Melanoma Patients: a Meta-analysis. J Natl Cancer Inst. Nov 16 2010.

144) Yoshizaki T, Sato H & Furukawa M. Recent advances in the regulation of matrix metalloproteinases activation: From basic research to clinical implication (Review). Oncol Rep 9: 607–6011. 2002.

145) Z.J. Smith and A.J. Berger, *Opt. Lett.* 30,1363–1365 (2005).

146) Zmudzinka M, Czarnecka-Operacz M, Silny W. Department of dermatology, university of medical science, ul.2008.

147) Zurada J, Malinowski A & Cloete I. Sensitivity analysis for minimization of input data dimension for feedforward neural network. *Proc IEEE Symp Circuits System* 6: 447–450.2000.

148) Zymanska E, Nowicki A, Mlosek K, Litniewski J, Lewandowski M, Secomski W, Tymkiewicz R. Skin imaging with high frequency ultrasound - preliminary results. J Ultrasound;12:9-16.2000.

Arabic summary

الملخص العربى

تصنف الأمراض الجلدية إما حسب مصدرها الرئيسي لأمراض جلدية أولية و أمراض جلدية ثانوية أو وفقا للعامل المسبب إلى : الأمراض الجلدية غير معدية مثل التهاب الجلد و الو ذمة الوعائية العصبية. والأمراض الجلدية المعدية (الفيروسية، البكتيرية، الصوفية والطفيلية) وغيرها من الأمراض مثل (الخلقية والآفات الخبيثة).

تستخدم طرق التصوير المختلفة في تشخيص الآفات الجلدية على النحو التالي:

تستخدم الموجات فوق الصوتية عالية التردد في تشخيص الأمراض الجلدية باستخدام ترددات عالية بين ٢٠و٢٥ ميغا هرتز . و تتولد صور الموجات فوق الصوتية في أوضاع مختلفة، مثل أحادى الأبعاد و ثنائي الأبعاد، وهذا النوع من التصوير يمكن استخدامه لتقييم خصائص الجلد لدا إصابته ببعض الأمراض مثل الأورام الجلدية، الصدفية، شيخوخة الجلد، الندابات، التئام الجروح و الحساسية الشديدة.

يستخدم التصوير بالرنين المغناطيسي في تقييم الأورام الجلدية ونظرا لصغر سمك الجلد فان التصوير بالرنين المغناطيسي يتطلب الدقة و الحساسية العالية. و نتيجة لتطور التكنولوجيا في مجال سطح الملف و الماسحات الضوئية جعلت التصوير بالرنين المغناطيسي مفيد لدراسة الهياكل السطحية للجلد. و بالتطبيق يمكن الحصول على صورة تفصيلية للورم، و عمقه ، وعلاقته بالأنسجة المجاورة.

يستخدم مطياف الرنين المغناطيسي لتمييز الجلد المصاب من الجلد الطبيعي. وفى الآونة الأخيرة ، يستخدم مطياف رمان لتشخيص الأورام السرطانية للجلد حيث انه أداة تحليلية حديثة متعددة المزايا بالنسبة للمريض.

يفيد استخدام الالاستوجراف في التمييز بين الآفات الحميدة والخبيثة ليس عن طريق مظهرها المرئي ولكن عن طريق قياس مرونتها أو صلابتها حيث أن الأورام الخبيثة أكثر صلابة من الأورام الحميدة ، و إذا أضيف إلى التصوير بالموجات فوق الصوتية عالية التردد فان لديها أمكانية تحسين دقة التشخيص السريري التقليدي لسرطان الجلد، والقضاء على اخذ خزعات غير ضرورية من الآفات الجلدية الحميدة.و هذا الإجراء مريحا وغير مكلفا.

الفحص بالأشعة السينية باستخدام تقنية التصوير الاشعاعى للثدي هو السمة المميزة في تشخيص تكلسات الشرايين لدى مرضى الكلى وهو فحص بسيط وامن وغير مكلف.

تفيد الأشعة المقطعية في تشخيص بعض أنواع أورام الغدد الليمفاوية السرطانية في الجلد عن طريق قياس سماكة الجلد وتحديد مدى انتشار المرض إلى الغدد الليمفاوية.

الهدف من البحث:

معرفة دور طرق التصوير المختلفة في تشخيص الأمراض الجلية و يتضمن كلا من:

الفحص بالأشعة السينية، الموجات فوق الصوتية، الأشعة المقطعية، الرنين المغناطيسي بأنواعه المختلفة و غيرها من طرق التصوير الجديدة.

جامعة بنها
كلية الطب البشرى
قسم الاشعة التشخيصية

دور طرق التصوير المختلفة فى تشخيص الامراض الجلدية

رسالة
توطئة للحصول على درجة الماجستير فى الاشعة التشخيصية

مقدمة من

الطبيبة/ شيماء فتحى محمد لطفى
بكالوريوس الطب والجراحة
جامعة قناة السويس

تحت اشراف

الاستاذ الدكتور/ مدحت محمد رفعت
استاذ الاشعة التشخيصية
كلية الطب البشرى
جامعة بنها

الدكتور/ هشام محمد فاروق
استاذ مساعد الاشعة التشخيصية
كلية الطب البشرى
جامعة بنها

٢٠١١